Drilling of CFRP/AA Multi-Material Laminates Using WC-Co CVD Diamond Coated Tools

José Nuno dos Santos Duro

Master Dissertation

FEUP Supervisor: Prof. Dr. Abílio de Jesus

INEGI Co-Supervisor: Dr. Tiago Silva

PALBIT SA Co-Supervisor: Eng. Daniel Figueiredo

U.PORTO

FEUP FACULDADE DE ENGENHARIA
UNIVERSIDADE DO PORTO

Master in Mechanical Engineering

July 2023

"We are what we repeatedly do.
Excellence, then, is not an act, but a habit"

Will Durant

Abstract

In recent years, promising solutions have emerged to address the need for reducing structural weight in the modern transportation industry. Alternatives may involve the utilization of hybrid composite configurations, such as multi-material assemblies combining fiber-reinforced polymers and aluminum alloys. Given the distinct mechanical and thermal characteristics of each component, the process of drilling, which is fundamental for creating holes in (typical) riveted or bolted assemblies, presents significant challenges when it comes to achieving damage-free holes with precise tolerances. Drilling multi-material laminates gives rise to several challenges, including the formation of metal burrs, incomplete fiber cutting, delamination damage, and tool wear, among others. Consequently, meticulous selection of cutting conditions and tools becomes imperative to mitigate these issues effectively.

In the present work, the drilling process of multi-material laminates (composed of CFRP and AA2024 layers) using two distinct geometries of CVD diamond coated WC-Co single-shot drilling tools, was studied. Experimental tests were performed on two different stacking sequences composed of three main layers: (i) type I, with a composite-aluminum-composite sequence and (ii) type II, with an aluminum-composite-aluminum sequence, with the goal of finding ideal operating conditions. Different configurations of feed rate and cutting speed were considered in order to evaluate different compromises between drilling operation productivity and hole quality. An additional wear inspection experimental campaigns was carried out in order to confirm whether the identified appropriate operational conditions are compatible with a reliable and predictable tool wear.

Results revealed considerably higher thrust force and torque in the aluminum layers, when compared to the CFRP layers. Delamination was observed primarily in the type I laminate configuration when employing conventional twist drills, indicating the higher susceptibility of that plate towards defects. The feed rate was verified as the parameter which most contributed to the appearance of this type of defects. During the analysis of burrs and uncut fibers, it was observed that burrs were, particularly, present in the configuration type II within the last aluminum layer when utilizing the conventional twist drill. On the other hand, uncut fibers were observed in the same type of plate but for the second geometry drill. The chip analysis showed the formation of CFRP small fragmented chips/dust and long, non-fragmented chips for the aluminum layers. After an approximate drilling distance of 1550 mm in both types of plates (approximately 345 holes), no significant tool wear was detected. However, in the case of drilling the configuration type II (AA/CFRP/AA) with the second geometry drill, some aluminum adhesion was observed on the cutting edge, indicating a potential wear tendency (associated with built up edge) for this specific configuration.

Keywords: fiber material laminates; CFRP/AA; drilling; feed rate; cutting speed; delamination; burr; uncut fibers; surface roughness; chips; tool wear.

Resumo

Nos últimos anos, surgiram soluções promissoras para abordar a necessidade de redução de peso estrutural na indústria moderna de transportes. As alternativas podem envolver a utilização de configurações híbridas, como montagens de multimateriais que combinam polímeros reforçados com fibras e ligas de alumínio. Dadas as distintas características mecânicas e térmicas de cada componente, o processo de furação, que é fundamental para criar furos em montagens (típicas) rebitadas ou aparafusadas, apresenta desafios significativos quando se trata de obter furos sem danos com tolerâncias precisas. Furar laminados de multimateriais acarreta vários desafios, incluindo a formação de rebarbas metálicas, corte incompleto de fibras, danos por delaminação e desgaste da ferramenta, entre outros. Consequentemente, a seleção meticulosa das condições de corte e das ferramentas torna-se imperativa para mitigar esses problemas de forma eficaz.

No presente trabalho, foi estudado o processo de furação de laminados de multimateriais (compostos por camadas de CFRP e AA2024) utilizando duas geometrias distintas de ferramentas de furação de WC-Co de uma única passagem revestidas com diamante CVD. Foram realizados testes experimentais em duas sequências de empilhamento diferentes, compostas por três camadas principais: (i) tipo I, com uma sequência compósito-alumínio-compósito e (ii) tipo II, com uma sequência alumínio-compósito-alumínio, com o objetivo de encontrar as condições operacionais ideais. Diferentes configurações de taxa de avanço e velocidade de corte foram consideradas para avaliar diferentes compromissos entre produtividade da operação de furação e a qualidade do furo. Uma campanha adicional de inspeção de desgaste foi realizada para confirmar se as condições operacionais adequadas identificadas são compatíveis com um desgaste confiável e previsível da ferramenta.

Os resultados revelaram uma força de avanço e torque consideravelmente mais elevados nas camadas de alumínio, quando comparados às camadas de CFRP. A delaminação foi observada principalmente na configuração de laminado tipo I ao utilizar brocas helicoidais convencionais, indicando uma maior suscetibilidade dessa configuração a defeitos. Verificou-se que a taxa de avanço foi o parâmetro que mais contribuiu para o aparecimento desse tipo de defeito. Durante a análise das rebarbas e fibras não cortadas, observou-se que as rebarbas estavam particularmente presentes na configuração tipo II (AA/CFRP/AA), na última camada de alumínio, ao utilizar a broca helicoidal convencional. Por outro lado, foram observadas fibras não cortadas no mesmo tipo de configuração, mas para a segunda geometria de broca. A análise das aparas mostrou a formação de pequenos fragmentos/pó de CFRP e aparas longas e não fragmentadas para as camadas de alumínio. Após uma distância aproximada de furação de 1550 mm em ambos os tipos de configuração (aproximadamente 345 furos), não foi detetado desgaste significativo na ferramenta. No entanto, no caso da furação da configuração tipo II com a segunda geometria de broca, observou-se alguma aderência de alumínio na aresta de corte, indicando uma possível tendência de desgaste (associada a uma borda construída) para essa configuração específica.

Palavras-chave: laminados de multimaterial; CFRP/AA; furação; avanço; velocidade de corte; delaminação; rebarba; fibras não cortadas; rugosidade superficial; aparas; desgaste da ferramenta.

Acknowledgements

First of all, I would like to express my sincere gratitude to my supervisors at FEUP and INEGI. To Prof. Dr. Abílio de Jesus, for all his guidance, interest in the work, and advice for its development. To Dr. Tiago Silva, for having been tireless in following, daily, this work, help in the most difficult decisions, guidance, and motivation. I am very grateful for having had the opportunity to work with them, which increased my knowledge and my critical thinking skills.

To PALBIT SA and my supervisor at PALBIT SA, Eng. Daniel Figueiredo. I am very grateful for having given the opportunity to work in my thesis in a business and industrial environment and I would like to highlight my gratitude for the constant interest they have shown and for all the help made available. To Pedro Tavares, for all the support with the drilling tools and with the roughness analysis of the holes and to Dr. Cristina Fernandes for the help in the SEM analysis of the drilling tools.

To INEGI, for making available to me, on a daily basis, its equipment and for the constant help in the development of my thesis. To Rúben Costa, my sincere gratitude for all the support and dedication throughout the experimental procedure of my work. To Vitor Sousa and José Bouças, for all the help and availability during the drilling tests.

To DEMec (Department of Mechanical Engineering of the Faculty of Engineering of the University of Porto), mainly to Miguel Figueiredo for providing the X-ray analysis equipment. To Prof. Dr. Albertino Arteiro, for the availability in the collection of information about composite materials.

To CEMUP (Materials Centre of the University of Porto), for the availability to perform the SEM analysis of the coating of drilling tools.

To my friends, who have always been by my side in multiple situations in my life, for all their friendship, loyalty and for all the good moments.

To my family, in particular my parents, grandmother, aunt and cousin, who are mainly responsible for my having had the opportunity to enter this course. For all their support and patience, my sincere gratitude.

Finally, to Ana, for all the love, friendship, and for always being by my side to help me achieve my dreams.

Institutional Acknowledgements

The author gratefully acknowledges the funding from Project Hi-rEV – Recuperação do Setor de Componentes Automóveis (C644864375-00000002), cofinanced by Plano de Recuperação e Resiliência (PRR), República Portuguesa, through NextGeneration EU.

Contents

Abstract i

Resumo iii

Acknowledgements v

Institutional Acknowledgements vii

Contents ix

List of Abbreviations xi

List of Symbols xiii

List of Figures xv

List of Tables xxi

Chapter 1 – Introduction 1

1.1. Framework and Motivation 1

1.2. Objectives 2

1.3. Document's Structure 2

Chapter 2 – State-of-Art and Literature Review 5

2.1. Composite Materials 5

2.2. Drilling Process 10

2.3. Drilling Tool Geometry and Materials 16

2.4. CVD Diamond Coatings 18

2.5. Tool Wear 19

2.6. Chip Formation and Removal Mechanisms 23

2.7. Delamination and Fracture Modes 26

2.8. Burr 30

2.9. Hole Size and Surface Quality 32

2.10. Drilling of CFRP/AA laminates 35

Chapter 3 – Experimental Procedures 41

3.1. Cutting Tools 41

3.2. Workpiece Material Process and Definition 43

3.3. Instrumented Experimental Setup 45

3.4. Drilled Holes Analysis 49

Chapter 4 – Results Analysis and Discussion 57

4.1. Cutting Forces and Torque 57

4.2. Delamination Analysis 63

4.3. Burr and Uncut Fibers 66
4.4. Hole' Surface Roughness 69
4.5. Chip Analysis 72
4.6. Tool Wear Inspection 77
Chapter 5 – Conclusions and Future Works 79
5.1. Conclusions 79
5.2. Future Works 80
References 81
Attachment A: Technical Drawings of the Drilling Tools 87
Appendix A: Preliminary Drilling Campaign and Drilling Campaign 89
Appendix B: Delamination Preliminary Results 93
Appendix C: Tool Wear Analysis During the Drilling Campaign 97

List of Abbreviations

AA	Aluminum Alloy
AFP	Automated Fiber Placement
ANOVA	Analysis of variance
ATL	Automated Tape Laying
BUE	Built-Up Edge
BUL	Built-Up Layer
CFRP	Carbon Fiber Reinforced Polymer
CMC	Ceramic Matrix Composites
CVD	Chemical Vapor Deposition
DC	Direct Current; Diamond Coating
DIP	Digital Image Processing
DLC	Diamond-Like Carbon
FML	Fiber Metal Laminates
FRP	Fiber Reinforced Polymer
HFCVD	Hot Filament Chemical Vapor Deposition
HOOP	Hybrid Oscillatory Orbital Process
HSS	High-Speed Steel
MCD	Microcrystalline Diamond Coatings
MMC	Metal Matrix Composites
MRR	Material Removal Rate
NCD	Nanocrystalline Diamond Coatings
PCD	Polycrystalline Diamond
PEEK	Polyether-Ether-Ketone
PVD	Physical Vapor Deposition
Ra	Arithmetic average roughness
RF	Radio Frequency

RMS	Root Mean Square Roughness
RSM	Response Surface Methodology
RTM	Resin Transfer Molding
RUHM	Rotary Ultrasonic Helical Milling
Rz	Average maximum height of the profile
SEM	Scanning Electron Microscope

List of Symbols

A_{del}	Area of the delamination zone
A_{max}	Maximum area of the delamination zone
A_{nom}	Nominal area of the drilled hole
b	Chip width
Co	Cobalt
Cs	Cutting speed
D_{max}	Maximum diameter of the delamination zone
D_{nom}	Nominal diameter of the drilled hole
f	Feed rate
f_z	Feed per tooth
F_a	Two-dimensional delamination factor
F_d	Conventional delamination factor
F_{da}	Adjusted delamination factor
F_{dmin}	Minimum delamination factor
F_{ed}	Equivalent delamination factor
F_v	Three-dimensional delamination factor
F_z	Drilling-out direction force; Thrust force
h	Chip thickness
M_z	Drilling torque
n	Rotating speed

List of Figures

Figure 1. Materials used in the Boeing 787 body [5]. 6

Figure 2. Carbon fiber structure of the BMW i3 (a); Body of Audi R8 e-tron composed of aluminum frame combined with carbon fiber components (b) [9].. 7

Figure 3. Typical types of composite fabrics: (a) plain weave; (b) twill weave; (c) satin weave [13]. 8

Figure 4. Drilling main quantities: n (rotating speed, r.p.m.); f (feed, mm/rev); fz (feed per tooth, mm); h (chip thickness, mm); b (chip width, mm); D (diameter of the drill, mm); Fz (thrust force, N); Mz (torque, Nm) (adapted from [16]). 11

Figure 5. Conventional twist drill geometry (adapted from [19]). 12

Figure 6. Identification of three zones of the drill tip [15]. 13

Figure 7. Influence of the spindle speed and feed rate in drilling temperatures on CFRP/AA laminates [20]. 14

Figure 8. Rotary Ultrasonic Helical Machining (RUHM) (vf – helical speed; ap – helical revolution; e – radius of helical feed path; ns – spindle speed; vfa – axial feed speed of tool) [22]. 15

Figure 9. Oscillatory Orbital Drilling (OOD) (ns – rotational speed; va – axial feed rate; nw – orbital rotational speed) [23]. 16

Figure 10. Drilling tools geometries: (a) conventional twist drill; (b) double point angle twist drill; (c) brad and spur drill; (d) dagger drill; (e) step drill; (f) core drill and (g) special core drill [26]... 17

Figure 11. Different types of tool wear illustrated in a drill tool [1]. 20

Figure 12. Stages of tool wear: Regime I (early disintegration of the cutting edge); regime II (usable life of the cutting edge); regime III (fast degradation of the cutting edge) [40]. 21

Figure 13. Cutting mechanisms in the orthogonal machining of CFRP: (a) Type I – Delamination Type Chip Formation; (b) Type II – Fiber Buckling Type Chip Formation; (c) and (d) Type III – Fiber Cutting Type Chip Formation; (e) Type IV – Fiber Splitting Type Chip Formation; (f) Type V – Fiber Fracture Type Chip Formation [40]. 24

Figure 14. Comparison of chips obtained from (a) one-shot drilling process and (b) helical milling process [48]. 26

Figure 15. Schematic of delamination in composite materials: (a) Peel-up (entry) delamination and (b) push-out (exit) delamination [49]. 27

Figure 16. Graphical illustration of several delamination factor parameters [49]. 28

Figure 17. Fracture modes during (a) peel-up and (b) push-out delamination [66]. 30

Figure 18. Distinct types of burr formation: (a) uniform with drill cap; (b) uniform without drill cap; (c) crown-shaped burr [68]. 31

Figure 19. Relation between fiber cutting angle and burr area [71]. 32

Figure 20. Evolution of hole size in CFRP and Aluminum alloy AA7075 using: (a) DLC coated drill and (b) TiAlN coated drill [73]. 33

Figure 21. Average surface roughness (Ra) profile of (a) quasi-homogeneous material and (b) CFRP [76]. 35

Figure 22. Mechanical model of the drilling process using an orthogonal cutting model and coordinate transformation [78]. 36

Figure 23. Radial and thrust forces in drilling and helical milling (adapted from [48]). 38

Figure 24. One-shot drilling tool geometries used in the present study: type N geometry (drill 1) (a) and respective drill tip illustration scheme (b); type W geometry (drill 2) (c) and respective drill tip illustration scheme (d). 42

Figure 25. SEM analysis of the CVD diamond coating thickness and composition of the drilling tools. 43

Figure 26. CFRP/AA/CFRP plates (Type I) used in experimental procedures. 44

Figure 27. AA/CFRP/AA plates (Type II) used in experimental procedures. 44

Figure 28. Drilling tests setup: (a) DMG Mori DMU 60 eVo CNC machine; (b) and (c) clamping system. 45

Figure 29. Cutting loads acquisition system: (a) Kistler Type 9170A rotating cutting force dynamometer; (b) Kistler Type 5238B signal conditioner; (c) Kistler Type 5697 data acquisition system. 46

Figure 30. Acquisition thrust force loads in Kistler software for a hole made by drill 2 for the parameters of feed – 0.05 mm/rev and cutting speed – 300 m/min: (a) signal with drift; (b) signal with drift correction. 46

Figure 31. Dimensions between drilled holes: (a) Hole spacing from the borders and between each hole center for the drilling campaign (ii) with drill 2; (b) total of holes predicted in each plate. 49

Figure 32. Experimental apparatus required for the X-ray analysis of drilled holes: DinoLite AM-4031MZTL digital USB microscope (a); Liquid bath container (b) for plate submersion under methane di-iodine liquid (c); SATELEC X MIND X-ray emitter (d); Kodak RVG 5100 digital sensor (e). 50

Figure 33. Matlab delamination script’s fundamental operations. 51

Figure 34. Places where the methane di-iodine liquid did not drain effectively in the delamination area. 52

Figure 35. Use of the band saw machine to obtain the locations of the drilled holes to be measured. 53

Figure 36. Measurement of internal hole surface roughness using the ALICONA Infinite Focus SL. 53

Figure 37. Images of wear analysis in the drilling tool 2 taken in the DinoLite digital USB microscope. 55

Figure 38. Signature of thrust force signals in three holes obtained with the drilling tool 2 (feed – 0.05 mm/rev; cutting speed – 300 m/min) in the type I configuration plate. 57

Figure 39. Cutting forces for the type I plate: (a) thrust force and drilling torque results using drill 2 (feed – 0.05 mm/rev; cutting speed – 300 m/min), with signaled laminate interfaces’ cross by drill point; (b) drill point location diagram. 58

Figure 40. Cutting forces for the type II plate: (a) Thrust force and drilling torque results using drill 2 (feed – 0.2 mm/rev; cutting speed – 150 m/min), with signaled laminate interfaces’ cross by drill point; (b) drill point location diagram. 59

Figure 41. Evolution of the maximum thrust force in the plate type I along the 345 holes, using the drilling tool 2 (feed – 0.05 mm/rev; cutting speed – 300 m/min). 60

Figure 42. Evolution of the maximum torque in the plate type I along the 345 holes, using the drilling tool 2 (feed – 0.05 mm/rev; cutting speed – 300 m/min). 61

Figure 43. Evolution of the maximum thrust force in the plate type II along the 345 holes, using the drilling tool 2 (feed – 0.2 mm/rev; cutting speed – 150 m/min). 62

Figure 44. Evolution of the maximum torque in the plate type II along the 345 holes, using the drilling tool 2 (feed – 0.2 mm/rev; cutting speed – 150 m/min). 63

Figure 45. Comparison delamination analysis by: (a) microscope and (b) X-ray analysis in the preliminary drilling campaign (i) with the drilling tool 1: feed rate – 0.3 mm/rev and cutting speed – 150 m/min. 64

Figure 46. Delamination occurrence in: (a) drilled hole using the drilling tool 1 (with delamination) (feed – 0.05 mm/rev; cutting speed – 300 m/min); (b) drilled hole using the drilling tool 2 (without delamination) (feed – 0.05 mm/rev; cutting speed – 300 m/min)... 65

Figure 47. Adjusted delamination factor (Fda) for various combinations of feed and cutting speed (represented in Table 8) with the drilling tool 1. 66

Figure 48. Presence of burr defects in the holes produced by the drilling tool 1 (feed – 0.05 mm/rev; cutting speed – 300 m/min) in the configuration type II. 67

Figure 49. Presence of burr defects in the holes produced by the drilling tool 1 (feed – 0.05 mm/rev; cutting speed – 300 m/min) in the configuration type I. 68

Figure 50. Presence of uncut fibers in the holes produced by the drilling tool 2 (feed – 0.2 mm/rev; cutting speed – 150 m/min) in the configuration type I. Images taken by: (a) DinoLite digital USB microscope; (b) X-ray analysis. 69

Figure 51. Arithmetic average roughness (Ra) in the holes of the configuration type I. 70

Figure 52. Average Maximum Height of the Profile (Rz) in the holes of the configuration type I. 70

Figure 53. Arithmetic average roughness (Ra) in the holes of the configuration type II. 71

Figure 54. Average Maximum Height of the Profile (Rz) in the holes of the configuration type II. 71

Figure 55. Chip geometry in different stages during the drilling of the configuration type II with the drilling tool 2 with the drilling parameters: feed – 0.2 mm/rev and cutting speed – 150 m/min. 73

Figure 56. Chip geometry in different stages during the drilling of the configuration type I with the drilling tool 2 with the drilling parameters: feed – 0.05 mm/rev and cutting speed – 300 m/min. 74

Figure 57. CFRP fragmented chips. 74

Figure 58. Chip adherence to the drilling tool 2 observed during the drilling campaign (ii). 75

Figure 59. CFRP chips with adherence to the non-fragmented aluminum chips – images taken in the DinoLite microscope. 76

Figure 60. Circular surface scratches created by the entangled aluminum chips in the drill in the configuration type II with: (a) the drilling tool 1 (feed – 0.05 mm/rev; cutting speed – 300 m/min) and (b) drilling tool 2 (feed – 0.2 mm/rev; cutting speed – 150 m/min). 76

Figure 61. Wear analysis of the cutting edges of the drilling tool 2 after drilling: (a) 15 holes and (b) 345 holes (feed – 0.05 mm/rev; cutting speed – 300 m/min) in the configuration type I. 77

Figure 62. Wear analysis of the cutting edges of the drilling tool 2 after drilling: (a) 15 holes and (b) 345 holes (feed – 0.2 mm/rev; cutting speed – 150 m/min) in the configuration type II. 78

Figure 63. Technical drawing (in mm) of the drilling tool 1 (by PALBIT S.A.). 87

Figure 64. Technical drawing (in mm) of the drilling tool 2 (by PALBIT S.A.). 88

List of Tables

Table 1. Distinct delamination factors and their analytical expression (adapted from [48]). 29

Table 2. Drilling conditions of the main studies of the literature review. 38

Table 3. Drilling tool geometry specification for each type. 42

Table 4. Number of holes produced by the combination of drilling parameters of the preliminary drilling campaign (i). 47

Table 5. Number of holes produced by the combination of drilling parameters of the second drilling campaign (ii). 48

Table 6. Wear analysis experimental procedure for the configuration type I (CFRP/AA/CFRP) with the drilling tool 2 (feed – 0.05 mm/rev; cutting speed – 300 m/min). 54

Table 7. Wear analysis experimental procedure for the configuration type II (AA/CFRP/AA) with the drilling tool 2 (feed – 0.2 mm/rev; cutting speed – 150 m/min). 54

Table 8. Results of the two-dimensional delamination factors, conventional delamination factors, and adjusted delamination factors. 65

Table 9. Preliminary drilling campaign (i) and drilling campaign (ii). 89

Table 10. Delamination results using DinoLite USB microscope analysis (left) and X-ray analysis (right) for the preliminary drilling campaign (i) with the drilling tool 1. 93

Table 11. Wear inspection of the drilling tool 2 in the drilling campaign (feed – 0.05 mm/rev; cutting speed – 300 m/min) of the plate configuration of type I. 97

Table 12. Wear inspection of the drilling tool 2 in the drilling campaign (feed – 0.2 mm/rev; cutting speed – 150 m/min) of plate configuration of type II. 98

Chapter 1

Introduction

1.1. Framework and Motivation

Hybrid composite laminates, in particular carbon fiber-reinforced polymer and aluminum laminates assemblies (CFRP/AA), have steadily gained ground to fulfill the demands of structural weight reduction in the current aircraft and automotive sectors. These new structural materials offer improved mechanical qualities, such as high strength-to-weight ratio, good corrosion and impact resistance, and higher stiffness when compared to traditional materials. Cutting tools and hole quality are both severely hampered by the abrasive and anisotropic properties of fiber-reinforced composite materials. In order to minimize defects, it is crucial to choose the right cutting conditions, especially when it comes to surface integrity issues like delamination, uncut fibers, fiber pullout, and poor surface roughness, which can affect fatigue behavior.

The interaction and disparity in the components' thermal and mechanical characteristics might cause multiple problems during drilling. Poor hole quality is reportedly the cause of around 60% of component rejections, and it may be expensive for aerospace businesses [1]. As a result, careful hole drilling in Fiber Metal Laminates (FML)s is required to prevent significant workpiece damage. Due to the different mechanical and thermal behaviors of each layer, drilling, which is the fundamental hole-making process used in the aerospace industry, proves to be especially difficult when it comes to producing damage-free holes with precise tolerances for CFRP/AA laminates in one-shot operations using dry conditions. One of the main problems brought on by drilling multi-material is the creation of metal burrs. Other important problems may include heat damage, rapid and severe tool wear, large drilled holes, and delamination. To avoid such defects, it is vital to improve a number of drilling-related processes. The choice of suitable cutting parameters is crucial since they have a big impact on how much the workpiece is damaged. Moreover, the geometry of the tool may be adjusted to minimize burr and delamination, and the material and coating of the tool can affect its cutting performance and increase its wear resistance.

The present work focuses on drilling of CFRP/AA using CVD (Chemical Vapor Deposition) diamond coated tools. The carbon fiber composites have a thermoplastic matrix, and the aluminum alloy is the AA2024, since it is a commonly used in the aerospace industry. The drilling tool's geometry and coating, as well as the drilling parameters, feed, and cutting speed, will be changed in order to both study their effects and identify an ideal solution. The cutting loads – both in the form of thrust force and torque – as well as the hole quality indicators – such as delamination, burr, hole size, and hole's surface roughness – will be examined as outputs to compare the various combinations. To predict tool's life and failure mechanisms the tool wear conditions and chip removal mechanisms in the drilling operations will also be examined.

1.2. Objectives

The primary objective of this work is to evaluate the machinability of drilling operations on CFRP/AA multi-materials using CVD diamond coated tools. This will allow for the determination of the effective operating conditions to achieve an optimal performance on the hole-making of this multi-materials. The main actions used to achieve this objective will be:

- Development of a cutting setup based on relevant literature review on fiber reinforced composite materials;
- Experimental characterization tests towards a detailed assessment of the cutting process;
- Planning of instrumented drilling tests with operational parameters selection and using PALBIT-designed cutting tools;
- Characterization of the drilling mechanical process, through instrumented drilling tests (spindle load measurement), defects characterization and wear inspection of tools;

1.3. Document's Structure

In chapter 1, the study subject is briefly introduced, the chapter's goals are set forth, and a general description of the dissertation structure is presented.

In chapter 2, the state-of-art and literature review in the main topics of the work is made. This contains an introduction to composite materials and a description of the fundamentals of the drilling process. The exploration of various drilling tool geometries and materials is followed by a summary of CVD diamond coatings and tool wear. The chip formation and removal mechanisms are also investigated, with an approach to delamination and fracture modes, burr creation, as well as hole size and surface quality. Finally, more recent information regarding the drilling of CFRP/AA2024 multilayer laminates is analyzed to ensure a detailed review in the main topic of this work.

In chapter 3, all of the experimental procedures that have been used as well as various analysis techniques are exposed. The material, drilling tools, cutting loads acquisition, drilling parameters, drilled holes analysis, chip analysis, and drilling wear analysis consist of the experimented procedures conducted in this chapter.

In chapter 4, all of the experimental results are presented and examined, beginning with the drilling forces, and moving on the drilled holes analysis.

In chapter 5, the last chapter of this dissertation, are presented some detailed conclusions as well as some recommendations for additional research.

Chapter 2

State-of-Art and Literature Review

2.1. Composite Materials

A composite material is a mixture of two or more materials that exhibit superior qualities compared to those materials used separately. As compared to bulk materials, composite materials' key benefits are their high specific strength and stiffness which enables weight reduction multiple applications/components. Nowadays, composite materials are known as reinforcement arrangements [2]. The matrix helps maintain the integrity and structural strength of the composite material when it is subjected to external forces or loads. It binds the reinforcing elements to ensure that the load is distributed and transmitted efficiently within the composite structure. The resulting materials are very heterogeneous and frequently anisotropic. The qualities of the composite material include the kind of matrix and charge, the fibers, the caliber of the interface, and the production method [3].

Nowadays, composite materials are strongly applied in various industries, including the aerospace sector. Each airplane manufacturer has as one of its objectives choosing the most suited material to the intended use in order to create the lightest construction [4]. The first commercial jet aircraft constructed largely of composite materials was the Boeing 787. Figure 1 illustrates how the Boeing 787 employs more composite materials in the main structure and fuselage than any other Boeing commercial aircraft. By volume, the Boeing 787 is made up of 80% composite material. In terms of weight, the airplane is composed of 50% composite, 20% aluminum, 15% titanium, 10% steel, and 5% other materials [5]. For the airplane parts, composite materials are often used in the fuselage skins and bulkheads (which offer the structural stiffness needed for a safe flight), in the wing skins, spars, and ribs (which aid in weight reduction while boosting stiffness and strength), in the tail section (where they provide excellent strength and stiffness while being lightweight), in fan blades, spinning cones, and exhaust nozzles (in order to increase their longevity, reduce weight, and improve performance), as well as in landing gear components like doors, fairings, and struts (to reduce weight and enhance strength and durability) [6]–[8].

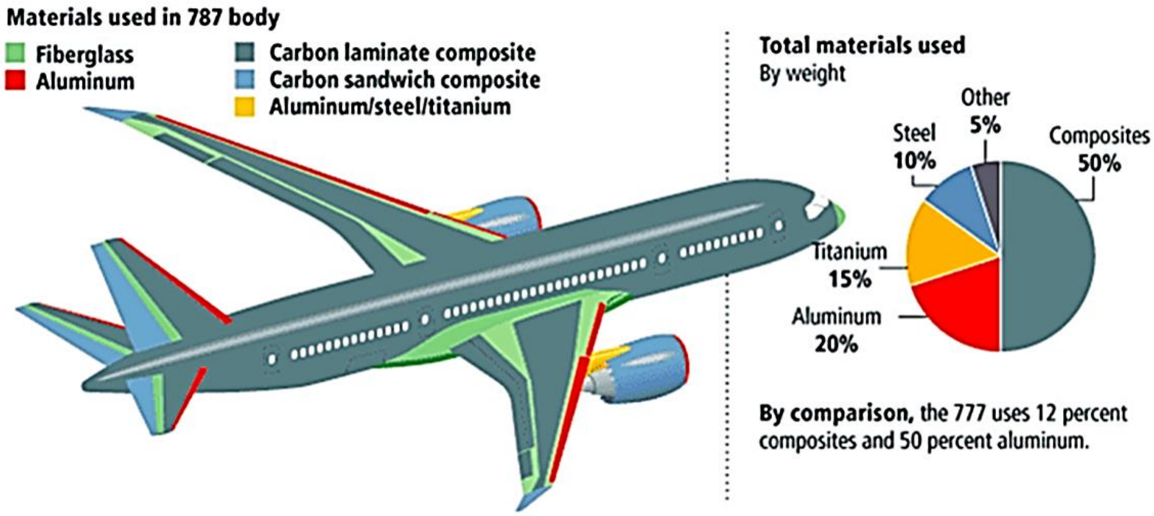

Figure 1. Materials used in the Boeing 787 body [5].

Besides the aerospace industry, it is important to highlight the viability of adopting composite materials in the transportation sector, particularly in automotive applications, which is the primary focus of this project.

The automotive industry has witnessed a significant evolution in the utilization of composite materials, particularly carbon fiber composites. The progressive adoption of carbon fiber composites in automobile manufacturing is rising because of their transformative impact on vehicle design, performance, and sustainability. Initially, the use of carbon fiber composites in automobiles was limited to high-end and performance vehicles due to cost constraints [4]. Challenges such as manufacturing complexity, limited production capacity, and uncertain material behavior posed barriers to widespread adoption. With advancements in manufacturing technologies and material science, carbon fiber composites became more accessible and affordable [2]. Breakthroughs in fiber reinforcement, resin systems, and curing processes improved the overall performance and reliability of these materials. Automakers began exploiting this attribute by integrating carbon fiber components into the vehicle's structure, such as chassis, body panels, and interior elements, being application examples the structure in carbon fiber of the BMW i3 (Figure 2a) and the aluminum space frame technology combined with carbon fiber components of the body of Audi R8 e-tron (Figure 2b) [9]. This approach led to significant weight reduction, enhancing fuel efficiency and overall performance .

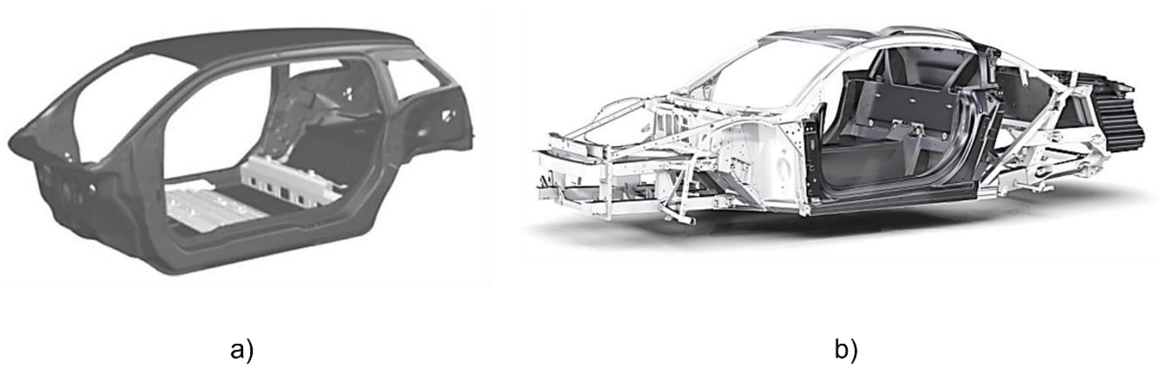

Figure 2. Carbon fiber structure of the BMW i3 (a); Body of Audi R8 e-tron composed of aluminum frame combined with carbon fiber components (b) [9].

Carbon fiber composites offer superior energy absorption capabilities compared to traditional materials. Their ability to withstand and distribute impact forces makes them ideal for enhancing vehicle safety and crashworthiness. Carbon fiber-reinforced composite structures are designed to protect occupants while maintaining structural integrity during collisions [6]. The inherent flexibility of carbon fiber composites allows for greater design freedom and innovative styling in automotive design. Aerodynamic profiles, and sleek contours can be achieved, giving automakers the opportunity to differentiate their products and create visually striking vehicles [9]. The use of carbon fiber composites aligns with the industry's drive towards sustainability. Lightweighting through composite materials reduces fuel consumption and carbon emissions. As demand increased and production techniques advanced, carbon fiber composites began to enter mass production models. Economies of scale, process automation, and efficient manufacturing strategies have steadily reduced the cost of carbon fiber composites, making them more economically viable for broader vehicle applications [9]. Continued research and development in carbon fiber composite technology are expected to further enhance their properties and reduce manufacturing costs. However, challenges such as recyclability, repairability, and end-of-life considerations remain focal points for ongoing innovation [6].

In comparison to other FRPs, such as metal matrix composites (MMC) and ceramic matrix composites (CMC), FRPs are the most significant and well-liked composite material for the production of lightweight structural elements [10]. A FRP material consists of a number of plies or laminae, which are referred to as layers. A ply is a single layer of woven fibers in the case of a fabric, or many fibers arranged in a single direction for unidirectional composites [11]. The most popular material in the composites sector is 2D woven fabric. It has two yarn sets, the warp (0º) and the weft (90º), which are perpendicular to one another in the fabric plane. The woven fabric is created by weaving together warp and weft threads in a pattern and a type of weave. The three basic weave kinds created by traditional weaving are plain, twill, and stain, as illustrated in the Figure 3. The simplest and most prevalent type of weave is the plain weave, in which each weft yarn alternately passes over and beneath each warp thread. The weft strands in a twill weave create a diagonal pattern by passing over several warp yarns and then going under several warp yarns. In the satin weave, in which the weft yarns travel over numerous warp strands before sliding beneath one, the fabric has a smooth appearance on one side [12].

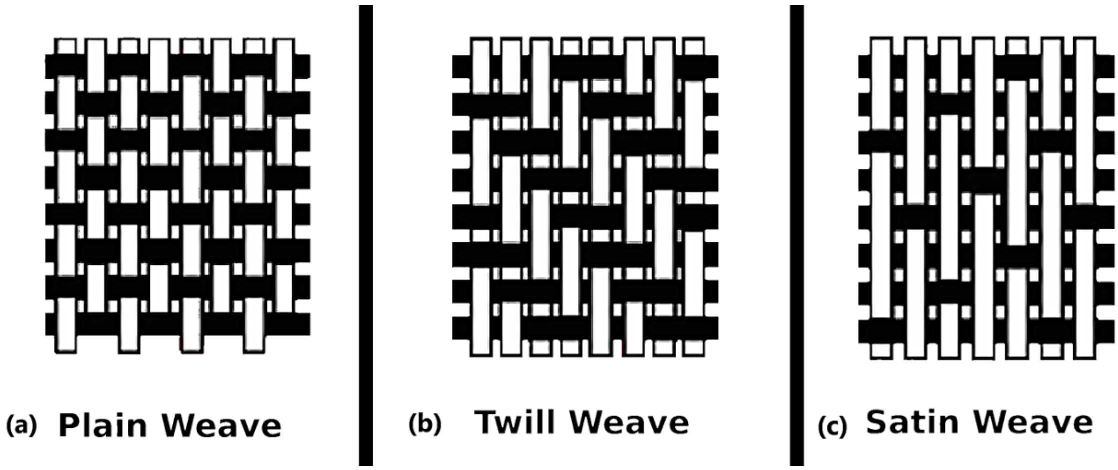

Figure 3. Typical types of composite fabrics: (a) plain weave; (b) twill weave; (c) satin weave [13].

The matrix might be made of an elastomer, thermoplastic, or thermosetting material [4]. The most common alternatives for choosing a matrix are thermoplastic and thermoset, and there are several matrix options available within the two major categories. The main distinction between the two is that whereas thermosetting resins cannot be altered after the chemical reaction that causes their cure has taken place, thermoplastic materials may be periodically softened by heat [6]. The manufacturing process, the physical and mechanical characteristics of the finished product, and the environmental resilience of the resulting composite all significantly change between the two options. For thermoplastics, long-term loads induce creeping because the Young's modulus and strength of thermoplastic materials are lower than those of thermosetting materials [14]. Processing temperatures for materials made of thermoplastics are greater than those for materials made for thermosets [14].

Regarding the thermoplastic matrices, the linear chains that compose them can change while they are still molten. The thermoplastic matrices are heated in the majority of production procedures, then the completed product is shaped using molding, injection, extrusion, or thermoforming before being cooled to maintain its shape. Thermoplastics come in a broad variety of forms, each with a unique set of intriguing features. Thermoplastic matrix options range from nylon and polypropylene, which are often used, to matrices like polyether-ether-ketone (PEEK) resins, which are chosen for their great tolerance to high temperatures and strong solvents found in commercial aircraft environments. Comparable to the price disparities in fibers, for example (ranging from less than 0,5 $/kg for polypropylene to more than 220 $/kg for PEEK), there is a clear disparity between the pricing of the commodity resins and the resins that would be employed for aerospace applications [4]. Several manufacturers have chosen to advocate the use of a commodity method to create miniature aircraft structures made of polypropylene and glass [3]. Because their wide-scale employment is still in the future, aerospace high-performance thermoplastic composites offer a comparatively high potential benefit [3].

On the other hand, the thermosetting matrices are typically liquid at ambient temperature, but during application, under the influence of heat and a substance called a hardener, they solidify. Afterwards, there is a chemical change that creates a strong three-dimensional link between the molecules. Due to the irreversible nature of this process, the substance is rendered insoluble and infusible in the majority of solvents (alcohols, ketones, and hydrocarbons). They are useful for molding big components with short, long, or woven threads, because they are generally more stiff than thermoplastic matrices, have better creep resistance, and are less brittle [4]. Polyesters, phenoplasts, polyurethanes, polyimides, and epoxy resins are the most widely used thermosetting matrices, with the latter being the preferred application for advanced composites. These resins are more expensive than polyesters and do not have the same high-temperature properties as polyimides, but they have a lot of advantages such as the good adhesion to resin and fibers, minimal shrinkage when curing, resistance to solvents and chemicals, good electrical qualities, and resistance to fatigue [3].

The fibers serve to carry most of the load and contribute to the composites' high strength and stiffness. Glass, carbon, and aramid fibers are the most often used fiber materials. E-glass (electrically isolating), S-glass (high breaking resistance and toughness), M-glass (high modulus), and R-glass (resistance) are examples of common glass fibers. High strength, high modulus, high tenacity, and intermediate modulus carbon fibers are other fibers that are used in a wide range. 90% of all fibers used in polymer composites for structural applications are glass fibers, making them the most prevalent and frequently utilized, being less expensive than aramid and carbon fibers [6]. Glass is drawn through an aperture to create glass fibers or filament, and around 200 filaments come together to make a strand. Carbon and graphite fiber are sometimes used interchangeably [11]. While the latter is stronger than the first one, they are both referred to as the same material in the composites industry. Originally, the aerospace industry employed carbon fibers to strengthen composite materials. The applications are now being expanded to include sectors like marine and automotive [14]. They possess excellent heat conductivity, high tensile strength, and high modulus of elasticity, besides being stronger and more rigid than glass and aramid fibers. The aramid (aromatic polyamide) fibers are made of para-linked aromatic aramides in a linear polymer chain. The most common application for aramid fibers is Kevlar [11]. Aramid fibers have a lower compressive strength than glass fibers but a greater tensile strength and modulus. Because of their extremely high impact and penetration resistance, armor made of aramid fibers is typically employed in ballistic body armor [11].

There are several different manufacturing processes used in the production of composite materials, each with its unique advantages and limitations. A common technique for making composites is called Hand-lay-up, which entails manually attaching layers of reinforcing fibers to a mold before soaking them in liquid resin [11]. While labor-intensive, this method gives the reinforcing fibers' placement better control and enables the construction of intricate structures. In resin transfer molding (RTM), dried reinforcing fibers are injected into a pre-made mold together with resin. In order to achieve appropriate resin infiltration, the mold is subsequently sealed, and pressure is applied. This technique is frequently employed to produce massive, intricate objects with precise tolerances.

Continuous reinforcing fibers such carbon fiber, are wound around a revolving mandrel in a manufacturing process called filament winding in a specified pattern. The fibers are then coated with resin to form a sturdy framework. The manufacture of cylindrical forms such as pipelines, tanks, and pressure vessels frequently use this method. In pultrusion, reinforcing fibers are drawn into a resin solution and then through a heated die to produce a solid structure with a constant cross-section. This method is frequently used to create structural forms like beams and rods. Manufacturing processes that are very productive can involve injection molding. In this process, thermoplastic and thermoset matrices are treated in conjunction mostly with short fibers but also with long ones. The mechanical performance is subpar compared to continuous fiber composites because of the indeterminate fiber orientation and poor fiber content, as well as lack of continuous fibers in the direction of load. Depending on the extensiveness of the treated material, two processes – Automated Tape Laying (ATL) and Automated Fiber Placement (AFP) – are often used for fiber deposition. AFP placement heads may lay up to 32 tows of narrow slit tape, allowing for more intricate curvatures, while ATP are typically built to process tapes of 75-300 mm in width. Thermoforming is the process of shaping composite materials into the required shape after heating them up until they are soft and malleable. Hot air, infrared heating, and radiant heating are few of the techniques that may be used in this process. The material is cooled after shaping in order to preserve its new shape [11].

2.2. Drilling Process

In the machining process of drilling, holes are made by removing material using revolving cutting tools. To cut through tiny layers of material and create chips, the drill uses rotating and feeding actions. The drill's main cutting edge removes material, and the chisel edge assists in plastic deformation [15]. There are a few key motions that take place through the drilling process. The initial contact of the drill tip with the workpiece is referred to as penetration. The drill begins to pierce the material when it comes into contact with the workpiece's surface. The drilling process starts with the penetration phase. The drill's movement into the workpiece when drilling is known as feeding. It controls how quickly the drill penetrates the material. The drill may drill further into the workpiece with the help of the feed action, gradually producing the hole. The cutting speed fluctuates during drilling according to the distance from the drill center. The drill's peripherical cutting edge experiences the maximum cutting speed. The cutting speed has an impact on how much material is removed during drilling . Figure 4 shows the drilling main quantities, such as the rotating speed (n – r.p.m.), the feed (f – mm/rev), the feed per tooth (fz – mm), the thrust force (Fz – N), the torque (Mz – Nm), the chip width (b – mm), and the chip thickness (h – mm) [16]. For the drilling process to be successful, these quantities must be properly controlled and coordinated in order to produce the appropriate hole diameters, surface quality, and material removal efficiency.

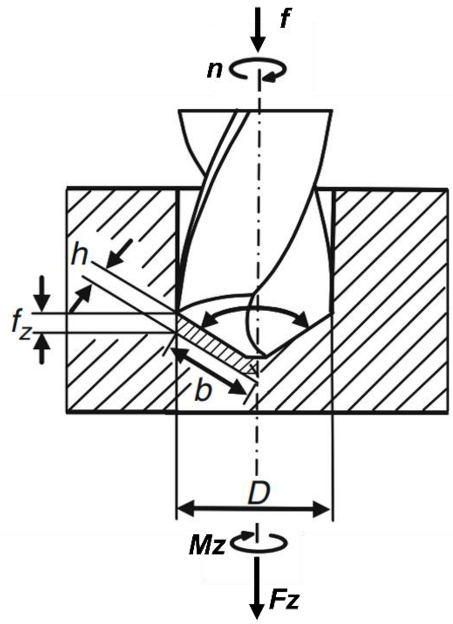

Figure 4. Drilling main quantities: n (rotating speed, r.p.m.); f (feed, mm/rev); fz (feed per tooth, mm); h (chip thickness, mm); b (chip width, mm); D (diameter of the drill, mm); Fz (thrust force, N); Mz (torque, Nm) (adapted from [16]).

Drilling is a commonly used machining operation and has significant economic importance. Drilling operations are limited by the drill geometry, the workpiece material's plastic deformation, and fracture properties. At the drill center, the cutting speed is near to zero. The cutting edge has the maximum cutting speed, known as the peripheral cutting speed, and both the cutting speed and rake angle change with regards to the distance from the drill center [1]. In order to minimize positional errors, favor tight tolerances, and lower production costs, hybrid composite laminates in aircraft assembly are primarily fastened by rivets and bolts, which requires producing a larger number of holes through drilling processes [17]. In the drilling process the typical drilling tool is the twist drill, which has a very complex geometry, as illustrated in Figure 5. The shank, which is attached to the drilling machine by a clamp, the flutes, and the point are its three basic components [18].

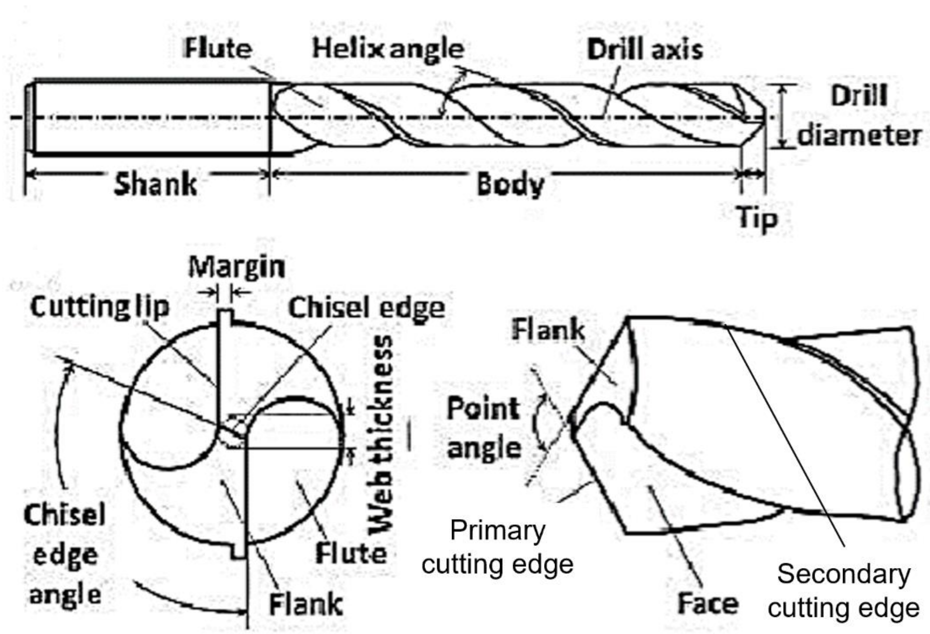

Figure 5. Conventional twist drill geometry (adapted from [19]).

For evaluating the machinability of laminated composites and hybrid composite laminates, drilling forces are crucial indications. They directly affect the drilling process' quality, specifically the likelihood of delamination. Drilling forces may be split up into two primary categories: thrust force and torque, and they can both be continuously measured [1]. Whereas torque shows the load amount needed to twist the drill bit during drilling, thrust force reflects the tribological behavior of the tool-chip contact. Figure 6 depicts the zones of the drill tip for identifying thrust force, where each cutting zone is used to determine the thrust force model [15]. In zone 1, the chip formation occurs, providing the axial force. A material removal occurrence in zone 2 varies from the ones in zone 1, because of the low tangential speed and of negative rake angles. Zone 3 has an extremely slow cutting speed, being indentation (plastic deformation) the dominant effect [15]. Similar thrust force profiles exist for drilling CFRP/AA laminates, and drilling aluminum results in larger thrust force than drilling composites. The presence of chip clogging and the variable chip separation mode may both be used to explain the variation in drilling force signals [17]. Kumar et al. [15] aimed to develop a theoretical model that can predict the drilling-countersinking thrust force of CFRP laminates. The model demonstrated good agreement with the actual data, regarding the comparison of the experimental results with its theoretical predictions. In order to determine how different factors, including feed rate, countersink angle, and drill bit diameter, affected the drilling-countersinking thrust force, a sensitivity analysis was also carried out. The results have shown that while the feed rate has no impact on the thrust force, the drill bit diameter and countersink angle do. The drilling parameters, such as tool shape, cutting speed, and feed rate, may be optimized using the model. This can assist to lower the thrust force and the danger of delamination, as well as the damage to the CFRP structure [15].

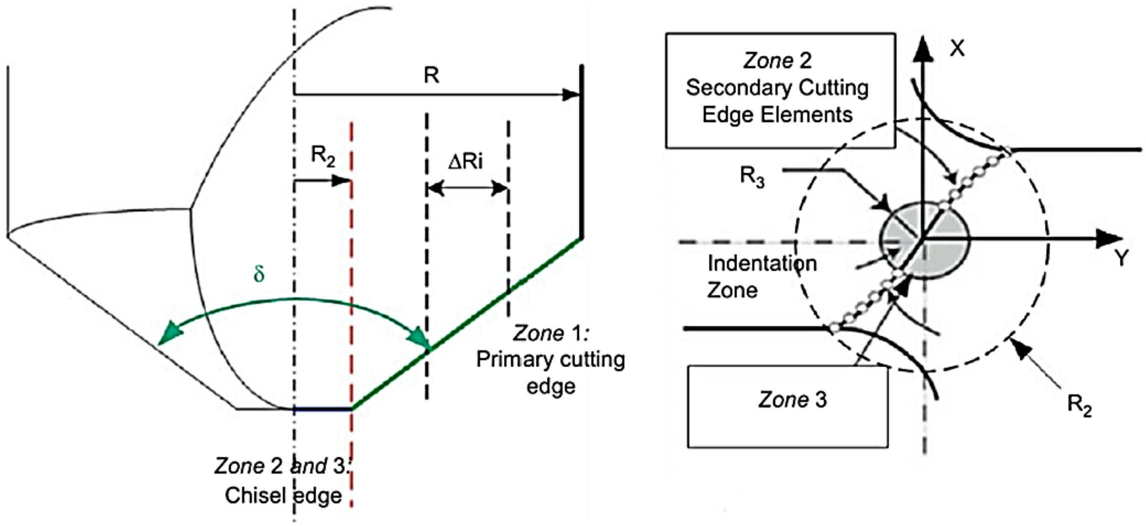

Figure 6. Identification of three zones of the drill tip [15].

Drilling temperatures play a critical role in assuring the quality of the drilled hole for hybrid composite laminates. In particular, when the drilling is carried out in dry circumstances because of the environmental issues related with cutting fluids, monitoring drilling temperatures is crucial to understand the physical mechanisms involved in one-shot drilling operations [1]. The development of drilling temperatures during the drilling of a CFRP/AA multi-material was initially presented by Wang et al. [20]. In this research, it was found that when the CFRP component is being drilled, the temperature rises rapidly until a maximum value is reached close to the conclusion of the process. The abrasiveness of carbon fibers and tool wear, generate significant quantities of friction and heat. The results of this research by means of the influence of feed rate and spindle speed in drilling temperatures are presented in Figure 7. When drilling both CFRP and aluminum layers at once, a quick increase in thrust force is accompanied by sharp decrease in temperature, which progressively changes during the course of drilling the aluminum component. Differences in the thermal conductivity characteristics of the two drilling materials are the reason for this particular progression of thermal behavior. Aluminum alloys are well recognized for having a high thermal conductivity, which makes it easier to remove the excess heat generated when drilling the top layer of CFRP [17]. While drilling a multi-material made of 5 mm thick CFRP and 5 mm thick aluminum AA5056, in the study of Sato et al. [21], a distinct evolution of the cutting temperature was noticed. This study’s spindle speed, at 900 r.p.m., is lower than the spindle speed proposed by Wang et al. [20] (2000 r.p.m.). Moreover, Wang et al. [20] picked a value of 0.02 mm/rev for this cutting parameter whereas Sato et al. [21] used 0.01 mm/rev for their multi-material stack drilling. In these circumstances, more cutting heat is produced because drilling the CFRP layer at a slower pace causes more abrasive friction and produces longer, non-fragmented chips that are challenging to remove. To guarantee the quality of drilled holes for hybrid composite laminates, it is essential to understand drilling temperatures. It's important to keep track of these using a variety of approaches to see how they affect the drilling efficiency of aerospace assemblies, especially when drilling is done in dry environments [20], [21].

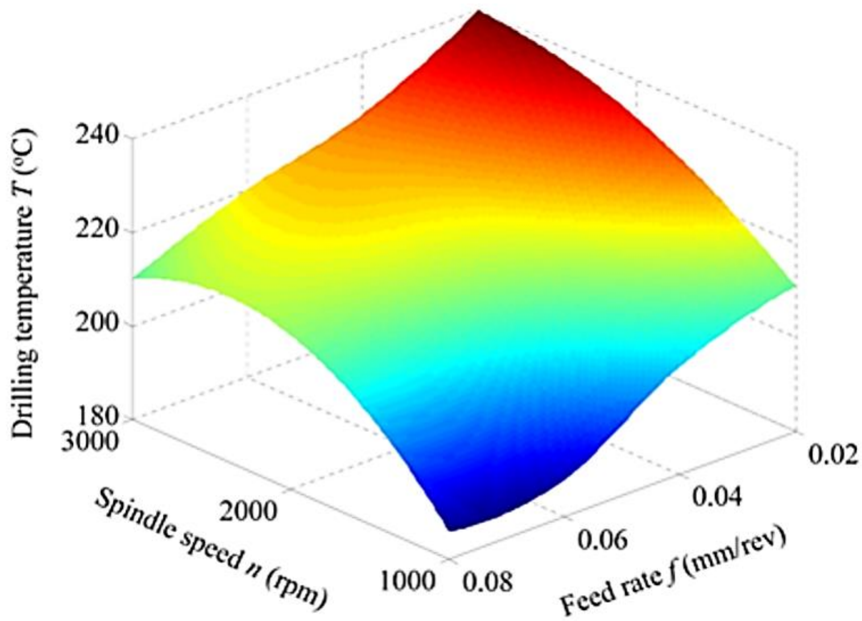

Figure 7. Influence of the spindle speed and feed rate in drilling temperatures on CFRP/AA laminates [20].

In conventional drilling of composite materials, a hole is made using a rotating drill bit with sharp edges. In this process, the material may get weaker, and the precision of the hole may decrease as a result of delamination, fiber fraying, and heat accumulation [1]. Nevertheless, rotary and ultrasonic vibrations are used in helical or orbital drilling, such as in rotary ultrasonic helical machining, to create high-quality holes in composite materials. By lowering heat accumulation and reducing delamination and fraying of the fibers, this innovative technique can increase the quality and precision of the holes [22]. There are many drilling processes apart from the conventional ones, in order to improve the quality of the final product. A scientific investigation into the use of rotary ultrasonic helical machining (RUHM), illustrated in Figure 8, for drilling small-diameter holes in carbon fiber reinforced plastics is presented by Geng et al. [22]. The study investigates the impact of different process factors on drilling load and hole quality using an experimental methodology. Spindle speed, feed rate, and ultrasonic power are some of the process variables that were examined. The experimental findings demonstrated that as spindle speed and feed rate increased, the drilling loads (thrust force and torque) also increased. In contrast to the spindle speed and feed rate, the ultrasonic power had more substantial impact on the drilling load. It was also concluded that higher ultrasonic power produced holes with smoother surfaces, less diameter deviations, and better roundness. The study sheds light on the mechanics of RUHM, including how helical motion and ultrasonic vibrations affect surface quality and material removal. In addition, the study revealed that helical drilling required less drilling torque and force than conventional drilling. This is explained, because the helical drilling process distributes the cutting pressures more equally, resulting in lower deformation and damage of the CFRP workpiece. Also, the helical drilling method decreased delamination, a problem that frequently arises while drilling CFRP. The authors also looked at how the shape of the tool affected drilling and discovered that the tool generated better holes with reduced hole diameter variation and increased roundness because of its sharper cutting edge and smaller point angle [22].

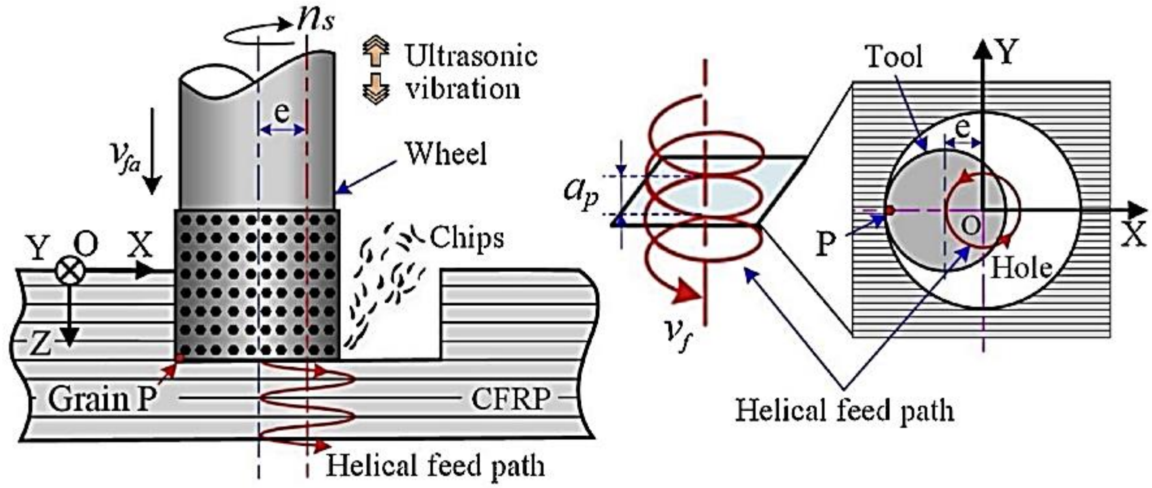

Figure 8. Rotary Ultrasonic Helical Machining (RUHM) (vf – helical speed; ap – helical revolution; e – radius of helical feed path; ns – spindle speed; vfa – axial feed speed of tool) [22].

Another technique, hybrid oscillatory orbital process, for drilling composite materials is covered by Sultana et al. [23]. To lessen delamination and enhance hole quality in composites, the authors suggest a hybrid oscillatory orbital process (HOOP), illustrated in Figure 9, which combines oscillation with orbital motion. The study examines how different drilling parameters affect the performance and hole quality with the HOOP technique. On composite made of carbon/epoxy, studies were carried out utilizing super abrasive diamond tools. To assess how well the HOOP procedure worked, it was compared with conventional drilling techniques. According to the study's findings, the HOOP procedure, as opposed to conventional drilling, enhances hole quality and lessens delamination. The authors noted that the use of oscillation and orbital motion minimizes the tool and workpiece's surface area in contact, reducing heat generation and friction. In turn, this causes less delamination and better hole quality. The study also revealed that the performance of the HOOP process is significantly influenced by the spindle speed, feed rate, oscillation amplitude, and oscillation frequency. The authors noted that increasing feed rate and spindle speed produced a greater cutting force and better hole quality. Nevertheless, using a too high cutting force might shorten the life of tools, causing tool wear. The authors also observed that boosting oscillation's amplitude and frequency decreased delamination and enhanced hole quality. The work reveals that drilling composites with super abrasive diamond tools utilizing the hybrid oscillatory orbital approach is successful. Comparing the HOOP procedure to conventional drilling techniques, the former increases hole quality and lowers delamination. The study emphasis how crucial it is to optimize drilling parameters including spindle speed, feed rate, oscillation amplitude, and frequency to get the best outcomes. The HOOP process could help to improve the efficiency and quality of composite drilling, which could lead to significant costs savings and improved performance. Overall, the drilling process, such helical and orbital drilling offers significant advantages over conventional drilling in composite materials, including improved hole quality, accuracy, and increased efficiency [23].

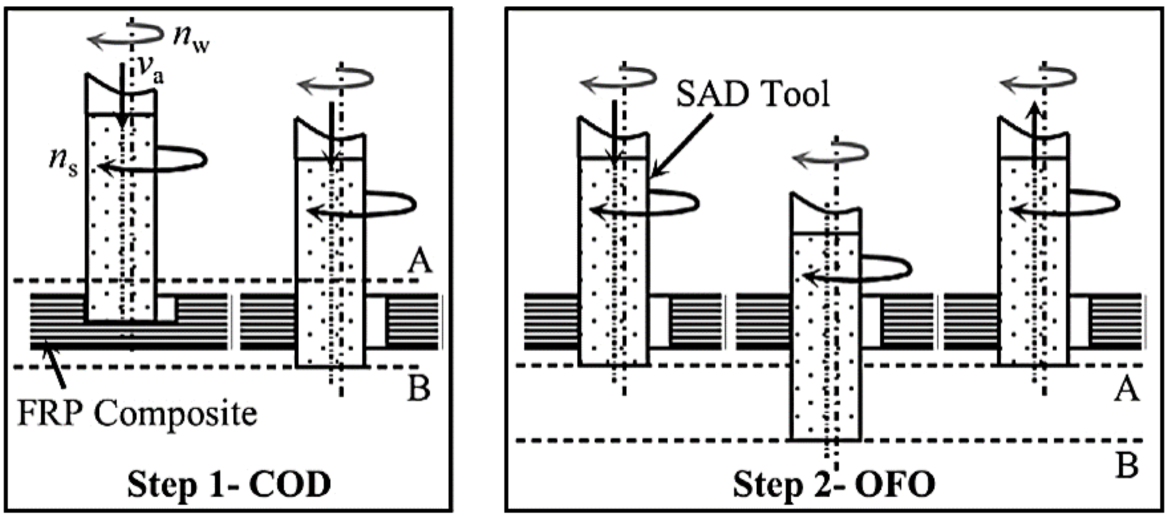

Figure 9. Oscillatory Orbital Drilling (OOD) (ns – rotational speed; va – axial feed rate; nw – orbital rotational speed) [23].

2.3. Drilling Tool Geometry and Materials

Depending on the material being drilled, several types of tool materials, such as high-speed steel (HSS), cemented or tungsten carbides, or polycrystalline diamond (PCD), may be selected [1]. The suggested tool materials for drilling composites and aluminum alloys are cemented and tungsten carbides due to their good compromise between hardness, toughness, and wear resistance compared to HSS, even at high temperatures, as detailed by Aamir et al. [24]. As a result, most experimental research and studies of CFRP/AA laminates in the literature were carried out using tools made of cemented or tungsten carbide [24], [25].

The choice of tool material and coating is crucial for achieving high-quality drilled holes in aerospace industry applications that involve drilling CFRP/AA laminates or FML composites. However, the selection of an appropriate drill bit geometry also plays a vital role in the drilling process's success, as it impacts hole surface quality, delamination, and tool performance [1]. There are several cutting tool morphologies available for drilling operations, as illustrated in Figure 10, but conventional twist drills are commonly used, given their relatively broad availability, for instance [26]. Special core drills (Figure 10g) are made especially for specialized applications or materials and may have unique features or specifications to meet those particular requirements. In contrast, core drills (Figure 10f) are general-purpose drilling tools used to create cylindrical holes in a variety of materials [26].

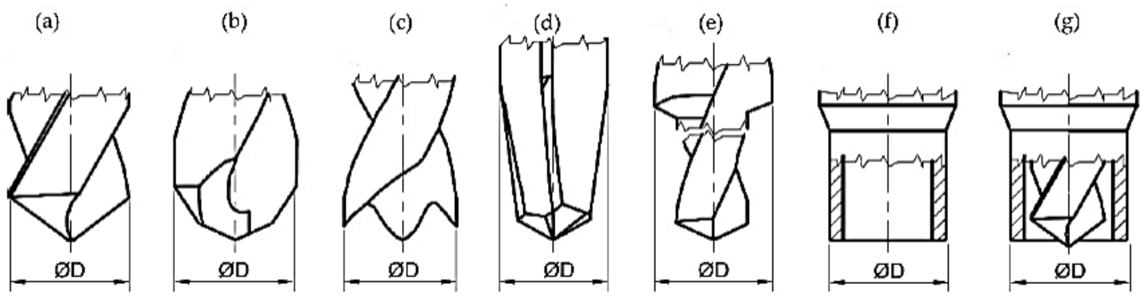

Figure 10. Drilling tools geometries: (a) conventional twist drill; (b) double point angle twist drill; (c) brad and spur drill; (d) dagger drill; (e) step drill; (f) core drill and (g) special core drill [26].

The comparison of the performance of a typical twist drill and a step drill was conducted by Brinksmeier et al. [27], focusing on the impact of tool morphology on the deviation of the drilled-hole diameter when drilling CFRP/AlCuMg2 laminates of various thickness and cutting speed. Both of the drills utilized in the investigation had comparable geometry, including uncoated carbide tools with a 130º point angle and a 30º helix angle. As compared to diameter deviations observed after drilling with a traditional twist drill, it was discovered that the step drill caused a better distribution of the mechanical load on the cutting edges. The drill bit's point angle has an impact on the cutting forces and chip formation during drilling. The authors discovered that, in comparison to a greater point angle (130º), a smaller point angle (90º) led to a bigger variation of the drilled hole diameter. The variance in the diameter of the drilled hole is also influenced by the drill bit's helix angle. According to the authors, a larger helix angle decreases cutting forces and enhances chip evacuation, which lowers the chance of deflection and enhances hole diameter accuracy. Soo et al. [28] used diamond-coated tungsten carbide drills with double point angles (130/60º and 140/180º) to drill CFRP/AA7010-T451 laminates and examined the effects of the double cone morphology on thrust force and hole quality. With the cutting parameters used in the investigation, it was found that the double cone drill was ineffective for drilling the multi-material in dry circumstances. The early failure of the drill was attributed by the authors to inadequate chip evacuation and consequent material adhesion. Instead, the flat point drill, according to the authors, generated holes with high diameter precision and a consistent metal exit burr. Zhang et al. [17] examined the impact of the brad and spur drill on cutting forces, surface roughness, and hole accuracy. It was concluded that this morphology had a better performance than the typical twist drill. Particularly, the surface roughness in the CFRP layer was improved by the brad and spur-like drill, which also lowered thrust forces. The average diameter roughness variation from nominal value varied from 14 µm for the twist drill to 5 µm for the brad and spur-like drill, which further encouraged higher hole precision. The greater self-centering ability of this tool's morphology, as well as the short chisel edge's more effective contribution to the decrease in cutting resistance and the expansion of the heat dissipation, were the explanations for this favorable outcome [17], [27], [28].

2.4. CVD Diamond Coatings

Diamond is considered the most wear-resistant material given is excellent compromise between hardness, toughness, and thermal conductivity. Applications include cutting tools, radiation detectors, optical windows, laser diode heat sinks, and electronic thermal management substrates. Except for highly specific applications, natural diamond is too expensive for the majority of these items. Yet chemical vapor deposition (CVD) diamond technology is quickly emerging as a way to generate diamond coatings and free-standing diamond components for several applications at an affordable cost. Many applications are already being produced commercially and are growing quickly [29]. Regarding the topic of this project, CVD diamond coated tools will be used for the drilling process.

As the name suggests, chemical vapor deposition (CVD) entails a gas-phase chemical reaction that takes place above a solid surface and results in deposition on that surface. All CVD methods for creating diamond films need a way to activate gas-phase precursor molecules that contain carbon. This often entails thermal activation (such as hot filaments), plasma activation (such as direct current (DC), radio frequency (RF), or microwave waves), or utilization of combustion flame (such as oxyacetylene or plasma torches). Before initializing the process, to provide a clean surface free of impurities, the substrate that has to be coated is firstly cleaned and prepared by polishing and/or etching. The following stage is creating a gas combination that will be used to deposit the diamond coating. This mixture will include a hydrocarbon gas (like methane or acetylene) and a carrier gas (like hydrogen). The gas flow is halted after the necessary diamond coating thickness has been reached, and the substrate is then allowed to cool gradually. To increase the quality and characteristics of the coating, the diamond-coated substrate may also go through post-treatment procedures including polishing or annealing [30]–[33].

Since carbon fibers may have an abrasive impact on the tool's cutting surfaces during the drilling operations of carbon fiber reinforced polymers (CFRP), traditional cutting tools soon lose their sharpness. Because of the significant loads on the cutting edge in the lack of coolant, very strict restrictions are placed on the diamond coating (DC) [34]. The results of experiments for cutting the edges of carbon fiber polymers are provided by Tsao et al. [35] and Duboust et al. [36], and it is clear from these findings that a diamond-coated tool has a greater wear resistance than an uncoated conventional tool. However, as the feed rate of the diamond-coated device rises, CFRP delamination takes place. While drilling CFRP with several drills, including a DC drill, it was discovered that a diamond-coated drill's cutting length is 80% longer than a conventional tool. Diamond-coated tools offer superior quality and a longer service life. High geometric flexibility and record breaking diamond coatings characteristics are combined in tools with CVD diamond coatings. Low coefficient of friction, good thermal conductivity, high hardness, and wear resistance all help prolong the life of tools by reducing heating and cutting forces. Nonetheless, the diamond coatings' service life may be shortened by poor adhesion [34].

2.5. Tool Wear

One of the major problems that can have a considerable impact on the quality of drilled holes, production costs, and drilling efficiency of multi-material laminates, notably CFRP/Al hybrid composites, is tool wear. In order to identify the primary wear mechanisms happening during drilling operations – which are responsible for the reduction in tool life and have the potential to cause catastrophic tool failure – it is crucial to continuously monitor these defects [1]. Several forms of wear can be noticed on the cutting tool after drilling both composites and metallic materials, as seen in Figure 11 [1]. The two most frequently employed primary processes of tool wear are flank wear and, to a lesser extent, crater wear. The friction between the tool's flank and the wall of the drilled hole causes flank wear, whereas the friction between the chips and the tool's rake face causes crater wear. More precisely, abrasive wear and tool edge chipping are the most common wear mechanisms brought on by drilling CFRPs. In contrast, the primary wear processes impacting cutting tools while drilling aluminum alloys are diffusion and adhesion wear (BUE – built up edge). BUE is a structure that develops irregularly and unstably when material is successively deposited on the tool-chip contact [37]. At very low cutting speeds (less than 25 m/min), this tool wear occurs in the tool rake face and functions as a fresh cutting edge, however chemical action diffusion is preferred under harsh cutting circumstances (more than 300 m/min) because the temperature rises [38]. Moreover, it appears that the wear processes present in the drilling of CFRP/AA laminates are a mixture of related wear phenomena unique to the drilling of each material independently, namely abrasive wear and adhesion wear [39].

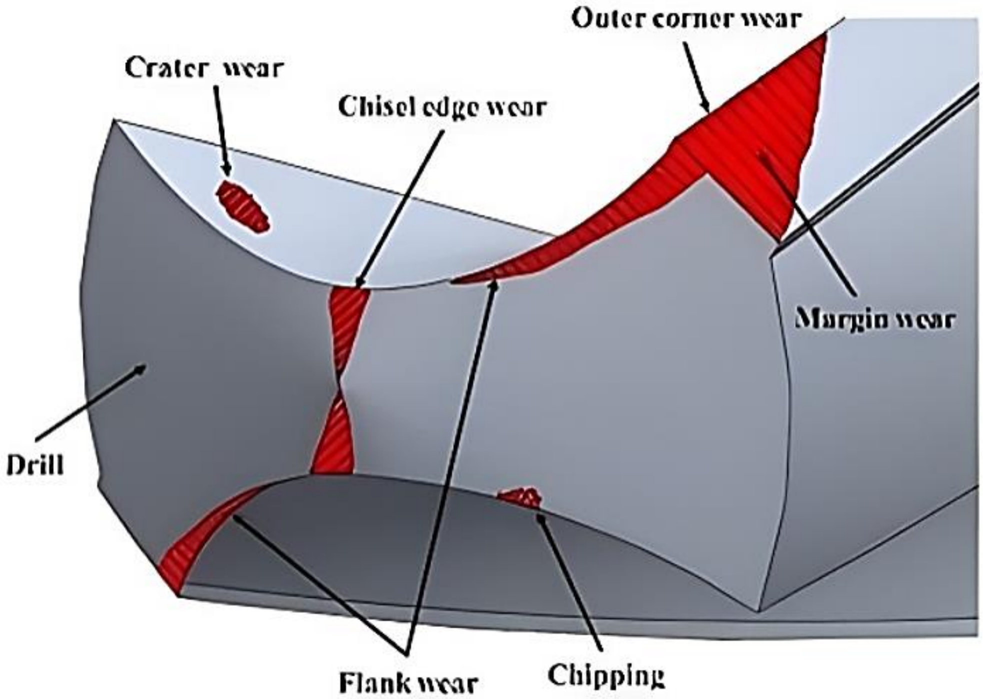

Figure 11. Different types of tool wear illustrated in a drill tool [1].

The stages of tool wear can be divided into three regimes: I, II, and III, as shown in Figure 12. In regime I, the wear of the cutting edge starts at a rapid rate. This is brought on by the cutting edge's weak regions and sharp corners breaking down initially. Because of the high stresses produced by the cutting forces, this regime is characterized by a rapid rise in wear rate, and the cutting edge may show chipping or breaking. Regime I often lasts for a short while before giving way the next stage. In regime II, the cutting edge is stabilized, and the tool material is gradually and uniformly removed as the wear progresses. This regime reflects the usable life of the cutting edge, and wear in this regime is predictable and has been described analytically. The cutting edge retains its geometry and cutting performance despite the comparatively low wear rate. However, ultimately the geometry of the cutting edge will become dysfunctional, causing rapid or catastrophic wear to begin. In regime III, the cutting edge degrades quickly, and the wear rate quickly rises. A dramatic decline in cutting performance and possible tool unusability define this phase. In regime III, the cutting edge may show significant fractures or breaking due to fracture wear (chipping) or delamination wear. The early disintegration of the cutting edge (regime I), the usable life of the cutting edge (regime II), and the fast degradation of the cutting edge (regime III) may all be used to characterize the stages of tool wear [40].

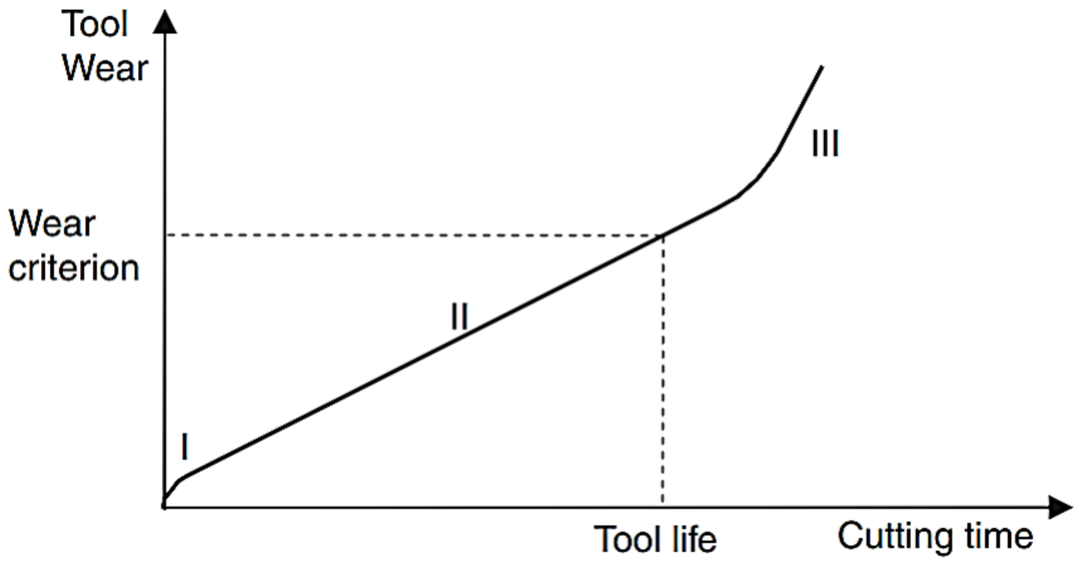

Figure 12. Stages of tool wear: Regime I (early disintegration of the cutting edge); regime II (usable life of the cutting edge); regime III (fast degradation of the cutting edge) [40].

Materials with a diamond film coating placed on a tungsten carbide substrate are known as diamond-coated carbides. Unfortunately, due to significant residual stresses in the film and substrate created during the CVD process, the diamond film’s adherence to the substrate is troublesome under actual cutting circumstances. High thermal residual strains that are created in the coating and substrate after cooling are also a result of differences in the thermal expansion coefficients of the diamond layer and the substrate. When working with fiber reinforced composites, two wear mechanisms – uniform abrasion and fracture-controlled delamination of the diamond film – have an impact on the wear characteristics of diamond-coated tools. When the film adhesion is adequate, the diamond-coated tools wear by uniformly abrading the diamond film. This causes the diamond film to thin and eventually to fracture, causing the film to be removed from the substrate locally. Nevertheless, when the film adhesion is insufficient or when the residual stress conditions in the film are unfavorable, localized fracture begins at the cutting edge’s nose in the form of radial crack, which causes the diamond film to delaminate widely. The amount of stresses in the diamond film affects whether or not cracks may form, and the edge geometry, specifically the ratio of film thickness to nose radius, controls whether or not a change from compressive to tensile stresses takes place [40]. This has an impact on how the diamond-coated tools wear.

Regarding PCD (polycrystalline diamond) tools, their wear is defined by a number of distinct parameters. Due to microchipping, initially weakly held particles may be lost from the cutting edge. After this, consistent flank wear caused by abrasion is frequently seen. The rake face becomes rounded as a result of this wear, and the wear land on the rake face is narrower than on the clearing face. On the flank face, shallow abrasive grooves that run in the direction of cutting may also occur. Similar to the wear mechanism seen when using tungsten carbides, consistent abrasion wear is the predominant wear mechanism when machining homogeneous composites at low feed rates. Microchipping and fracture, on the other hand, become the main wear mechanisms as the work material becomes less homogenous or when employing high feed rates, particularly in interrupted cutting. The cutting edge may sustain serious damage from chipping that occurs at a scale far bigger than the diamond grain size. In the long term, coarse PCD grades often outperform fine ones because they offer a lower rate of flank wear [40]. On the other hand, fine grain PCD is less vulnerable to cutting edge microchipping than coarse grain PCD. The cobalt binder that held the diamond grains together is firstly removed from between the grains, which makes it easier for the diamond grains to come loose from the cutting edge [40].

A diamond coated carbide drill was used in the research of Fernández-Pérez et al. [41] to perform an experimental investigation to look into the wear processes and delamination during CFRP drilling. The authors discovered that tool wear increased with both thrust force and torque, and that the coating's adhesion to the substrate is essential for delaying tool wear. The authors discovered that the wear mechanism involved the combination of two events: diamond coating detachment followed by severe abrasion of the carbide substrate. After about 4 minutes, the abrasive wear that was caused by the localized diamond coating layer detachments started to lessen the edge's sharpness. With minor changes to the cutting geometry, the quantity of material lost from the tool's edge in the form of flank wear increased as the total length of cutting time increased. The increase in thrust forces and subsequent delamination can be attributed to the favoring of abrasive wear to higher cutting speeds. The major wear process was found to be significant abrasion on the exposed carbide substrate and coating separation from the cutting edge's rake surface. In order to postpone tool wear and extend tool life, the coating layer's excellent adhesion to the carbide is essential. The delamination near the hole's exit is the quality criterion that determines the tool life. The beginning of flank wear is primarily responsible for the emerge of the machining induced damage. Hrechuck et al. [42] presents a scientific analysis of the tool wear during the drilling of CFRP composites using cemented carbide drills. They used a drilling machine with a fixed spindle speed of 10000 r.p.m. and various drilling parameters. An optical microscope and scanning electron microscope were used to measure the tool wear (SEM). The results of the trials demonstrate that the drilling parameters have an impact on tool wear. The feed rate, point angle, and drilling speed were shown to have the greatest effects on tool wear. Because of the rise in cutting power and temperature, higher feed rates are associated with greater tool wear. A smaller point angle results in less tool wear, as well as representing a decrease of cutting force and temperature. Montoya et al. [43] presents a scientific analysis of the performance of coated and uncoated carbide tools in drilling thick CFRP/AA laminates. According to the results, coated carbide tools had lower tool wear than the uncoated carbide tool. The tool that had been coated had signs of adhesive wear, but the uncoated tool had signs of abrasive wear. The coating on the carbide tool contributed to a decrease in adhesive wear and extension of tool life. The study also determined that the cutting speed and feed rate had a big impact on tool wear. When the feed rate and cutting speed increase, the tool wear also increases. The authors associated this to an increase in temperature during drilling, which increased tool wear [41]–[43].

2.6. Chip Formation and Removal Mechanisms

Chip removal concerns may be regarded as one of the major difficulties in drilling CFRP/AA laminates, as they have an impact on the drilled hole wall surface. In fact, while drilling CFRP/AA laminates, the formation of non-fragmented chips in the aluminum component relies on the rolling up of these chips around the drill bit, which if inappropriate may compromise the geometrical and dimensional properties of the composite hole. During the single shot drilling operation, the cutting tool has an influence on the size and form of chips [1]. When using single shot drilling, the cutting conditions for metal and composite are very different in terms of chip production [44]. While the development of continuous chips is preferred when drilling composite materials because powder-like chips erode the surface quality, the formation of fragmented metal chips is necessary to ease their evacuation and prevent the worsening of the drilled-hole surface roughness. Nevertheless, multilayer CFRP are made of layers that produce dust-type chips, making it difficult to produce such composite chips. Moreover, polymer composite chips are continuous at low feeds, matching cutting circumstances that also produce lengthy, non-fragmented chips while drilling metals [45].

During the orthogonal machining of unidirectional CFRP there are several types of chip formation, as illustrated in Figure 13. When machining at 0º fiber orientation and positive rake angles, Delamination Type Chip Formation (Type I) occurs. At the fiber-matrix interface, the tool starts a fracture that eventually develops into a small chip section [40]. Repeating this technique yields a succession of tiny chips with machined surfaces that show fibers partially obstructed in the epoxy resin matrix. When machining at 0º fiber orientation and 0º or negative rake angles, Fiber Buckling Type of Chip Formation (Type II) occurs. The fibers bend as a result of compressive force applied in their direction. The fibers subsequently break apart into tiny discontinuous pieces in a direction perpendicular to their length. By machining fiber orientations larger than 0º and less than 90º, as well as for all rake angles, Fiber Cutting Type Chip Formation (Type III) occurs. The mechanism of chip generation consists of interlaminar shear fracture along the fiber-matrix interface during cutting tool advance, followed by fracture from compression-induced shear across the fiber axis. Depending on how much interlaminar shear occurs, this kind of chip may be continuous or discontinuous. Fiber Splitting Type Chip Formation (Type IV) occurs when cutting with a 90º fiber orientation and a negative rake angle. The fibers split and fracture at the fiber-matrix contact as the tool slides in the direction of the fibers. The outcome consists in small and discontinuous chips. Finally, Fiber Fracture Type Chip Formation (Type V) happens while cutting with positive rake angles and fiber orientation over than 90º. The tool creates a high degree of fiber damage by causing the fibers to fracture perpendicular to their length, producing a succession of tiny chips with a machined surface [40].

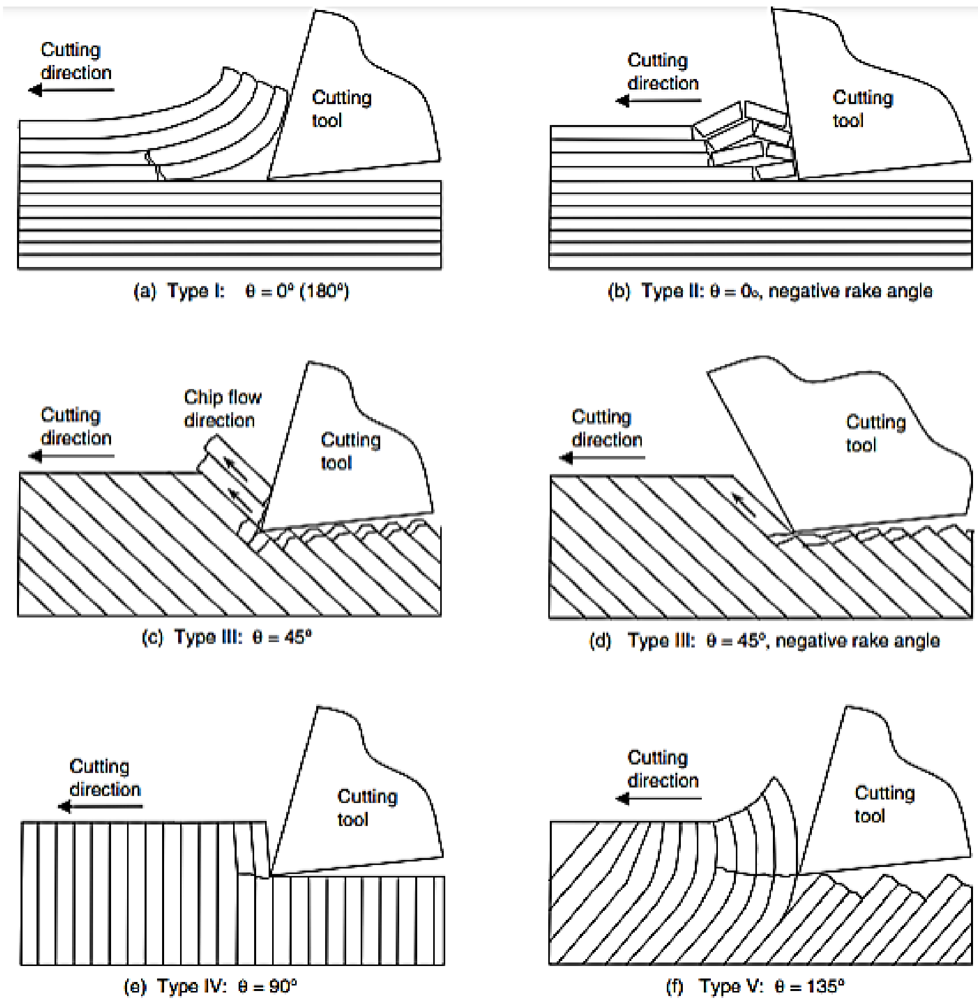

Figure 13. Cutting mechanisms in the orthogonal machining of CFRP: (a) Type I – Delamination Type Chip Formation; (b) Type II – Fiber Buckling Type Chip Formation; (c) and (d) Type III – Fiber Cutting Type Chip Formation; (e) Type IV – Fiber Splitting Type Chip Formation; (f) Type V – Fiber Fracture Type Chip Formation [40].

The matrix material used in a composite can have a significant influence on the chip formation process during machining. The brittle fracture of the matrix and the fibers in thermoset matrix materials, which are more brittle than thermoplastics but stronger, lead to chips that are broken apart and powdery. The matrix's brittle fracture close to the tool tip is also noticeable. The ductile thermoplastic matrix, in contrast, uses plastic deformation to make continuous and curling chips. This is explained by the polymer's high degree of elongation under stress and the hydrocarbon chains sliding during cutting owing to the rise in temperature. Moreover, the cutting conditions can have an impact on chip morphology. Thermoset matrices crack early under conditions of high cutting speeds and low feed rates due to high strain rates, producing smaller chip segments. On the other hand, the high temperature created by machining causes the thermoplastic material to deform significantly, producing lengthy ribbon-like chips. In spite of this, for both thermoset and thermoplastic matrixes, low cutting speeds and high feed rates lead to larger chips [40].

The fiber material is another important parameter affecting chip formation. Glass fibers create chips that exhibit partial bending and breaking, which causes the fiber and matrix material to separate. On the other hand, carbon fibers create chips by sharp fracture with minimal distortion, leading to serrated fracture surfaces with individual facets angled toward the fiber axis. Moreover, CFRP is more prone to debonding during machining because of the self-lubricating properties of carbon and graphite fibers. In contrast, aramid fibers are more resilient than glass and carbon fibers, which enables them to bend significantly in front of the moving cutting edge. As a result, aramid fibers are very difficult to cut and produce twisted and tangled fiber chips [40].

The development of chips when drilling a CFRP/AA7075-T6 composite is one of the major factors examined by Hassan et al. [46]. The chip production mechanism altered as the drilling parameters and twist drill geometry varied, according to the investigation of chip formation using high-speed cameras. The study found that a ductile mode of deformation occurred while drilling with a lower point angle and a higher cutting speed because the resulting chips were smaller and tightly coiled. In contrast, larger and more fragmented chips were produced while drilling with wider point angle and slower cutting speed, indicating a brittle mode of deformation. This observation is consistent with the literature on the mechanism of chip production, where it is known that the chip formation process can be strongly impacted by the cutting speed and tool geometry. Also, it was noted that the CFRP layer's delamination had an impact on the mechanism of chip generation, resulting in irregular chips and poor hole quality. The ideal spindle speed and feed rate for chip production was found to be 2600 rev/min and 0.05 mm/rev, respectively, resulting in the generation of short, fractured chips and tight helical chips. This combination facilitates drilling's evacuation process and, as a result, produces improved surface finish. Sridhar et al. [47] also investigated the chips in the drilling of CFRP/AA2024. In contrast to those formed while drilling aluminum alone, the study found that the chips produced during the drilling of multi-material carbon fiber reinforced aluminum laminates were more discontinuous and irregular. This shows that the chip formation mechanism is significantly impacted by the addition of carbon fibers to aluminum. The fact that the chips left behind when drilling CFRP are irregular and discontinuous suggests that the material is more brittle and breaks more easily. On the other hand, the chips that were produced when drilling AA2024 were more continuous and constant. This is explained by the fact that aluminum is ductile, which enables the creation of longer, more continuous chips during drilling. Bolar et al. [48] investigates the drilling and helical milling process for hole-making in CFRP/AA2024. It was discovered that a number of variables, including the tool geometry, cutting speed, feed rate, and angle of entry, had an impact on the chip production process during drilling and helical milling. The analysis of chip morphology revealed that drilling and helical milling produce different types of chips, as verified in Figure 14. The chips generated during drilling were irregular and discontinuous, with a propensity to build up on the cutting edge of the tool. With multi-material carbon reinforced aluminum laminates, this means that drilling is a less effective procedure for creating holes, and the built-up edge formation can cause tool wear and a decline in the quality of the drilled holes. On the other hand, the chips generated via helical milling had a better surface finish and were more regular and continuous. In comparison to drilling, the study indicated that helical milling generated better-quality holes with less delamination and fiber pull-out. The uniform and continuous quality of the chips created during helical milling can be associated to the contact of the cutting edge with the material and the more gradual penetration of the tool in the material [46]–[48].

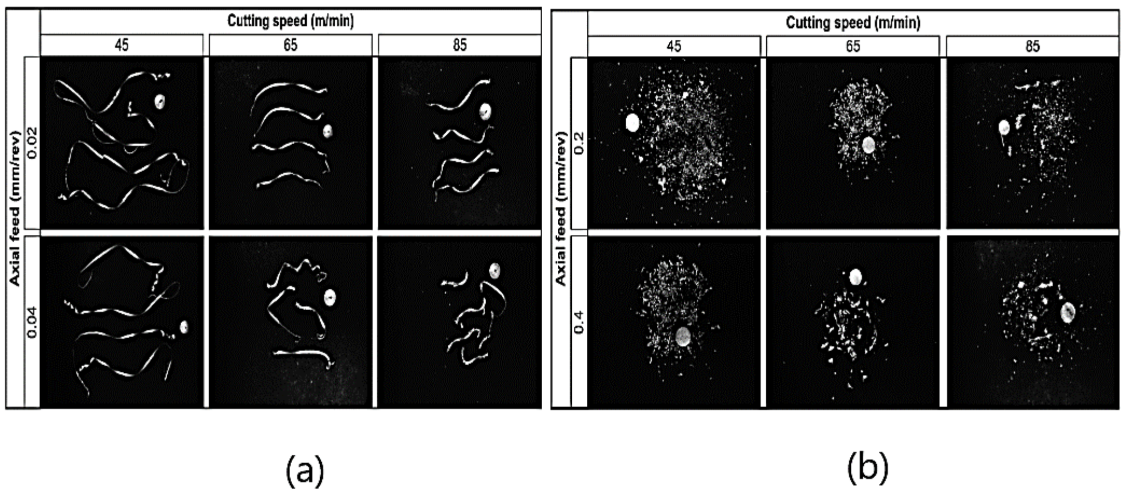

Figure 14. Comparison of chips obtained from (a) one-shot drilling process and (b) helical milling process [48].

2.7. Delamination and Fracture Modes

Delamination is characterized as a failure of the interply that takes place during the drilling of composite laminates. It is widely acknowledged as the primary mechanism of failure when drilling composite materials. It also poses a serious problem since it significantly lowers the material's fatigue strength, which can worsen the long-term performance of FRPs. When the thrust force is greater than the material's interlaminar bond strength, drilling-induced damage manifests as splitting between two adjacent layers [1]. As explained in Figure 15, this phenomenon may be seen at both the machined-hole entry (peel-up delamination,), Figure 15a, and exit (push-out delamination), Figure 15b [49]. The plies separate from one another and form a peel-up delamination zone around the drilled-hole entry circumference when the drill penetrates the top surface of the laminate. This is caused by the contact between the composite material and the cutting edges of the drill, which creates a peeling force acting in the axial direction through the slope of the drill flutes. The friction between the drill and the workpiece material, considering the tool shape, might affect the peeling force indicated before. The uncut plies beneath the cutting tool begin to thin down as the drill approaches the drilled composite's exit side, which causes them to start deforming and causing push-out delamination. Due to the drill's larger thrust force and decreased inter-ply bonding strength, push-out delamination has been reported to be more severe than peel-up delamination in many applications [49]. The process of delamination in drilling hybrid composite laminates is the same as drilling single FRPs [50]. The choice of the stacking sequence will only have an impact on how severe the delamination is. Since the bottom-supporting metal component serves as a backup plate and inhibits the deformation of the higher composite part, drilling from a laminate composite part to a metal part results in less push-out delamination than drilling from a metal to a FRP part. Furthermore, peel-up delamination is enhanced in this structure by metal chip evacuation [51].

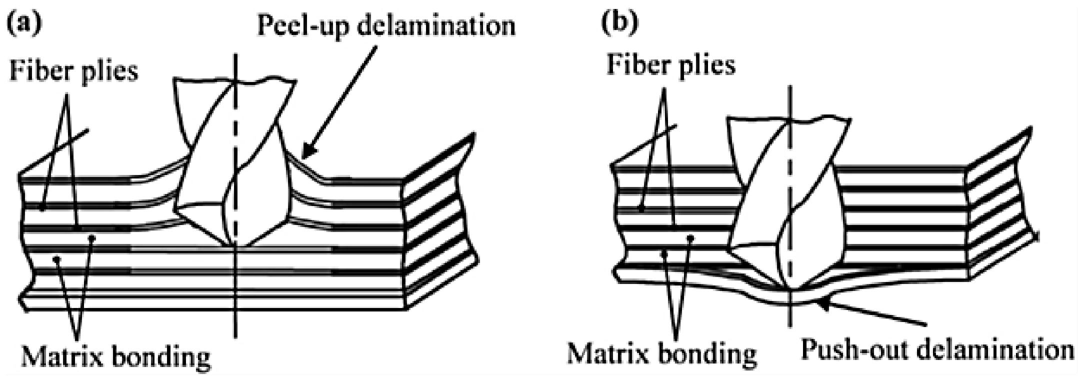

Figure 15. Schematic of delamination in composite materials: (a) Peel-up (entry) delamination and (b) push-out (exit) delamination [49].

The critical thrust force at which push-out delamination occurs is known as the critical thrust force. This value was determined using the linear elastic fracture mechanics and the conventional laminate plate theory. The first critical thrust force in twist drills model was created by Hon-Cheng and Dharan [52] and considered mode I fracture, isotropic material, a single point thrust load, and a circular delaminated region. Although later models have improved it, this model is still fairly conservative. According to Lachaud et al. [53], the material is orthotropic, and the thrust power is focused on the hole's center. For unidirectional composite materials, an elliptical delaminated region was taken into consideration by Zhang et al [54]. Rahmé et al. [55] split the stress into two zones, while Piquet et al. [56] defined uniformly distributed pressure. Mixed-mode I + II delamination was taken into consideration by Girot et al. [57], while thermo-mechanical loads were taken into account by Massoom and Kishawy [58]. The models that used mixed-mode I + II delamination produce the most accurate findings. Therefore, more testing is necessary to determine the mixed-mode I + II critical fracture energy than to just determine the critical fracture energy for mode I. Among models that take pure mode I fracture into consideration, Piquet et al. [56]'s model appears to be the most accurate.

The degree of delamination or damage at the entry and exit of a drilled hole in the composite laminate is measured by the delamination factor. This is described as the ratio of the diameter of the drilled hole to the largest diameter of the delamination region. The proportion representing the delamination factor can vary from 0% (no delamination) to 100% (complete delamination) [1]. Many methods have been developed in recent years to evaluate the degree of drilling-induced delamination. The delamination factor, which may be described in two dimensions (2D), and three dimensions (3D) is the basis for all of these models. The first study to propose a delamination parameter was by Chen [59], where a one-dimensional feature measured on the drilled hole was used. This conventional delamination factor, designated by F_d, is calculated as the difference between the nominal diameter of the drilled hole (D_{nom}) and the maximum diameter (D_{max}) of the observed delamination zone (Figure 16). Based on the computation of the ratio of the area (A_{nom}) linked to the maximum diameter (D_{max}) of the delamination zone to the nominal area of the drilled hole, Faraz et al. [60] developed a 2D delamination factor, designed by F_a. Nevertheless, since only the size of the delamination zone is considered, this indication ignores the role that fracture length plays in drilling-induced delamination. A 3D delamination component was more recently suggested by Xu et al. [49] to account for the interlaminar failure seen inside the FRP. The arithmetic mean of the 2D delamination factor, F_a, for each delaminated layer served as the basis for calculating this factor. F_d continues to be the most often used delamination factor for determining the degree of drilling-induced delamination because it is simpler to apply, even though all of these more sophisticated delamination factors can properly estimate the true extent of delamination damage. The delamination factors, F_d (conventional delamination factor), F_a (two-dimensional delamination factor), F_{dmin} (minimum delamination factor), F_{da} (adjusted delamination factor), F_{ed} (equivalent delamination factor), and F_v (three-dimensional delamination factor) are expressed in Table 1.

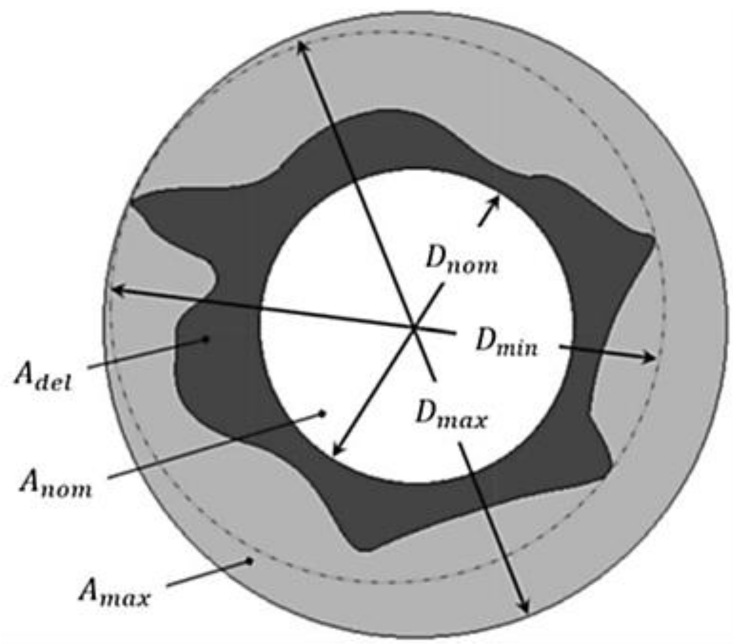

Figure 16. Graphical illustration of several delamination factor parameters [49].

Table 1. Distinct delamination factors and their analytical expression (adapted from [49]).

Delamination Factor	Expression
$\boldsymbol{F_d}$ (conventional delamination factor)	$F_d = \frac{D_{max}}{D_{nom}}$
$\boldsymbol{F_a}$ (two-dimensional delamination factor)	$F_a = \frac{A_{del}}{A_{nom}}$
$\boldsymbol{F_{dmin}}$ (minimum delamination factor)	$F_{dmin} = \frac{D_{min}}{D_{nom}}$
$\boldsymbol{F_{da}}$ (adjusted delamination factor)	$F_{da} = F_{da} + \frac{A_{del}}{A_{max} - A_{nom}} (F_d^2 - F_d)$
$\boldsymbol{F_{ed}}$ (equivalent delamination factor)	$F_{ed} = \frac{1}{D_{nom}} \sqrt{\frac{4(A_{del} + A_{nom})}{\pi}}$
$\boldsymbol{F_v}$ (three-dimensional delamination factor)	$F_v = \frac{1}{p} \sum_{k=1}^{p} \frac{A_{del}^k}{A_{nom}}$

Several studies were carried out in order prevent delamination damage. In the study of John et al. [61], using a backing material that supports the composite material being drilled is one of the most popular methods for reducing delamination damage. The backing material, which is positioned behind the workpiece to offer support and avoid delamination, can be either a solid or a liquid. Using specialized drill bits, such as stepped or countersink drill bits, is another method for reducing delamination. These drill bits can aid in minimizing the force applied to the workpiece and lessen the possibility of delamination. It was also discussed the usage of laser drilling and ultrasonically assisted drilling, both of which have special drilling techniques that can lessen delamination damage. Additionally, the necessity of optimizing drilling parameters, such as the cutting speed, feed rate, and drill bit shape was also examined. By minimizing the force applied to the workpiece, these parameters may be optimized to lower the likelihood of delamination [61].

Several non-destructive measuring techniques have been developed to track the dimensions of delamination, such as its size, shape, and position. These techniques often incorporate image capture hardware and image processing software. The delamination caused by drilling must be quantified using these dimensional properties. Optical microscopy, digital scanning [62], ultrasonic C-scan [63], [64], and X-ray are the non-destructive approaches used by many studies to assess delamination, as detailed in various review publications [1].

It is important to establish the material's fracture energy in relation to its delamination by experimental testing, based on the fracture modes, in order to compute the critical thrust force. These modes correspond to the kinds of relative displacement that loaded cracked surfaces experience. There are three fracture modes and depending on the area of the crack being studied, they can either occur alone or together. While the crack is forming perpendicularly to the fracture plane, Mode I takes place (tensile stress). In Mode II, the fracture surfaces glide against one another in opposing directions (sliding shear stress). The fracture planes experience lateral displacement in Mode III, but the stress is turning rather than sliding. In Figure 17 is presented these fracture modes occurring during peel-up and push-out delamination [65].

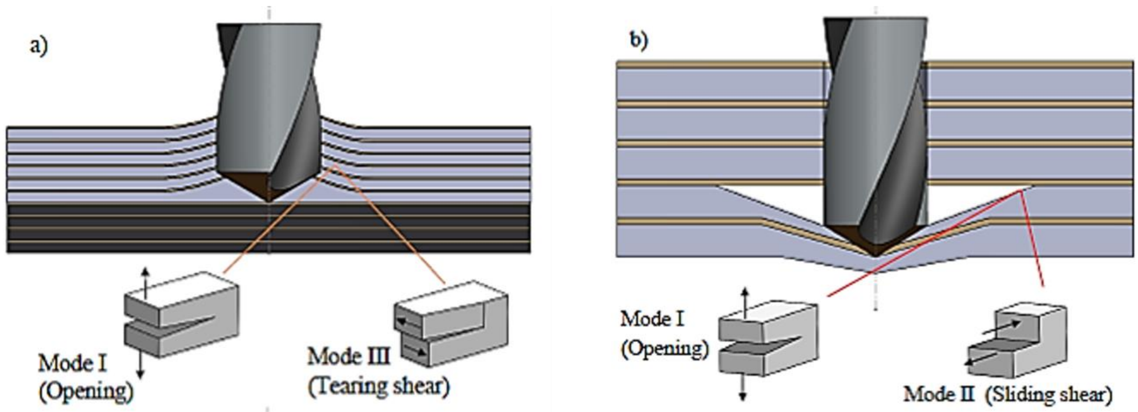

Figure 17. Fracture modes during (a) peel-up and (b) push-out delamination [66].

2.8. Burr

The geometrical defect known as a burr is present in several drilling operations and is visible as a raised portion at the entry and exit of the drilled hole, particularly in aluminum alloys [1]. The plastic deformation of the uncut material during drilling is the cause of the production of burrs, which are often greater near the exit of the hole than at the entry. Exit burrs are developed in the opposite side of the drill entrance and can impair the surface quality of the material. Moreover, the combination of greater stresses and reduced resistance in the workpiece material with a plastic deformation fracture leads to burr development. The plastic deformation is directly influenced by both high localized temperature and thrust force [67]. According to the characteristics of the workpiece material, drilling parameters, and cutting forces, two types of burrs, uniform (with or without drill caps) and crown, may be distinguished at the drilled aluminum plate, as explored by Devitte et al. [68] and shown in Figure 18.

Figure 18. Distinct types of burr formation: (a) uniform with drill cap; (b) uniform without drill cap; (c) crown-shaped burr [68].

Devitte et al. [68] used a Response Surface Methodology (RSM) to improve the drilling procedure for metal composite aeronautical structures. The study discovers that burr development is highly influenced by cutting speed, feed rate, and drill point angle. It was proposed that RSM may be used to find the best drilling settings to reduce burr development. Lee et al. [69] aimed to investigate the burr formation and tool wear characteristics during the drilling process of CFRP and its hybrid composites. Regarding the challenging task due to the anisotropic nature of the material, causing burr formation and tool wear, this study conducts drilling experiments on CFRP and its hybrid composites to investigate the effect of the hybridization of CFRP with other materials on burr formation and tool wear. According to the study's results, burr size grows with feed rate, drill point angle, and spindle speed. Burr formation is affected by the inclusion of additional materials in the composite structure because hybrid composites create more burrs than pure CFRP composites. In another study, Geier et al. [70] presents a novel approach to measure drilling-induced burr occurrence in CFRP composites using digital image processing (DIP). The technique entails utilizing a high-resolution camera to take pictures of the drilled hole and then processing those pictures with an image processing software. Based on the intensity gradient of the picture, the computer recognizes the presence of the burr and measures its height. The study's results demonstrate that the DIP approach can reliably forecast the development of burrs in CFRP composites. The study also demonstrates that burr creation is significantly influenced by high values of spindle speed and feed rate, going in accordance with the other studies. This technique (DIP) has the ability to reduce the cost and time associated with drilling process design and optimization of cutting parameters. The results of this study may have a strong impact on the creation of new drilling methods and the enhancement of current drilling procedures for CFRP composites [70]. The influence of fiber orientation on burr development during the drilling process is examined by Xu et al. [71]. The study discovered that the fiber orientation of the CFRP has a substantial impact on burr development, relation exemplified in Figure 19. It was also determined that the orientation of the fibers with respect to the drill axis affected burr size and shape. The burrs tended to be bigger and more asymmetrical when drilling perpendicularly to the fibers, as well as smaller and more symmetrical when drilling parallel to the fibers. The anisotropic character of the CFRP, which means that its properties change depending on the orientation of the fibers, is what the authors ascribe to this differential in burr development. Due to the strong interfacial interaction between the fibers and the matrix material, the drill finds increased resistance while drilling perpendicularly to the fibers. Larger burrs with asymmetrical forms may be developed as a result of this increased resistance. In contrast, because of the reduced interfacial interaction between the fibers and the matrix material, drilling parallel to the fibers represents less resistance, resulting in smaller and more symmetrical burrs [72]. The study of Xu et al. [71] also showed that burr development in fiber-reinforced composites might be influenced by the kind of PCD drill employed. The drill's geometry and coating when drilling perpendicular to the fibers, might affect burr size and morphology. Overall, the studies indicate that burr development is a frequent issue in drilling operations for metal composite and CFRP composites. They point out a number of variables, including cutting parameters, tool geometry, and material properties, that affect burr development. Nevertheless, the studies also suggest several techniques, such as response surface methodology, analytical models, and digital image processing, for improving drilling procedures and forecasting burr development [68]–[72].

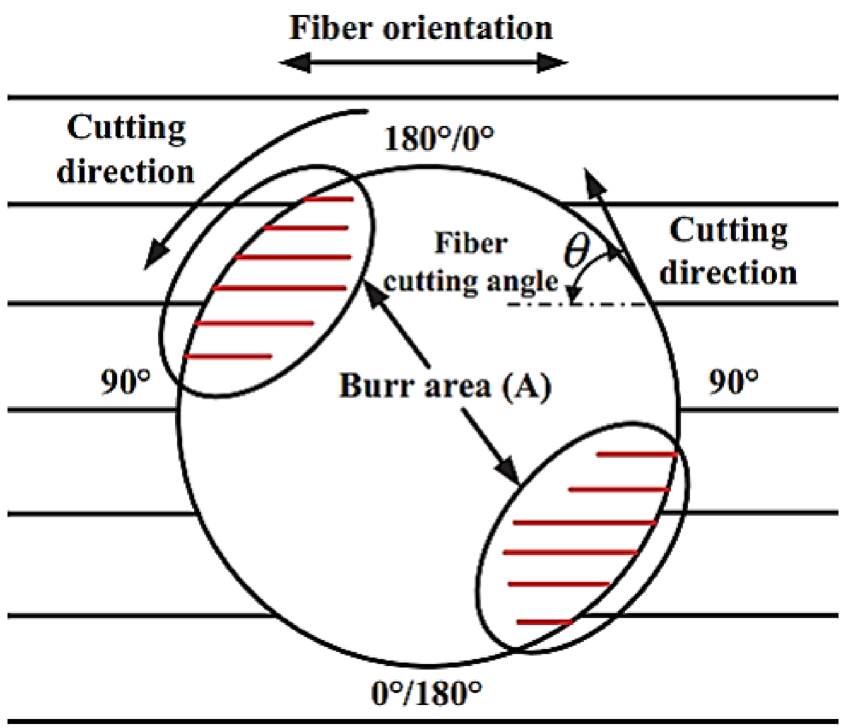

Figure 19. Relation between fiber cutting angle and burr area [71].

2.9. Hole Size and Surface Quality

While drilling multi-material laminates, dimensional problems are frequently observed. Due to the varied thermal and mechanical properties of metal alloys and composite materials, varying dimensional tolerances throughout the drilled hole may be seen. Additionally, the diameter of the entry layer of CFRP drilled hole remains larger than that of the metal part. This can be attributed to the detrimental abrasion of the CFRP hole wall caused by the unfavorable evacuation of metal chips during the drilling of multi-material laminates [1].

D'Orazio et al. [73] investigated the effect of tool wear on hole quality in drilling of CFRP and aluminum alloy AA7075 laminates, using two types of coated tools, Diamond-Like Carbon (DLC) and nanocomposite TiAlN. One of the study's key conclusions was that tool wear has a considerable impact on hole quality, especially in terms of hole size. The diameter of the holes decreases as the tools deteriorate, which may affect how well the parts fit and work. In terms of tool wear and hole quality, the authors concluded that the nanocomposite TiAlN coated tool performed better than the DLC coated tool, as shown in Figure 20, and also that the hole size in CFRP tends to be higher than in the aluminum alloy. The wear of the cutting tool, the material characteristics of the stacked material, and the drilling parameters are some of the reasons of the hole size issues in the drilling process, mostly caused by cutting tool wear [73].

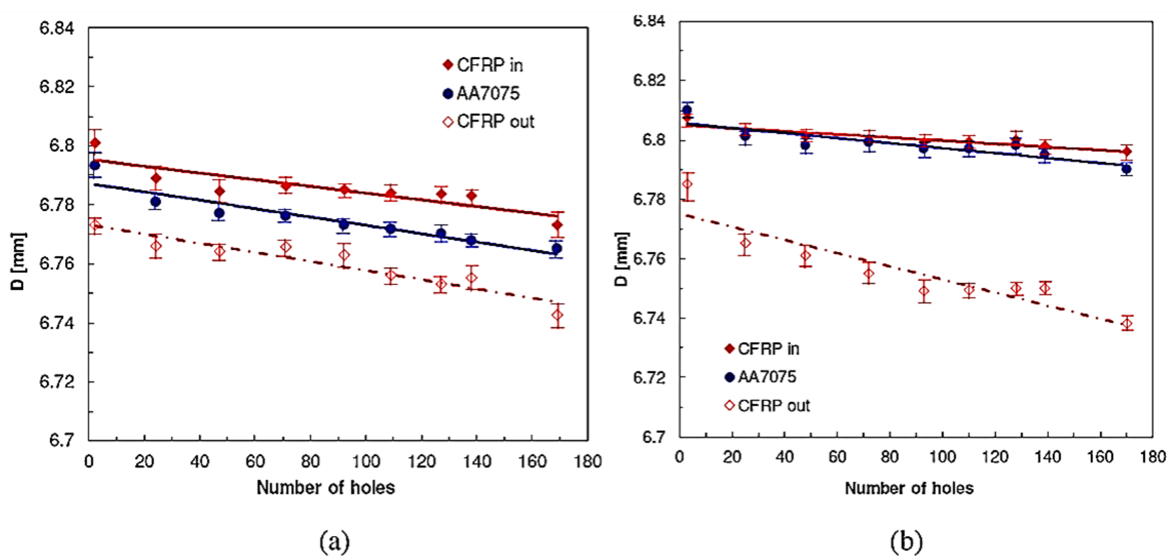

Figure 20. Evolution of hole size in CFRP and Aluminum alloy AA7075 using: (a) DLC coated drill and (b) TiAlN coated drill [73].

In the investigation of Zhang et al. [74], the study's results show that a number of variables, including drill wear, drilling parameters, and the existence of material flaws, have an impact on the distribution of hole size in CFRP/invar co-cured material. The study discovered that drill wear was the most important factor impacting hole size distribution, and that an increase in drill wear was associated with considerable rise in hole size variance. The research also revealed that the drilling parameters, including feed rate and cutting speed, affected the distribution of hole sizes. More hole size variation and worse hole quality were linked to higher feed rates and cutting speeds. This is because increased hole size variation can be caused by more deformation generated by higher drilling forces which arise due to higher feed rates and cutting speeds. The distribution of hole size was also impacted by material defects, such voids, fractures, and inhomogeneity. The presence of defects led to worse hole quality and a bigger size variation. This is due to the possibility of flaws causing the material to fracture and delaminate during drilling, which would result in a wider range of hole sizes [74].

It is commonly acknowledged that one of the key outcomes used to assess the drilling capabilities of composites is hole surface roughness. The surface quality is measured by keeping an eye on the surface imperfections of the workpiece. Hole surface roughness is significantly influenced by drilling parameters and drill bit geometry [1]. The excellent quality of the hole surface roughness obtained following the drilling of composite panels is ensured by the lack of any surface defects in the wall of the drilled hole. The cutting parameters and cutting tool characteristics have a significant influence on the drilled-hole surface roughness during the drilling process. It is crucial to examine the surface integrity of drilled holes because flaws in the surface have a direct impact on how well structural components assemble and can lead to serious problems including excessive wear, fatigue, and a reduction in the material's corrosion resistance [1].

The hole surface quality is a very important parameter, since that, currently, in aeronautical industry, CFRP panels have a maximum permissible value of arithmetic average roughness (Ra) of 3,2 μm while aluminum panels have a maximum acceptable value of 1,6 μm [1].

The Taguchi method is used by Kuo et al. [75], while drilling CFRP/AA laminates, to offer a statistical study of the hole surface quality. Spindle speed and vibration frequency were determined to have the greatest effects on hole surface quality. Moreover, utilizing metrics like average roughness (Ra) and root mean square roughness (RMS), the study provides a thorough investigation of hole surface roughness. According to the investigation, the improved vibration-assisted drilling method significantly reduced hole surface roughness when compared to conventional drilling. The use of vibration-assisted drilling helps to reduce the amplitude of surface roughness, resulting in a smoother and more uniform surface finish. Moreover, Geier et al. [76] showed that, in comparison to uncoated cutting tools, diamond-coated cutting tools produced a smoother surface finish and less burr development. The use of diamond-coated tools contributed to a smoother and more uniform surface finish by lowering the occurrence of delamination and fiber pullout during machining, since in composite materials it is more difficult to achieve good hole surface quality. Figure 21 represents the influence of fiber pull-out and uncut fibers in the surface roughness of composite materials. The surface roughness profile in quasi-homogeneous materials is better than in CFRP, because reinforcing and non-reinforcing fibers can be bent (bending dominant chip removal method) during the machining of fiber reinforced composites instead of being cut, which can leave a lot of uncut fibers on the machined surfaces [75], [76].

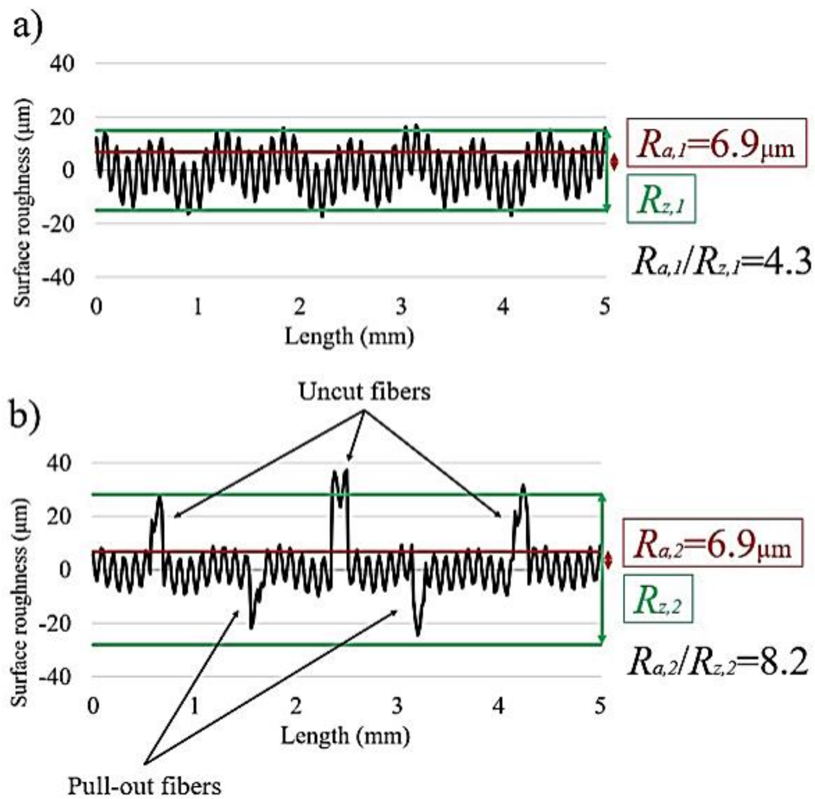

Figure 21. Average surface roughness (Ra) profile of (a) quasi-homogeneous material and (b) CFRP [76].

2.10. Drilling of CFRP/AA laminates

One of the fiber metal laminates, carbon fiber reinforced aluminum laminate, constitutes a replacement material with advantages over the original materials. The improvements in this field’s inventions have led to higher strength and stiffness to weight ratios. This type of composites is being utilized in a range of applications, enabling to replace the metals employed in various sectors, such as the aeronautics and automotive, thanks to its many benefits such as lightweight, and resistance to corrosion [77]. In order to create composites with improved fracture development properties, carbon fibers and aluminum alloys are frequently combined in a variety of patterns. By focusing on the matrix and reinforcements as the two key components of composite materials, it is possible to categorize them as metal, polymer, ceramic, and carbon metal matrix composites or stable reinforcements such natural and synthetic fiber reinforcement [77].

According to Zhong et al. [78], the most difficult cutting circumstances typically arise in the interface while drilling CFRP/AA/CFRP co-cured materials, as illustrated in Figure 22. The principal cutting edge’s drilling impact on CFRP/AA/CFRP co-cured materials is a difficult three-dimensional drilling procedure. Because of the various material characteristics of the two layers, the interface between the CFRP and AA layers presents a problem for the cutting process. Because of the interaction between the cutting tool and the two distinct materials, the cutting conditions at the interface are complicated. The authors present a strategy to characterize this drilling process by creating a mechanical model of the drilling process using an orthogonal cutting simplification and coordinate transformation. Two assumptions are made by them concerning the drilling procedure. To begin, they contend that the material properties and cutting tool pressure are the primary elements influencing the spring-back of the hole wall. The displacement of the hole wall after drilling is referred to as spring-back, and it can be troublesome in precision manufacturing applications. Second, the authors contend that the drilling-out direction (F_z) force is the only factor influencing the delamination of the CFRP layer [78].

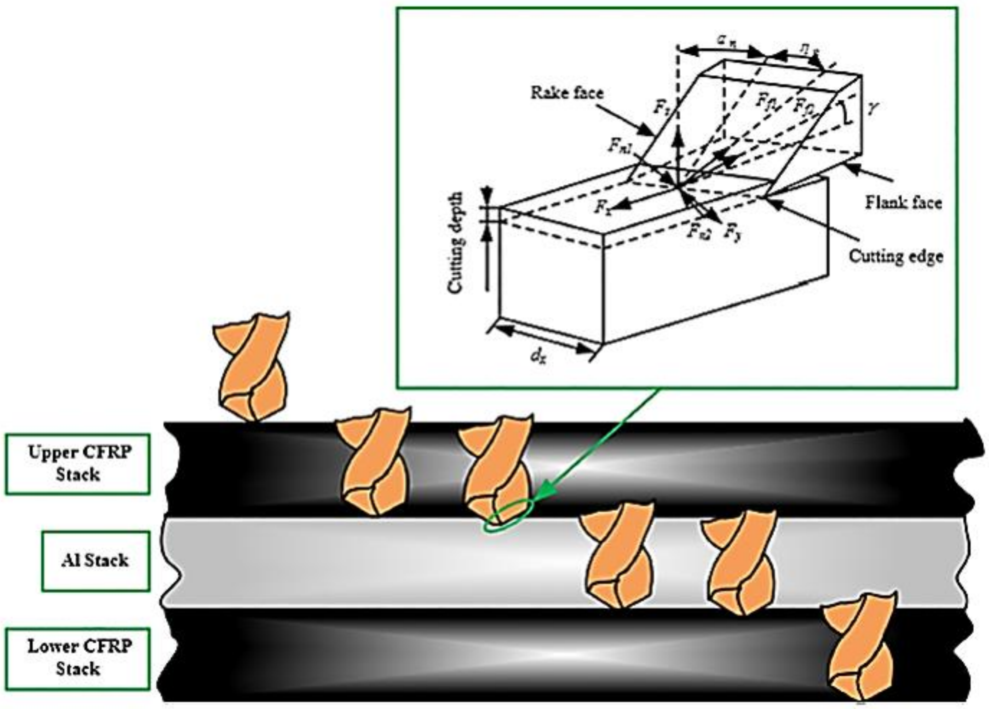

Figure 22. Mechanical model of the drilling process using an orthogonal cutting model and coordinate transformation [78].

Several recent studies on this subject analyze the thrust force in the drilling process of CFRP/AA. Sridhar et al. [47] aimed to investigate the effect of drilling parameters on thrust force while drilling carbon fiber reinforced aluminum laminates. The thermal softening of the carbon fiber prepreg, which made it easier to remove material and reduced the thrust force, was observed by the authors to have a significant impact on the thrust force when drilling at a spindle speed of 4000 rev/min. However, when increasing the axial feed rate, the uncut chip's thickness at the cutting edges values rose, and bigger thrust forces were originated. According to the study's 2D response plot, using lower axial feeds and faster spindle speeds can result in lower average thrust force. The axial feed and spindle speed had a considerable impact on the thrust force, according to the ANOVA (Analysis of Variance) results, whereas the interaction effect had a significant but less apparent impact. The ANOVA findings by Sridhar et al. [47] indicate that axial feed (80.35%) and spindle speed (17.15%) were the two parameters that had the greatest influence on the thrust force. Drilling at a spindle speed of 4000 rev/min with an axial feed of 0.1 mm/rev resulted in the lowest thrust force. Zhong et al. [78] examined the influence of cutting parameters on the thrust force during the drilling process of CFRP/AA/CFRP co-cured material. For the specified cutting parameters, the thrust force magnitudes of an uncoated drill and a drill coated with TiAlN were evaluated in the investigation. It was discovered that, regardless of whether the feed rate was decreased or not, the maximum thrust force with the TiAlN-coated drill was lower than with the uncoated drill as the cutting speed rose. For the intended cutting parameters, the maximum thrust force for drilling an aluminum stack was higher than for drilling a CFRP stack. The results showed that the TiAlN coating was successful in lowering the maximum thrust force and that cutting speed was the major factor influencing how much force the drill bit generated. In the study of Bolar et al. [48] two methods of creating holes – mechanical drilling and helical milling – were compared. The raw force signals obtained using these approaches demonstrated that the components' different material qualities were responsible for the thrust force signal's peaks and valleys. The valleys represented the milling of carbon fiber layers, while the peaks indicated the signals received while cutting aluminum layers. The plastic deformation related with the metal cutting was ascribed to the force peaks when machining aluminum layers, whereas the lower thrust force signal while milling carbon fiber matrix was connected to the lower resistance provided by the brittle matrix material. According to Bolar et al. [48], the cutting mechanics caused the thrust force to be greater during drilling than during helical milling. The primary cutting edges, being the principal edges in the cutting action during drilling, increase axial cutting and the thrust force magnitude. The periferical cutting edges on the milling cutter's end and perimeter are used to remove material during helical milling, which results in a better load distribution and a substantially reduced thrust force magnitude. The study also discovered that mechanical drilling produced radial forces of greater magnitude than helical milling. This is explained by the fact that during mechanical drilling, chips are transported from the cutting zone through the helical flutes, and the continuous metallic chips abrade the hole surface, raising the frictional load and radial forces. In contrast, the created chips in helical milling are easily evacuated without increasing the frictional load. In Figure 23 the forces in the two processes are represented [48].

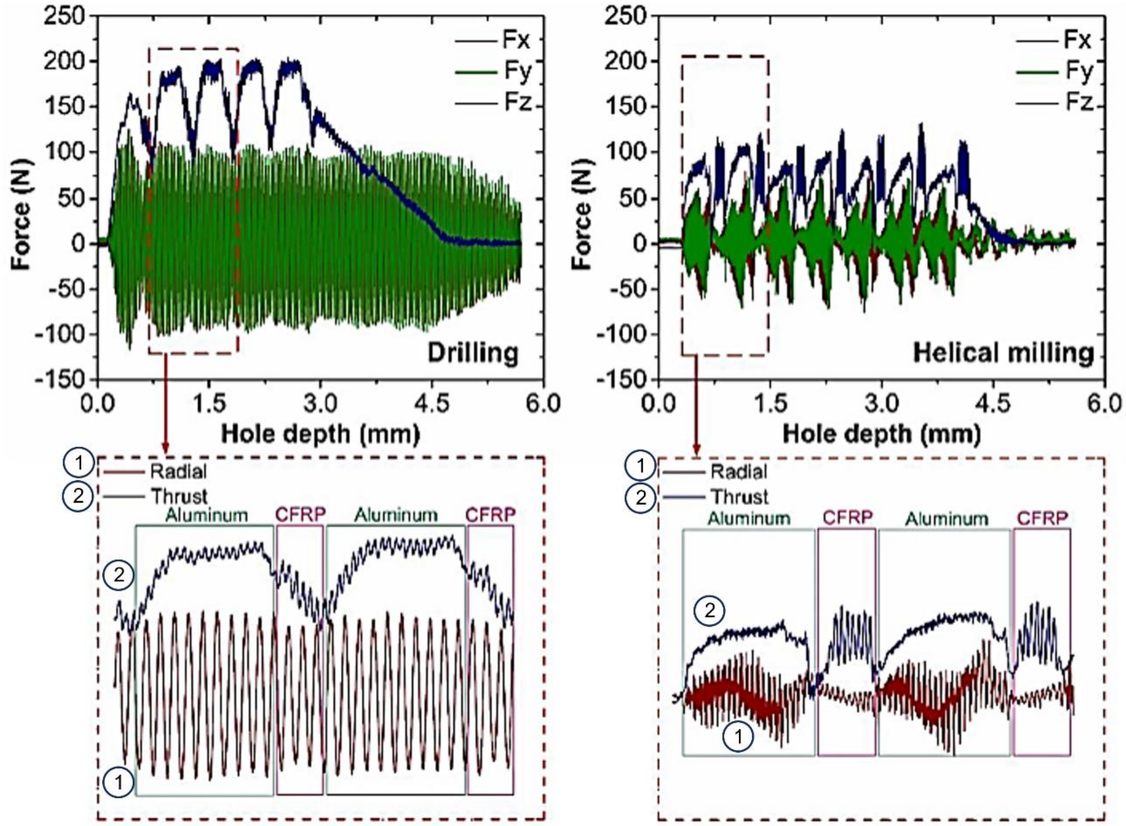

Figure 23. Radial and thrust forces in drilling and helical milling (adapted from [48]).

Regarding the purpose of the present work, in Table 2 is presented the parameters used in the main studies aborded in the chapter, in order to summarize the information acquired about the drilling of CFRP/AA laminates.

Table 2. Drilling conditions of the main studies of the literature review.

Author	Feed (mm/rev)	Cutting Speed (m/min)	Material	Drill Geometry	Drill Coating
Zhang et al. (2021) [74]	0.005, 0.01, 0.015, 0.02	38, 75, 113, 151	CFRP/AA	Twist drill (diameter - 6 mm; point angle - 140º; helix angle - 60º)	PVD TiAlN
Zhang et al. (2019) [18]	0.1	100	CFRP/AA	Countersinking drilling tool (diameter - 6.013 mm)	Not coated
Soo et al. (2019) [28]	0.15, 0.30	60, 120	CFRP/AA7010	Double Cone drill (diameter - 6.38 mm; point angles - 130º, 60º; helix angle - 30º), Flat point drill (diameter - 6.38 mm; point angles - 140º, 180º; helix angle - 30º)	CVD Diamond

Hassan et al. (2021) [46]	0.05, 0.1	23, 39	CFRP/AA7075-T6	Twist drill (diameter - 4.826 mm; point angle - 110º, 130º; helix angle - 15º, 30º)	Not coated
Sridhar et al. (2022) [47]	0.1, 0.2, 0.3, 0.4	21, 43, 64, 85	CFRP/AA2024	Solid carbide drills (diameter - 6.8 mm; point angle - 140º; two flutes)	Not coated
Bolar et al. (2022) [48]	0.02, 0.04	45, 65, 85	CFRP/AA2024	Carbide drills (diameter - 6.8 mm; point angle - 140º; two flutes)	Not coated
Xu et al. (2018) [49]	0.01, 0.015, 0.02, 0.025	20, 30, 40, 50	CFRP	Brad & spur drill; tungsten carbide twist drill; solid carbide dagger drill (diameters - 6.35 mm)	CVD Diamond (brad spur drill)
Devitte et al. (2021) [68]	0.05, 0.15, 0.25	20, 40, 60	GFRP/AA	Carbide drills (diameter - 6 mm; point angles - 118º, 135º, 130º; helix angles - 27.6º, 26.6º, 16.6º)	Not coated
Lee et al. (2021) [69]	0.1	50	CFRP	Carbide drill (diameter - 8 mm; point angle - 90º; helix angle - 30º)	Not coated
Geier et al. (2022) [70]	0.15, 0.35	100	CFRP	Fishtail drill; Brad & Spur drill	Not coated
D'Orazio et al. (2017) [73]	0.163, 0.2	128, 170.8	CFRP/AA7075	Two Twist drills (diameter - 6.8 mm; point angles - 118º, 140º)	Diamond and nanocomposite TiAlN
Kuo et al. (2017) [75]	0.04, 0.06, 0.08	130, 150, 170, 200	CFRP/AA7075-T6	Twist drill (point angle - 120º; helix angle - 20º)	CVD Diamond
Geier et al. (2020) [76]	0.035, 0.043, 0.064, 0.078, 0.093	50, 65, 100, 135, 150	CFRP	Double point angle twist drill; Compression end mill (diameters -10 mm)	CVD Diamond
Zhong et al. (2022) [78]	0.025, 0.05, 0.075, 0.1	15, 30, 45, 60	CFRP/AA2024	Two Twist drills (diameter - 6 mm; point angle - 135º; helix angle - 20º)	One uncoated and the other coated with TiAlN
Ekici et al. (2021) [79]	0.1, 0.14, 0.2	65, 85, 110	CFRP/AA5754	Three carbide drills (diameter - 6 mm; point angle - 118º; helix angle - 30º)	PVD TiN-TiAlN and TiAlSiMoCr
Pardo et al. (2020) [80]	0.1	41	CFRP/AA7010-T651	Twist drill (diameter - 6 mm; point angle - 118º)	Not coated
Nurhaniza et al. (2016) [81]	0.27, 0.3, 0.32	57, 75, 94	CFRP/AA2024-T3	End mill with double tooth cutter (diameter – 6 mm)	Polycrystalline Diamond (PCD)
Marques et al. (2022) [82]	0.03, 0.05, 0.07	80, 100, 120	CFRP/AA5754	Twist drill; Double-point angle drill; Chip-breaking drill	Diamond

Chapter 3

Experimental Procedures

In this chapter, the methodologies used during the development of the experimental work are examined. Two types of fiber metal laminates configurations (including AA2024 and CFRP materials) were found relevant to study and are thoroughly described in this chapter. The experimental drilling setup, parameter definition and analysis methods are also depicted along the chapter.

3.1. Cutting Tools

Regarding drilling tools, a type N geometry drill (referred as drill 1), presented in Figure 24, and a type W geometry drill (referred as drill 2), also presented in Figure 24, were used in this work. According to DIN 1836 [83], which classifies drills based on their helix angle, drill 1 can be identified as an N-type drill (helix angles between 18º and 30º), while drill 2 can be identified as a W-type drill (helix angles between 35º and 45º). N-type drills are suitable for a variety of materials and provide a good balance between chip removal and stability during the drilling process. They are widely used in conventional drilling operations. On the other hand, W-type drills are specifically designed for applications that require higher chip removal and cutting rates, making them particularly effective in wide range of materials. Compared to drill 1, drill 2, in addition to having a larger diameter, is a tool with a larger point angle and a slightly larger helix angle. The geometry of the drill 1 has a diameter of 6 mm, point angle of 120º, and helical angle of 30º. The geometry of the drill 2 has a diameter of 6.4 mm, point angle of 140º, and helical angle of 37º. The tungsten carbide tools were diamond coated through the hot-filament chemical vapor deposition (HFCVD) process. The characteristics of each drilling tool are summarized in Table 3. In Attachment A the technical drawings of each drilling tool are presented.

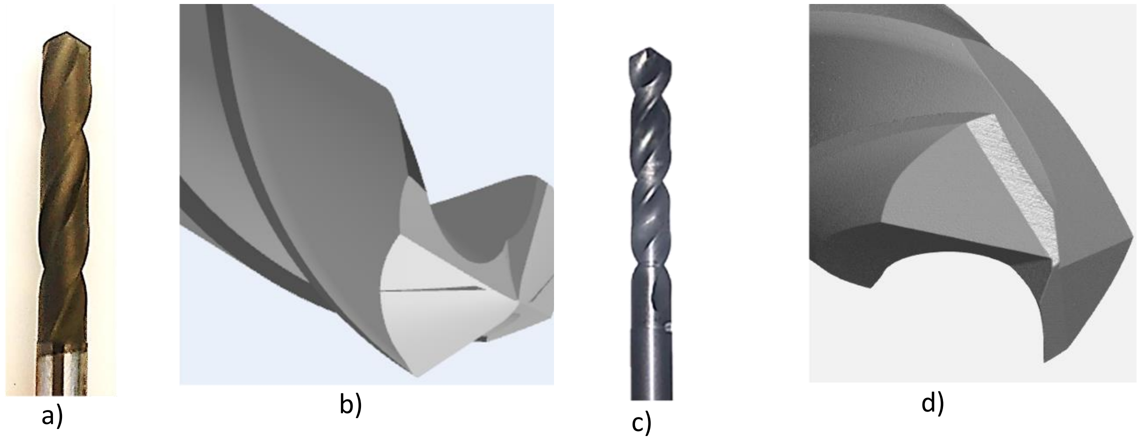

Figure 24. One-shot drilling tool geometries used in the present study: type N geometry (drill 1) (a) and respective drill tip illustration scheme (b); type W geometry (drill 2) (c) and respective drill tip illustration scheme (d).

Table 3. Drilling tool geometry specification for each type.

Drill Tool	Diameter (mm)	Point Angle (º)	Helical Angle (º)	Coating Type
Drill 1	6	120	30	HFCVD
Drill 2	6.4	140	37	HFCVD

The diamond coating has a microhardness of 10000 HV and a multilayer composition, using different diamond layers, composed of microcrystalline diamond coatings (MCD) and nanocrystalline diamond coatings (NCD), as shown in Figure 25. The excellent adhesion combined with the unique smoothness of this multilayer composition guarantees productive drilling of composite materials. In order to determine the thickness of the diamond coating in the drilling tool, a SEM analysis was made, confirming a specific thickness between 4.3 µm and 4.6 µm. The thickness of the coating it is an important aspect, since that with these values of thickness it is possible to guarantee a very sharp cutting edge, enabling the better separation of the fibers during drilling.

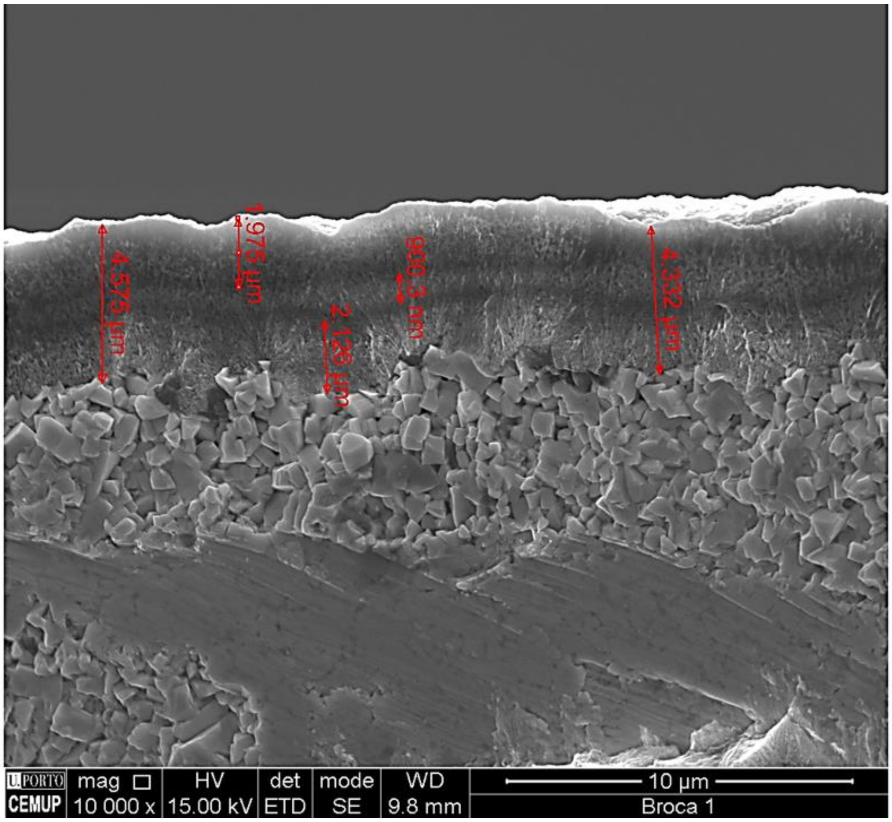

Figure 25. SEM analysis of the CVD diamond coating thickness and composition of the drilling tools.

3.2. Workpiece Material Process and Definition

Two different configurations of CFRP/AA2024 plates were manufactured and tested within the scope of this study. The plates had dimensions of 200x200 mm, and they were classified into two types: Type I – CFRP/AA/CFRP (Figure 26) and Type II – AA/CFRP/AA (Figure 27). Both configurations had a total thickness of 4.5 mm. In both configuration types of multi-material, each layer of AA and CFRP have a thickness of 1.5 mm.

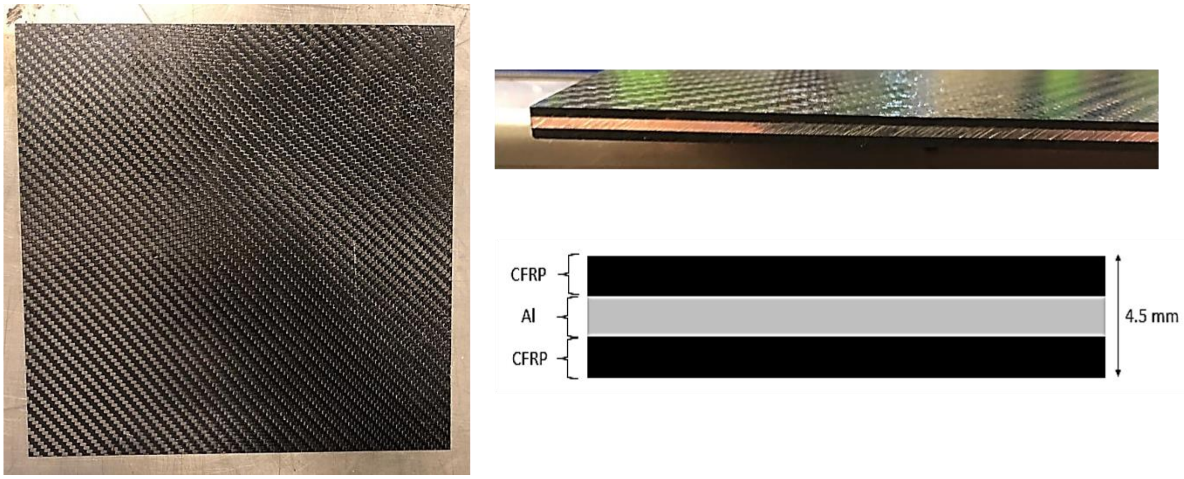

Figure 26. CFRP/AA/CFRP plates (Type I) used in experimental procedures.

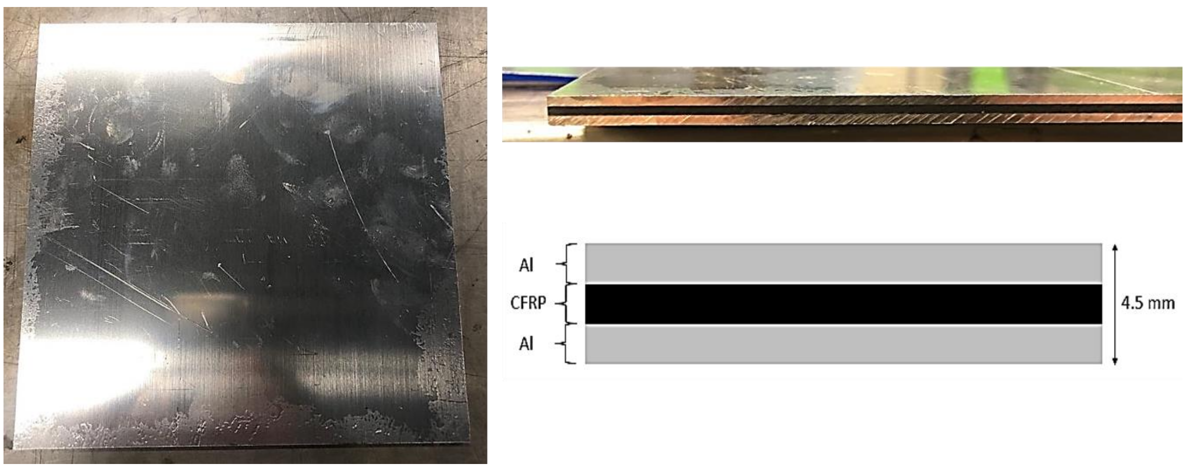

Figure 27. AA/CFRP/AA plates (Type II) used in experimental procedures.

The plates were manufactured by Beyond Composite. The fiber metal laminates manufacture process consisted of an aluminum surface treatment using sandpaper, to improve surface roughness. Acetone was employed to clean the surfaces, and an adhesion promoter (Sika Aktivator 205) was applied to enhance bonding between the layers. In the case of CFRP, a thermosetting epoxy resin was produced by mixing it with a catalyst. Subsequently, the CFRP layer (twill weave 2/2) were stacked while simultaneously impregnating seven weaves with the resin, thorough hot pressing process (temperature of 80 ºC, and pressure of 30 kPa). The resulting fiber volume fraction of composite layers is 79%.

3.3. Instrumented Experimental Setup

An universal machining center (DMG Mori DMU 60 eVo) was employed in all drilling experiments (illustrated in Figure 28a). The clamping system is shown in Figure 28b and 28c, fixed to the machining center table. It consists of a flat surface where the plate sits. This flat surface has a slot in the middle that provides tool clearance with adequate back support, enabling drilling operations. Two steel bars clamp the to-be-drilled plate against the flat surface.

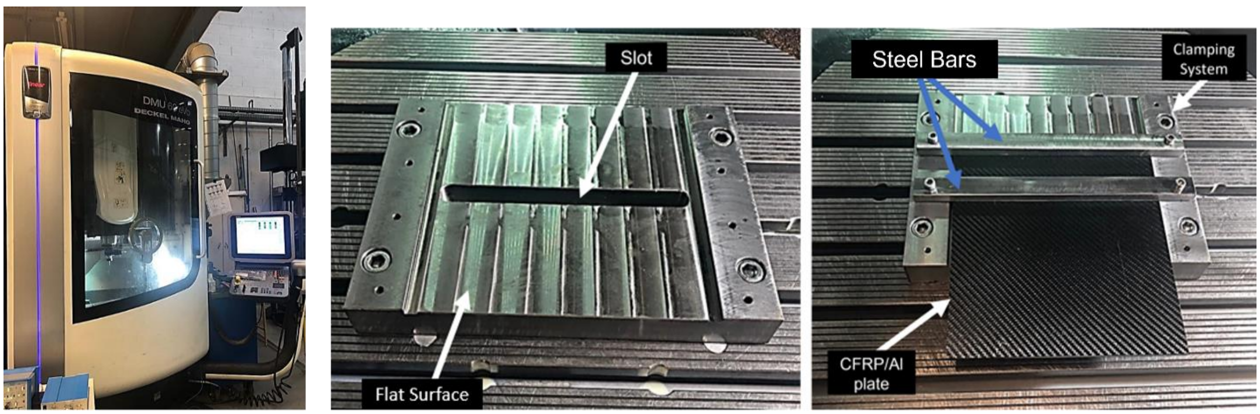

a) b) c)

Figure 28. Drilling tests setup: (a) DMG Mori DMU 60 eVo CNC machine; (b) and (c) clamping system.

A spindle-mounted dynamometer and data acquisition system, illustrated in Figure 29a, enabled cutting force and torque measurement. This dynamometer consists of two parts, the stator and the rotor, and it is positioned directly on the machine's spindle. The stator is then coupled with a Kistler Type 5238B signal conditioner (shown in Figure 29b), which is coupled with a Kistler Type 5697 data gathering system (shown in Figure 29c), allowing connection with the Kistler DynoWare program for results analysis.

a) b) c)

Figure 29. Cutting loads acquisition system: (a) Kistler Type 9170A rotating cutting force dynamometer; (b) Kistler Type 5238B signal conditioner; (c) Kistler Type 5697 data acquisition system.

Piezoelectric materials can exhibit temperature-dependent behavior, leading to variations in their electrical properties and signal output. The heating and cooling of the machine center (for instance the spindle) may translate in load and torque signal deviation (as illustrated in Figure 30a). To solve this problem, the software's drift adjustment tool was employed, as shown in Figure 30b. The measured values are deducted from the straight line that this drift compensation tool computes between the data set's start and finish locations.

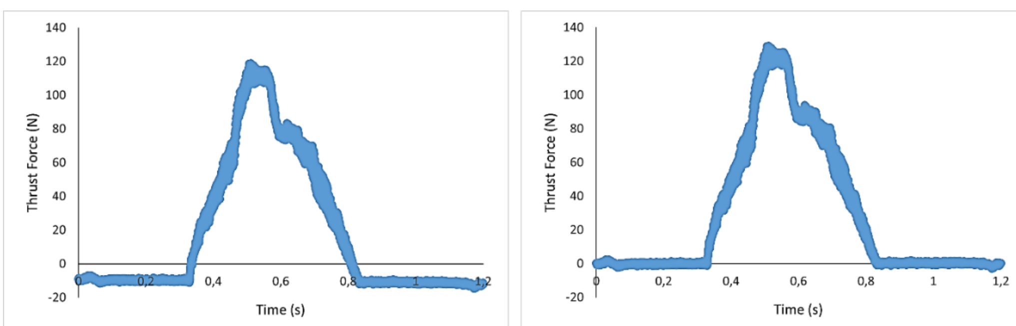

a) b)

Figure 30. Acquisition thrust force loads in Kistler software for a hole made by drill 2 for the parameters of feed – 0.05 mm/rev and cutting speed – 300 m/min: (a) signal with drift; (b) signal with drift correction.

Regarding the drilling parameters, an initial preliminary experimental drilling campaign (i) was conducted. This campaign involved testing highly productive drilling operating conditions, as presented in Table 4, using the two drilling tools and the two multi-material configurations. The material removal rate (MRR) of the two drilling tools and the number of holes produced by the combination of the drilling parameters are also presented.

Table 4. Number of holes produced by the combination of drilling parameters of the preliminary drilling campaign (i).

Feed (mm/rev) / Cutting speed (m/min)	0.05	0.1	0.15	0.2	0.3
50	Type I: Drill 1 (48 holes) (MRR: 3.75 cm3/min) Drill 2 (30 holes) (MRR: 4 cm3/min) Type II: Drill 1 (45 holes) (MRR: 3.75 cm3/min)				
100		Type I: Drill 1 (3 holes) (MRR: 15 cm3/min)	Type I: Drill 1 (44 holes) (MRR: 22.5 cm3/min)		
150				Type II: Drill 2 (15 holes) (MRR: 48 cm3/min)	Type I: Drill 1 (10 holes) (MRR: 67.5 cm3/min)
200					
300			Type I: Drill 1 (10 holes) (MRR: 67.5 cm3/min)		Type I: Drill 1 (10 holes) (MRR: 135 cm3/min)

In order to compare the performance of drilling tools 1 and 2 under more conservative operating conditions, both drilling tools were evaluated using identical parameters in the same multi-material configuration. For the type I configuration (CFRP/AA/CFRP), drilling tool 2 achieved superior results with a feed of 0.05 mm/rev and cutting speed of 300 m/min, as will be further analyzed in Chapter 4. Similarly, for the type II configuration (AA/CFRP/AA), drilling tool 2 exhibited superior performance with a feed of 0.2 mm/rev and cutting speed of 150 m/min.

Building upon the results obtained from the preliminary experimental campaign (i), a second experimental drilling campaign (ii) was conducted, as documented in Table 5. In this drilling campaign, exclusively drill 2 was utilized to assess the predetermined drilling conditions across a significant number of holes and verify the machinability in both multi-material configurations. All holes produced in the second drilling campaign are exhibited in Table 5. The preliminary drilling campaign (i) and the secondary drilling campaign (ii) images of the drilled plates are shown in detail in Appendix A.

Table 5. Number of holes produced by the combination of drilling parameters of the second drilling campaign (ii).

Feed (mm/rev) / **Cutting speed (m/min)**	**0.05**	**0.2**
150		Type II: Drill 2 (345 holes) (MRR: 48 cm3/min)
300	Type I: Drill 2 (345 holes) (MRR: 24 cm3/min)	

Besides the adjustment of the drilling conditions, a distance of 12.5 between the holes (Figure 31a) and their distance to the edges of the plate, also 12.5 mm (Figure 31b) were also elaborated for the drilling tool 2, in order to optimize the total number of holes per plate and to guarantee that hole spacing had no significant impact on delamination extend. With these distances, it is possible to predict a total of 225 holes per plate.

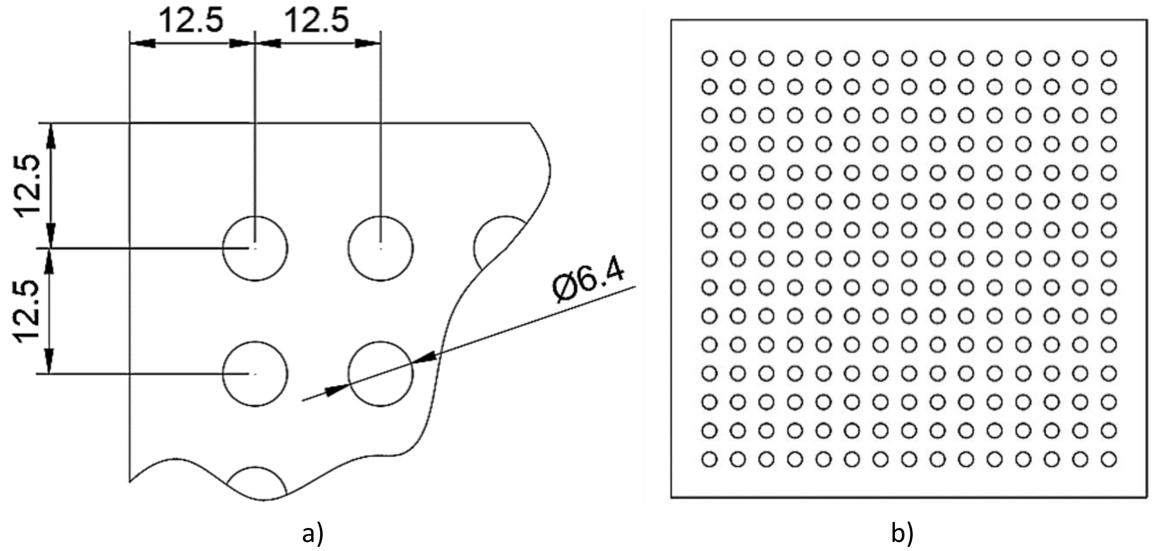

Figure 31. Dimensions between drilled holes: (a) Hole spacing from the borders and between each hole center for the drilling campaign (ii) with drill 2; (b) total of holes predicted in each plate.

3.4. Drilled Holes Analysis

Regarding delamination damage, the surface of the drilled holes was examined by taking pictures with a DinoLite AM-4031MZTL digital USB microscope, presented in Figure 32a, which enabled picture taking using the DinoCapture 2.0 software. To infer on eventual intra or inter delamination, an X-ray analysis was carried out. The plates were initially submerged for at least 30 minutes in a methane di-iodine liquid bath, as presented in Figure 32b to access the delamination damage.

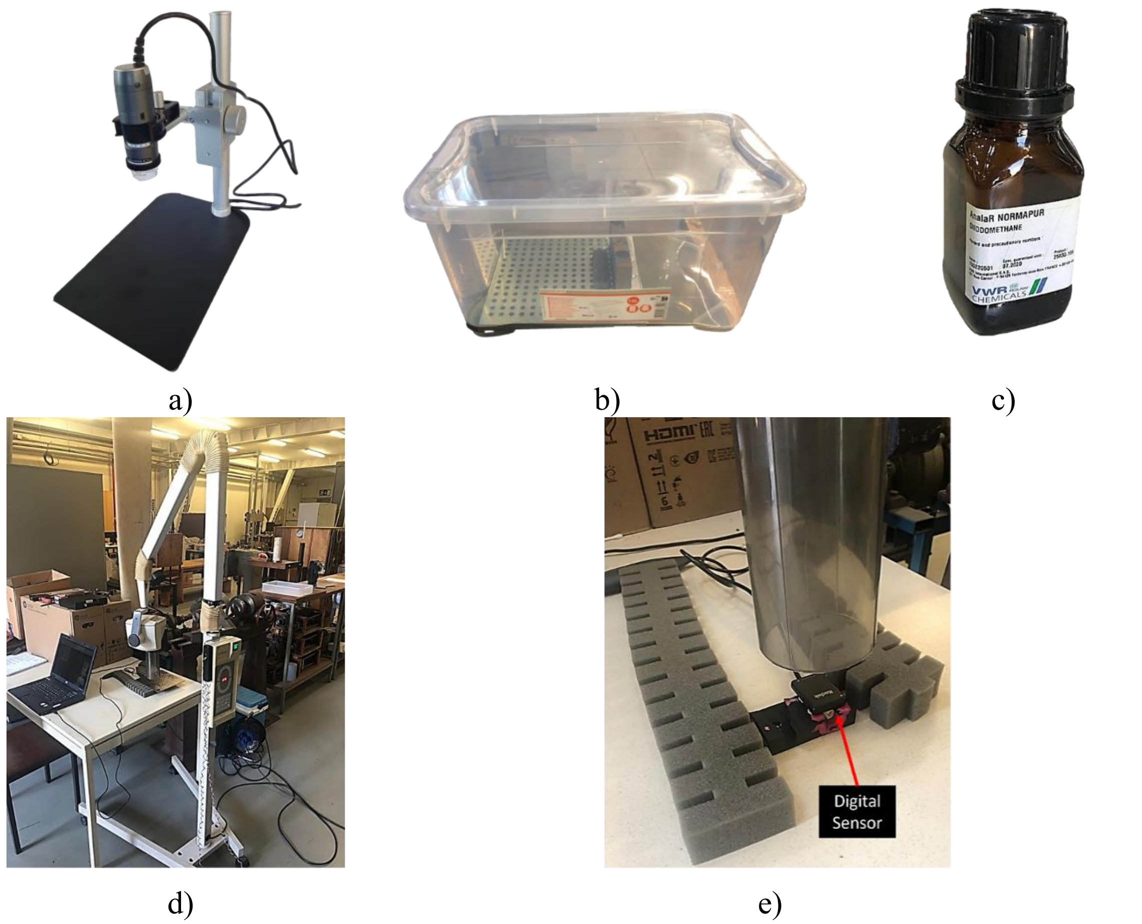

Figure 32. Experimental apparatus required for the X-ray analysis of drilled holes: DinoLite AM-4031MZTL digital USB microscope (a); Liquid bath container (b) for plate submersion under methane di-iodine liquid (c); SATELEC X MIND X-ray emitter (d); Kodak RVG 5100 digital sensor (e).

The contrast liquid seeps into the eventual internal delamination voids of the manufactured the hole, enabling its observation. Following the X-ray emission from a SATELEC X MIND, shown in Figure 32d, the photos were taken using a Kodak RVG 5100 digital sensor, which was positioned beneath the hole as it is highlighted in Figure 32e.

After taking the pictures through the X-Ray analysis, the delamination factors were then calculated from those pictures using a Matlab script developed by [82]. A basic graphical explanation of the Matlab script is illustrated in Figure 33. The image was transformed into a binary color map by applying a color threshold, which results in pixels being assigned either black or white.

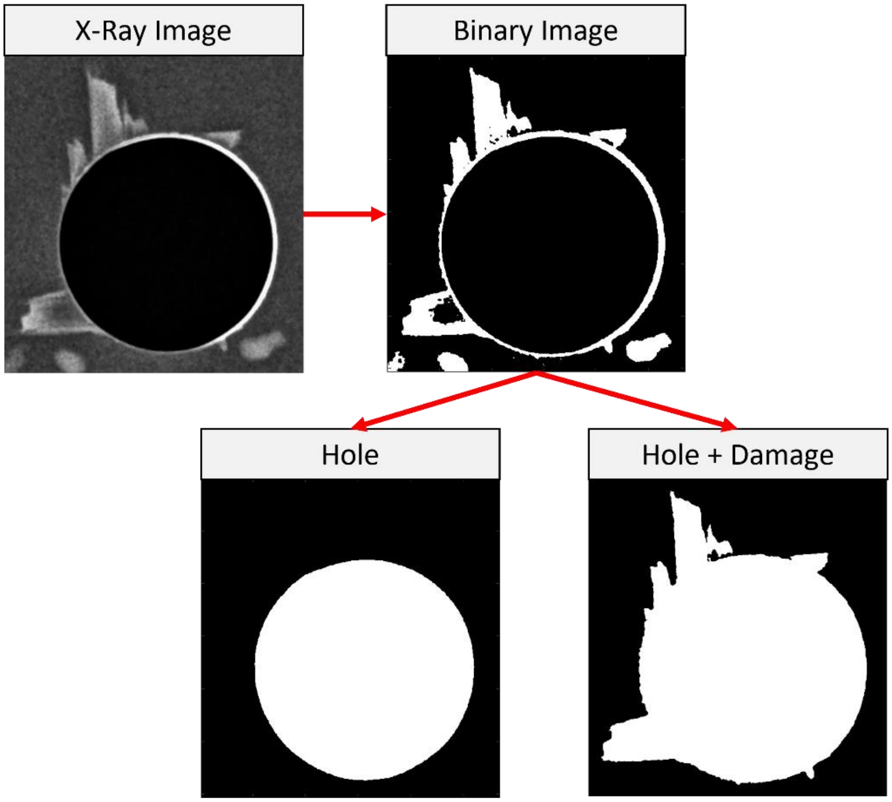

Figure 33. Matlab delamination script's fundamental operations.

The delamination analysis technique is highly influenced by the specific threshold of the white area applied to the binary image obtained from the X-ray picture. If the same threshold value is used for all X-ray images, there may be a challenge due to variations in brightness among the images. To address this issue in different scenarios, adjustments were made to the threshold value. Additionally, the correct threshold level that correlated with the apparent degree of delamination occasionally produced a binary image with an incomplete contour of the hole, making it impossible for the Matlab script to calculate an area value. For those cases, it was necessary to manually alter the binary image by adding white pixels until the hole contour was depicted. Due to image collection through the experimental procedure at the time of X-ray analysis, it was found that in some delamination defects, the methane di-iodine liquid did not drain properly inside the delamination area, as illustrated in Figure 34. Thus, the X-ray analysis procedure had to be repeated in order to not to translate into delamination factor deviation.

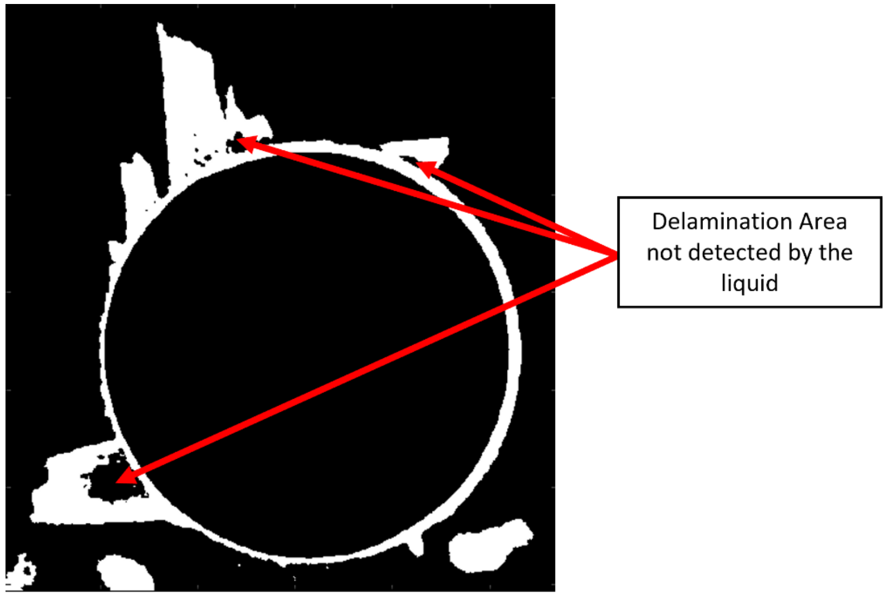

Figure 34. Places where the methane di-iodine liquid did not drain effectively in the delamination area.

The analyze of whether burrs or uncut fibers were present in the drilled holes was conducted by taking images of the drilled holes using the DinoLite digital USB microscope (the same presented before). Besides this procedure was also conducted an X-ray analysis to the drilled holes in order to verify the existence of uncut fibers in the configuration type II (AA/CFRP/AA).

Initially, to facilitate the measurement of the surface roughness of the holes, the multi-material plates were cut in a band saw machine (Figure 35) at the locations where the measurements were to be made.

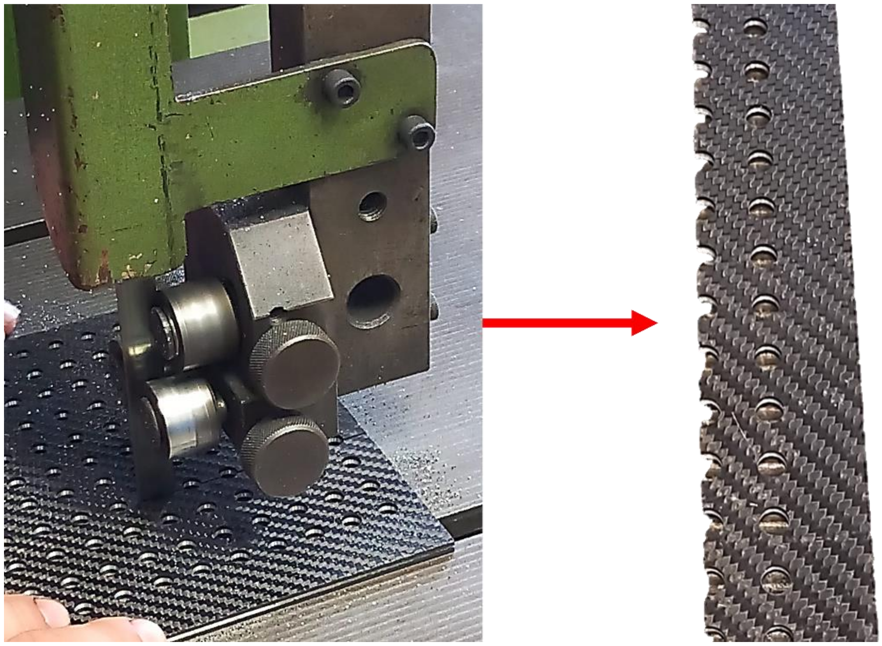

Figure 35. Use of the band saw machine to obtain the locations of the drilled holes to be measured.

The 3D surfaces of the drilled holes' walls were generated using the ALICONA Infinity Focus SL, a 3D measurement technology depicted in Figure 36. To infer on the surface roughness of the drilled hole walls, multiple probe lines were drawn so that roughness values (Ra and Rz) could be computed.

Figure 36. Measurement of internal hole surface roughness using the ALICONA Infinite Focus SL.

Roughness measurements of 3 holes in each plate configuration were carried out for each of the two drilling tools. That is, 3 holes for the configuration type I (CFRP/Al/CFRP) with the drill 1 (feed – 0.05 mm/rev; cutting speed – 300 m/min), 3 holes for the configuration type I (CFRP/AA/CFRP) with the drill 2 (feed – 0.05 mm/rev; cutting speed – 300 m/min), 3 holes for the configuration type II (AA/CFRP/AA) with the drill 1 (feed – 0.05 mm/rev; cutting speed – 300 m/min), and 3 holes for the configuration type II (AA/CFRP/AA) with the drill 2 (feed – 0.2 mm/rev; cutting speed – 150 m/min).

In order to analyze the chip formation and evacuation, samples of long and non-fragmented aluminum chips containing CFRP powder chip adhesion were taken. Thus, the chips were collected in two boxes when drilling the type I configuration (CFRP/AA/CFRP) and when drilling the type II configuration (AA/CFRP/AA). The chips where then analyzed using the DinoLite digital USB microscope.

Tool wear inspection was analyzed on the drilling tool 2 when drilling the two plate configurations. For each plate type (I and II), 345 holes were drilled with two drilling tools 2 (one for each configuration plate). Table 6 and 7 shows the number of holes where the tool wear was inspected in the DinoLite microscope (Figure 37), in order to evaluate its progression. For each configuration and for each tool the same total drilling distance of 1552.5 mm was calculated by multiplying the number of holes produced with each drilling tool by the thickness of the multi-material plate (4.5 mm).

Table 6. Wear analysis experimental procedure for the configuration type I (CFRP/AA/CFRP) with the drilling tool 2 (feed – 0.05 mm/rev; cutting speed – 300 m/min).

Wear Analysis in Configuration Type I (CFRP/AA/CFRP)	
Hole Number	Drilling Distance (mm)
15	67.5
90	405
180	810
270	1215
345	1552.5

Table 7. Wear analysis experimental procedure for the configuration type II (AA/CFRP/AA) with the drilling tool 2 (feed – 0.2 mm/rev; cutting speed – 150 m/min).

Wear Analysis in Configuration Type II (AA/CFRP/AA)	
Hole Number	Drilling Distance (mm)
15	67.5
90	405
180	810
270	1215
345	1552.5

Figure 37. Images of wear analysis in the drilling tool 2 taken in the DinoLite digital USB microscope.

Chapter 4

Results Analysis and Discussion

4.1. Cutting Forces and Torque

In terms of the consistency of the cutting forces, Figure 38 displays a graph illustrating the thrust forces of three holes obtained using drilling tool 2 (feed – 0.05 mm/rev; cutting speed – 300 m/min) on the type I configuration plate. Through analysis of the graph, it is evident that the results for these forces exhibited consistent patterns throughout the experimental drilling campaign (ii), as indicated by the similarity in the shape of the thrust force curves.

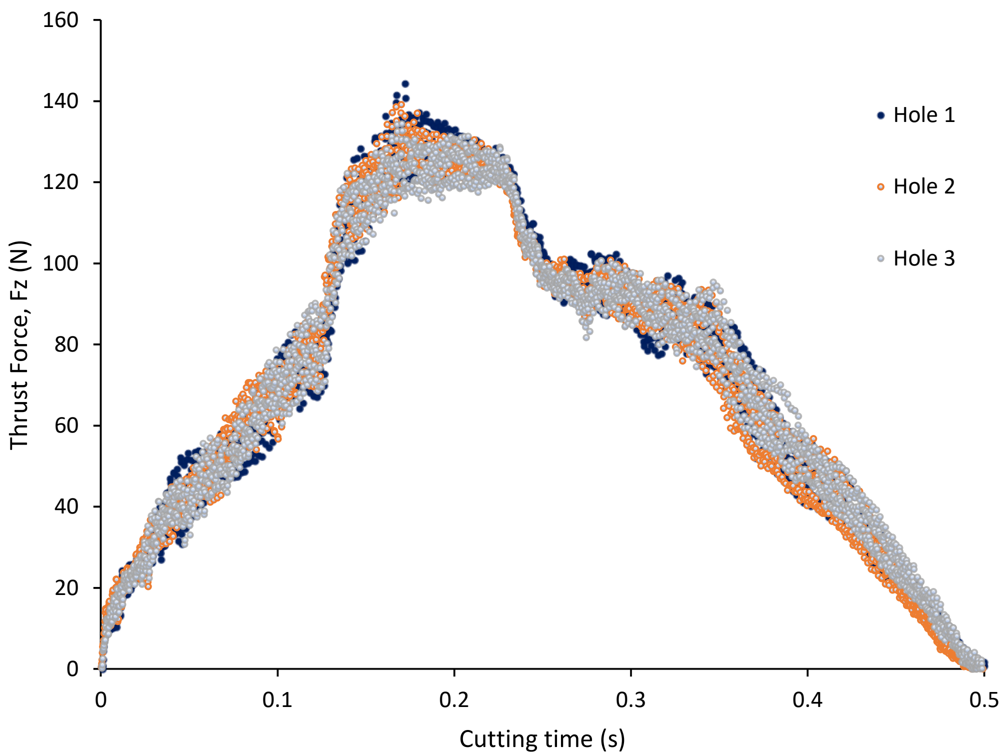

Figure 38. Signature of thrust force signals in three holes obtained with the drilling tool 2 (feed – 0.05 mm/rev; cutting speed – 300 m/min) in the type I configuration plate.

The thrust force and torque results for the two distinct plate configurations are presented in Figures 39 and 40. Thrust force in CFRP layers is lower when compared to the aluminum layers. This phenomenon can be attributed to the fact that the drilling process imposes compressive loads on the multi-material. The aluminum layers can better withstand these compressive loads due to their ductility and ability to undergo plastic deformation. In contrast, the CFRP layers, with their brittle nature, tend to fracture when subjected to significant compressive forces. Additionally, the thrust force during drilling the lower CFRP layer is higher than that of the upper CFRP layer (in the type I configuration plate). This arises to the fact that unlike in the upper layer, on the lower CFRP layer the secondary cutting edges of the drill are engaged, thus generating significant axial load. Moreover, the accumulation and entanglement of aluminum chips around the drilling tool as it progresses through the layers can also promote such results, as explained by Franz et al [1], [23]. The torque signals were significantly low during all the drilling campaign, and their measurements tend to be difficult to become correlated in the same instances of the thrust force signals.

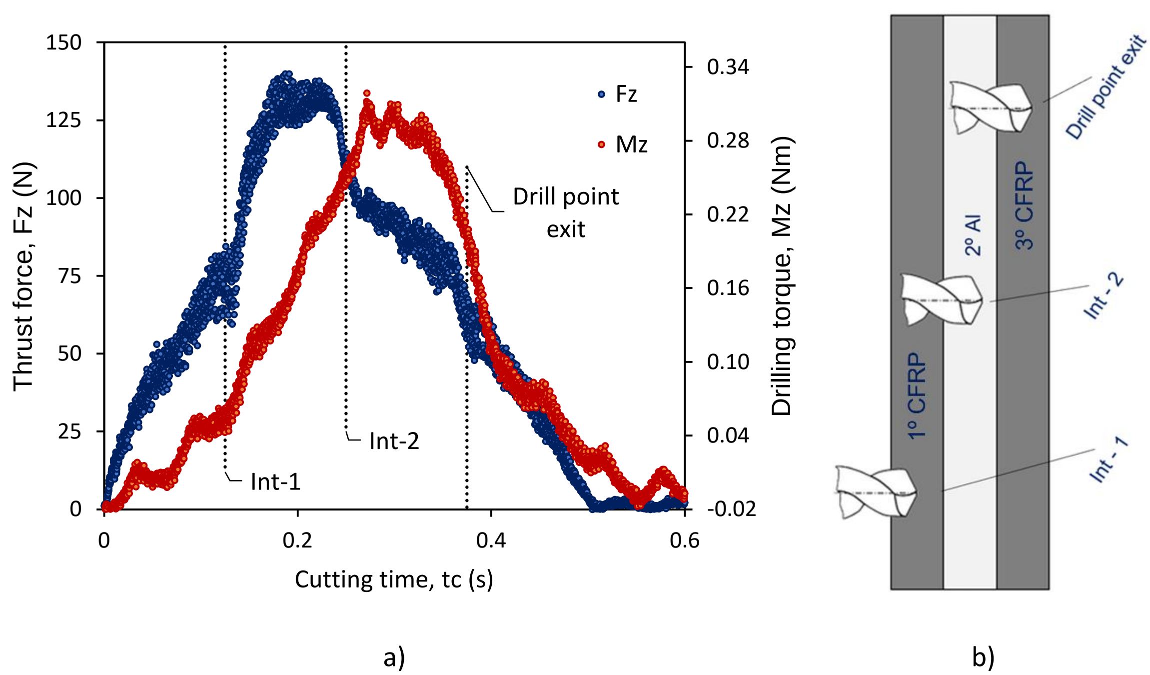

Figure 39. Cutting forces for the type I plate: (a) thrust force and drilling torque results using drill 2 (feed – 0.05 mm/rev; cutting speed – 300 m/min), with signaled laminate interfaces' cross by drill point; (b) drill point location diagram.

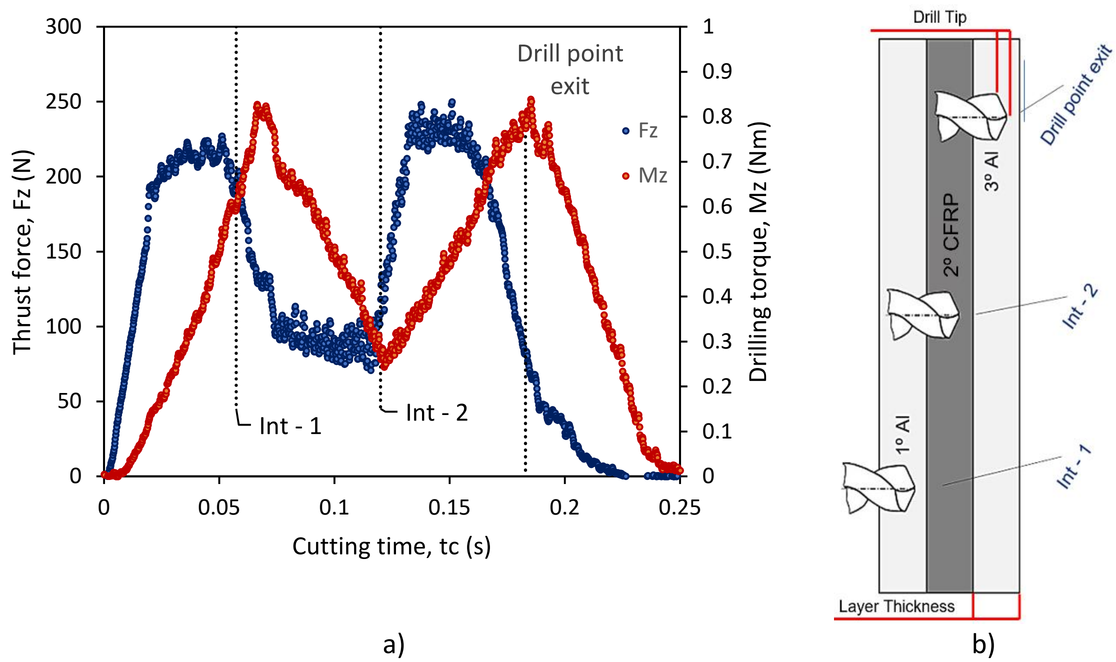

Figure 40. Cutting forces for the type II plate: (a) Thrust force and drilling torque results using drill 2 (feed – 0.2 mm/rev; cutting speed – 150 m/min), with signaled laminate interfaces' cross by drill point; (b) drill point location diagram.

To accurately analyze the maximum thrust force and torque values within each multi-material layer, it was essential to determine whether the depth of drilling tool 2's cutting edges was less than the thickness of each layer. By comparing the depth of the drill bit with the thickness of each layer of the multi-material in the previous image (Figure 40), it becomes apparent that during certain moments of drilling, the primary cutting edges of the tool only engage with a single layer of the multi-material. Consequently, this allowed for a clearer distinction between the cutting forces acting on each layer of the multi-material configurations.

As outlined in the experimental procedure, cutting force values were measured at points of interest for both types of multi-material configurations during drilling a total of 345 holes. The cutting force graphs obtained from the 345 holes in each multi-material configuration exhibited a consistent pattern, with variations observed only in the maximum and minimum values. For the type I plate the maximum values for the thrust force and torque were measured. Thus, in Figures 41 and 42 (thrust force and torque, respectively) show the evolution of this drilling forces for selected intervals of holes using the drilling tool 2 with the drilling parameters: feed – 0.05 mm/rev and cutting speed – 300 m/min. Regarding the maximum thrust force results between interface 1 (Int 1) and interface 2 (Int 2) (Figure 41), it can be observed that with increasing number of drilled holes there is a tendency for slightly larger cutting forces. This may suggest a tendency towards tool wear phenomena (i.e., built up edge) which will be further inspected in section 4.6. According to the study of Pardo et al. [80], as the tool wore down, the thrust force significantly increased. Also, the cutting edge rounding due to build up edge may have increased the thrust force linearly during drilling of the CFRP layer. On the other hand, the maximum torque results (Figure 42) increase since the first 15 holes until the last holes, and the increasing in the aluminum layer, observed in Figure 40 were more substantial than in the CFRP layer. This is in accordance with the study of Pardo et al. [80], where the torque signal magnitude rose by almost 150% when drilling the CFRP layer. On the other hand, frequent chip blockage made it difficult to calculate the overall increase in torque during drilling of the aluminum layer. But when concentrating on the first contact between the tool and the aluminum layer, prior to chip clogging, a torque increase of at least 300% was seen.

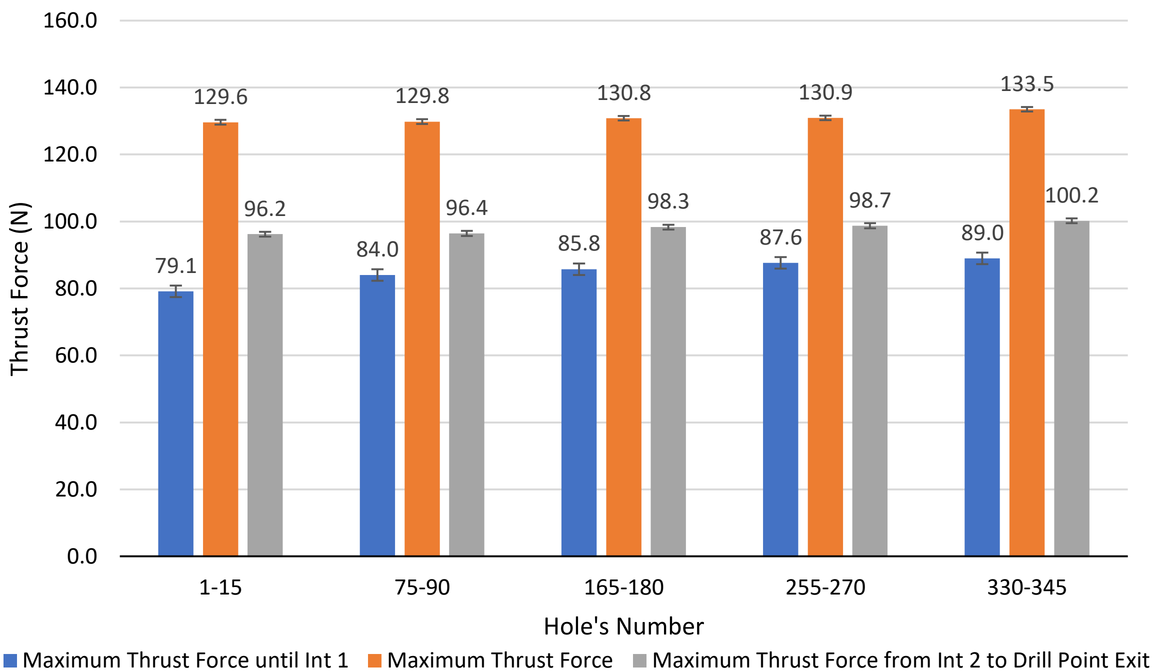

Figure 41. Evolution of the maximum thrust force in the plate type I along the 345 holes, using the drilling tool 2 (feed – 0.05 mm/rev; cutting speed – 300 m/min).

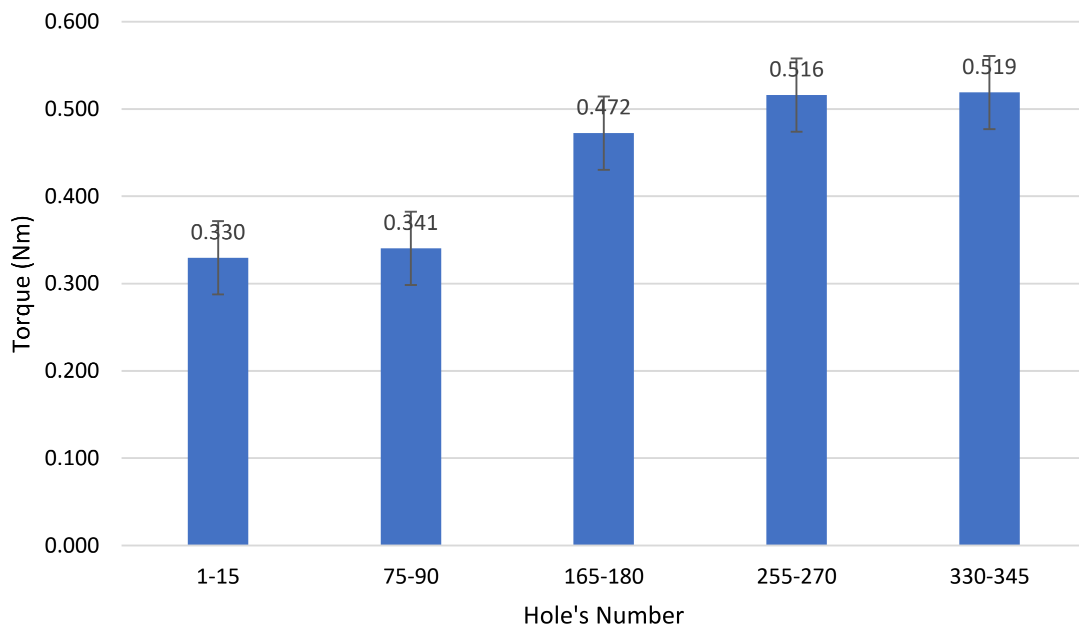

Figure 42. Evolution of the maximum torque in the plate type I along the 345 holes, using the drilling tool 2 (feed – 0.05 mm/rev; cutting speed – 300 m/min).

In Figures 43 and 44 the evolution of the maximum thrust force and torque is presented, respectively, until interface 1 (Int 1) and from interface 2 (Int 2) to the time of the drill point exit at type II configuration plate from the first 15 holes to the last 15 holes, using the drilling tool 2 with the drilling parameters: feed – 0.2 mm/rev and cutting speed – 150 m/min. The results are in accordance as before, where it is possible to see a lower increase of each drilling forces with the evolution of the first 15 holes drilled to a final total of 345 holes.

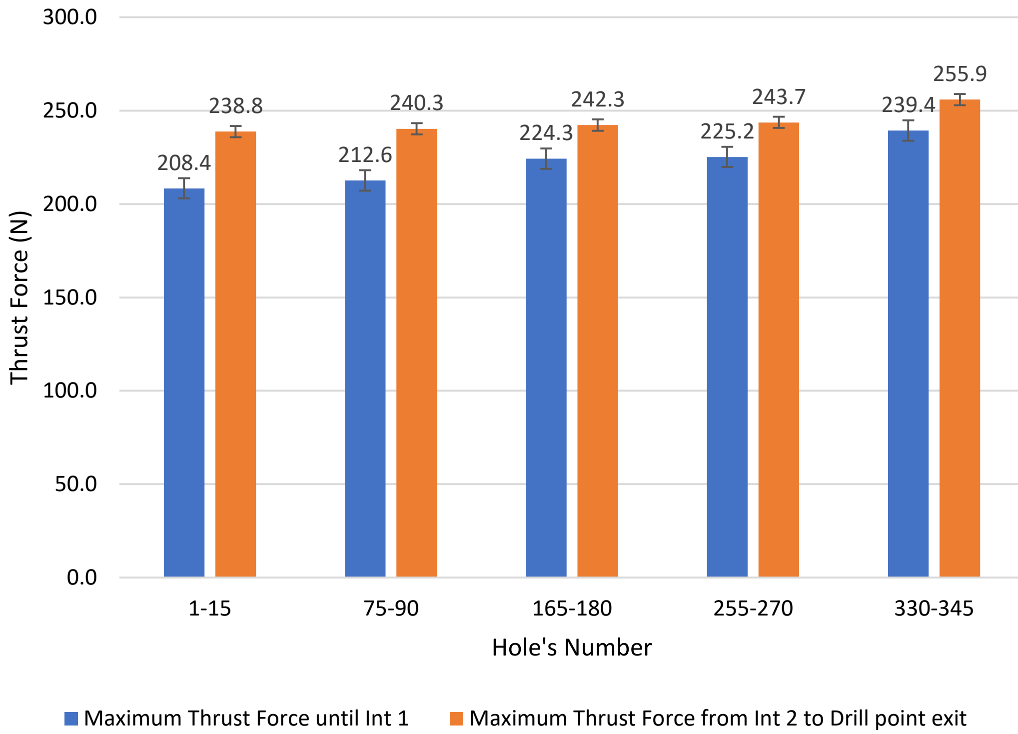

Figure 43. Evolution of the maximum thrust force in the plate type II along the 345 holes, using the drilling tool 2 (feed – 0.2 mm/rev; cutting speed – 150 m/min).

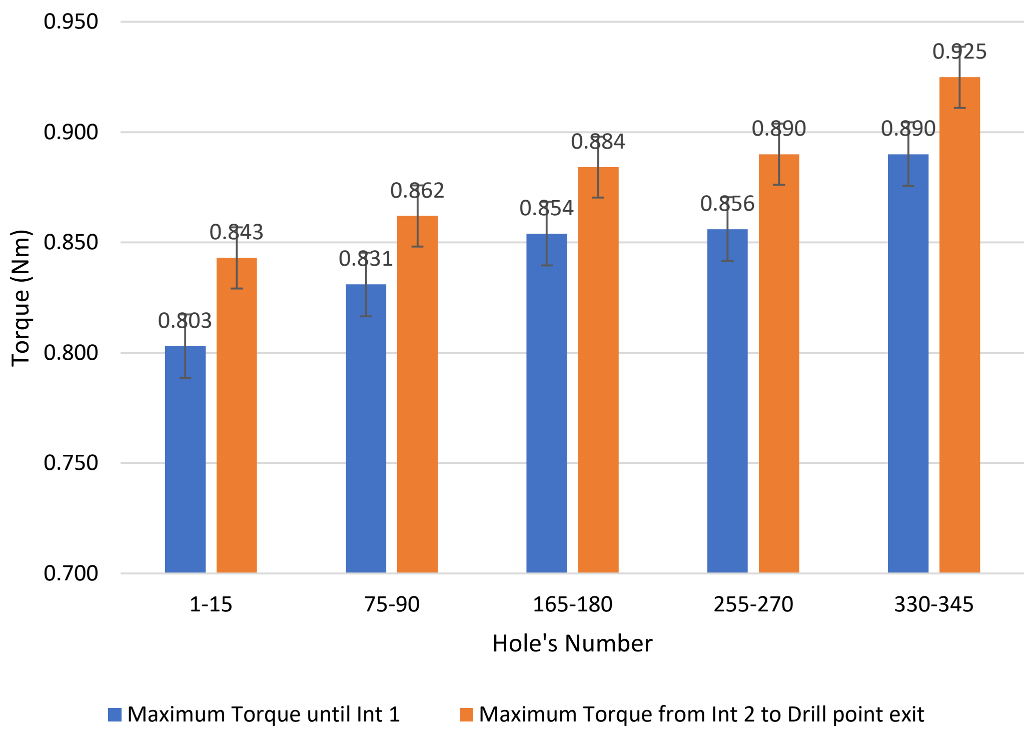

Figure 44. Evolution of the maximum torque in the plate type II along the 345 holes, using the drilling tool 2 (feed – 0.2 mm/rev; cutting speed – 150 m/min).

4.2. Delamination Analysis

Figure 45a and 45b present the delamination results of the same hole using two distinct methods, microscope, and X-ray analysis, respectively. This confirms that there is no intradelamination between CFRP and AA layers, given the two methods results consistency. Similar results (showing no delamination) were obtained for the type II plate. Consequently, the delamination defects were only observed in the plate of configuration type I, since, in the interior layer of the plate of configuration type II this type of defects was not observed. Further results of the delamination in the preliminary campaign are exhibited in Appendix B.

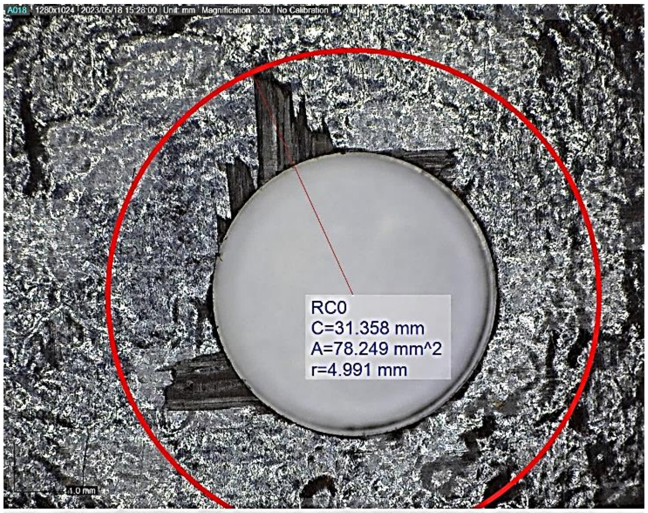

a)

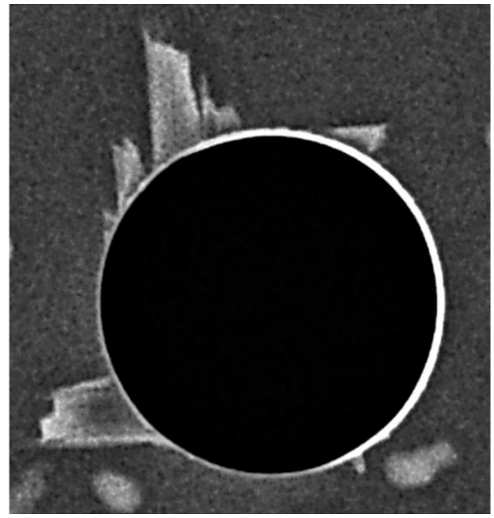

b)

Figure 45. Comparison delamination analysis by: (a) microscope and (b) X-ray analysis in the preliminary drilling campaign (i) with the drilling tool 1: feed rate – 0.3 mm/rev and cutting speed – 150 m/min.

The analysis of the delamination defects was studied essentially in the holes produced in the preliminary drilling campaign (i) in the plate of configuration type I with the drilling tool 1, since with the optimization of the parameters chosen for the drilling campaign with the drilling tool 2 (feed – 0.05 mm/rev; cutting speed – 300 m/min) this type of defects were not visualized, as presented in Figure 46. The delamination defects observed were only presented in the first layer of CFRP, so the type of delamination visualized is the peel-up delamination.

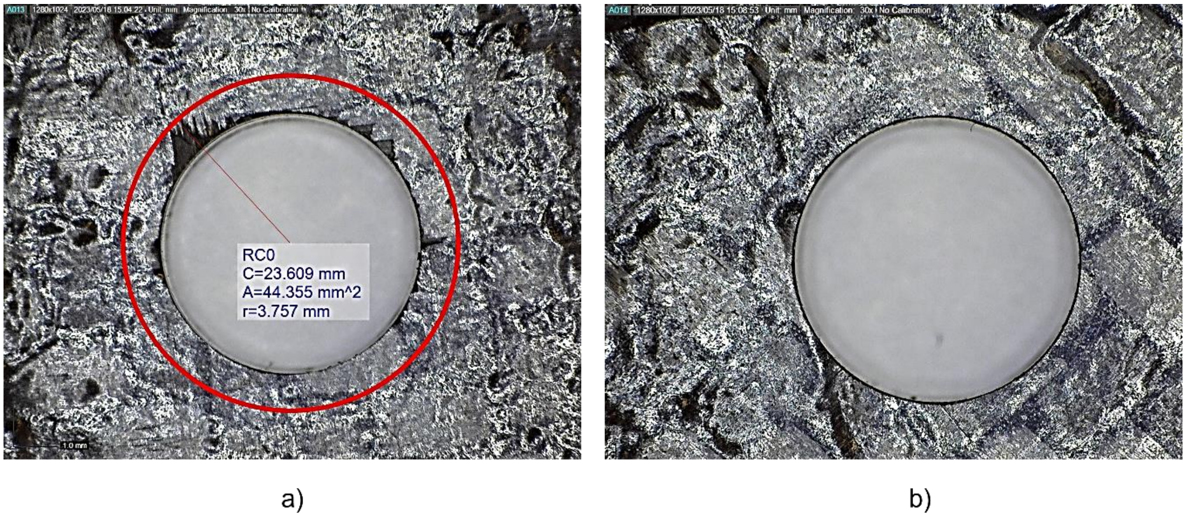

Figure 46. Delamination occurrence in: (a) drilled hole using the drilling tool 1 (with delamination) (feed – 0.05 mm/rev; cutting speed – 300 m/min); (b) drilled hole using the drilling tool 2 (without delamination) (feed – 0.05 mm/rev; cutting speed – 300 m/min).

In Table 8 are presented the values of the delamination factors obtained in the Matlab script, for the holes produced in the preliminary drilling campaign (i) with different drilling parameters. In Figure 47, the graphic corresponds to the adjusted delamination factor for the drilling tool 1 at various feed and cutting speed levels, which are highlighted in Table 8.

Table 8. Results of the two-dimensional delamination factors, conventional delamination factors, and adjusted delamination factors.

Hole Nr.	Feed (mm/rev)	Cutting Speed (m/min)	A_{nom}	A_{del}	D_{nom}	D_{max}	A_{max}	F_a	F_d	F_{da}
1	0.05	50	28.274	8.237	6	6.424	32.412	0.291	1.071	1.211
2	0.1	100	28.274	19.560	6	7.514	44.344	0.692	1.252	1.637
3	0.15	150	28.274	26.364	6	10.234	82.259	0.932	1.706	2.293
4	0.15	300	28.274	29.214	6	9.712	74.081	1.033	1.619	2.257
5	0.3	150	28.274	30.697	6	9.982	78.257	1.086	1.664	2.342
6	0.3	300	28.274	28.057	6	10.650	89.082	0.992	1.775	2.410

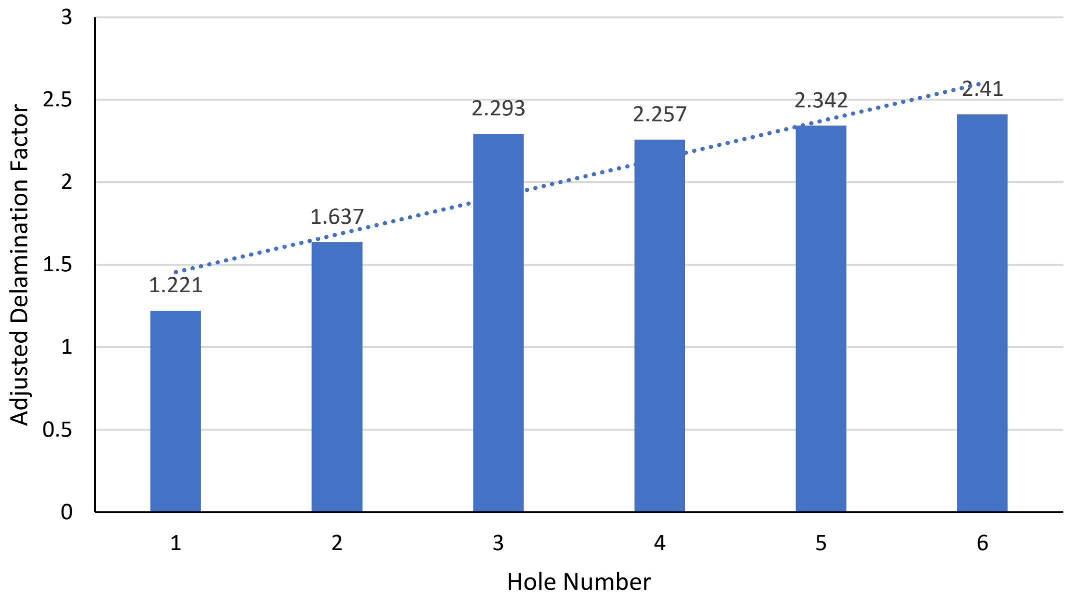

Figure 47. Adjusted delamination factor (F_{da}) for various combinations of feed and cutting speed (represented in Table 8) with the drilling tool 1.

From the analysis of the results in Table 8 and the graph in Figure 47, it can be seen that for the holes produced in the type I configuration plate with the drilling tool 1, the delamination damage increases with the increase of the drilling parameters. However, when analyzing the results for the maximum feeds (0.3 mm/rev) and for the maximum cutting speeds (300 m/min), it can be seen that the feed presents a greater contribution to the delamination increase. These aspects are in accordance with the study conducted by Geng et al. [66], where the relationship between delamination and feed rate and cutting speed demonstrates that raising the feed rate often causes an increase in delamination, however the impact of cutting speed on delamination can vary depending on the particular drilling conditions. Also, regression research and empirical models of the study of Geng et al. [66] have shed light on what might have happened in drilling scenarios. Based on these findings, it is frequently advised in industrial practice to maintain drilling efficiency while using a relatively high cutting speed and a low feed rate, which was what exactly had been used in this work in the drilling campaign (ii) of the configuration type I with the drilling tool 2 (feed – 0.05 mm/rev; cutting speed – 300 m/min).

4.3. Burr and Uncut Fibers

Both burr and uncut fiber defects were observed during the drilling of both types of multi-material configurations.

Regarding the burr defects, these were present in most of the holes produced by the drilling tool 1 during the preliminary drilling campaign (i), while this defect was not visualized in any hole in the drilling campaign (ii) with the drilling tool 2 with the optimized cutting parameters for the plate of configuration type II. Figure 48 illustrates the DinoLite digital USB microscope images of two holes obtained with the drilling tool 1 during the preliminary drilling campaign (i), where burr defects are clearly seen.

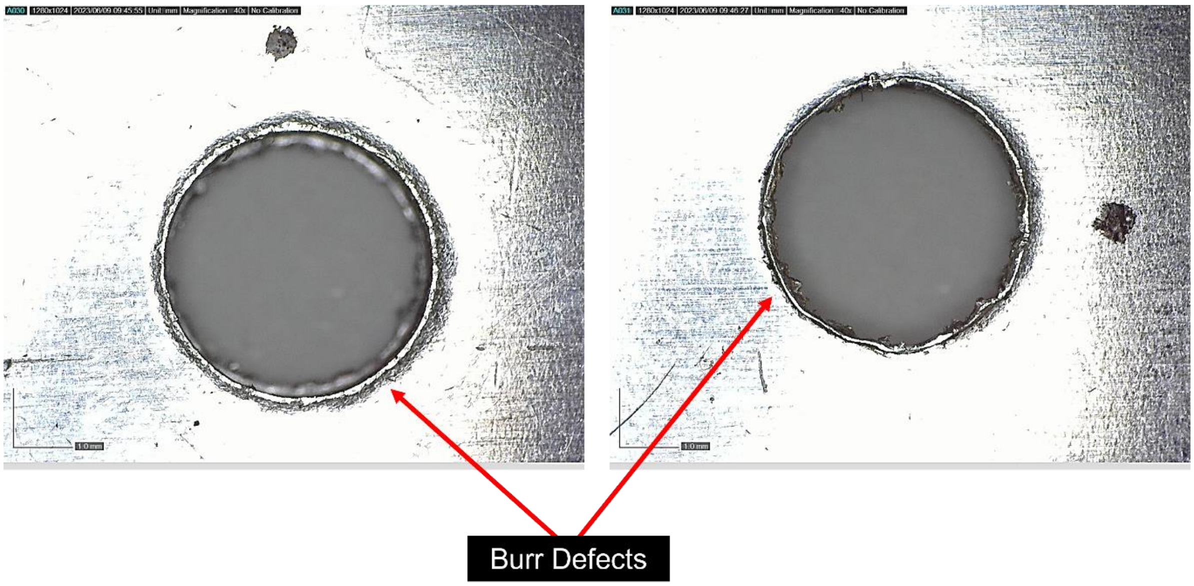

Figure 48. Presence of burr defects in the holes produced by the drilling tool 1 (feed – 0.05 mm/rev; cutting speed – 300 m/min) in the configuration type II.

Concerning the burr defects in the type I configuration, upon comparing the previous image (Figure 48) with Figure 49, it becomes evident that the burr defects in the type II configuration are more pronounced.

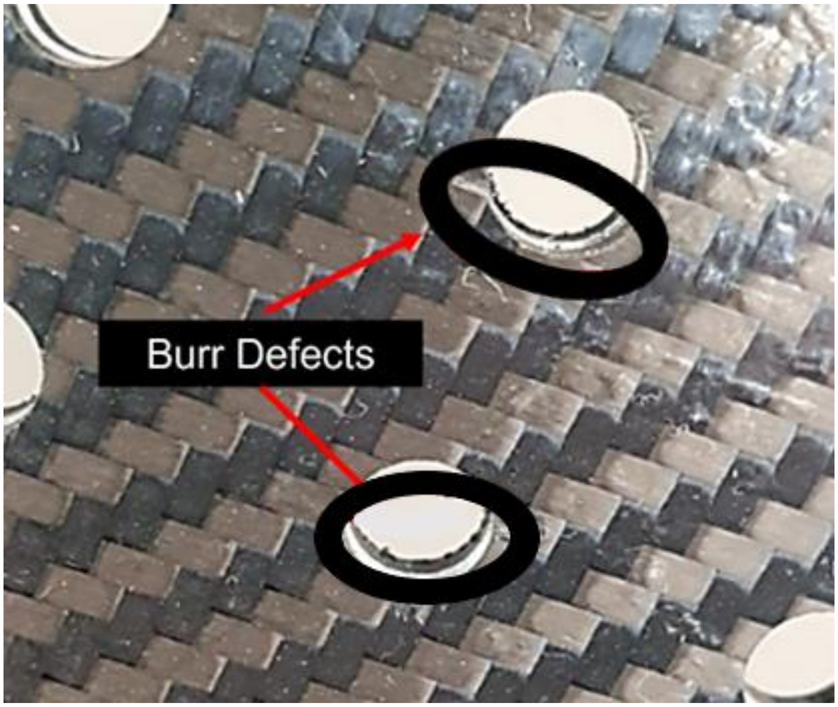

Figure 49. Presence of burr defects in the holes produced by the drilling tool 1 (feed – 0.05 mm/rev; cutting speed – 300 m/min) in the configuration type I.

On the other hand, in the drilling campaign (ii) with the drilling tool 2, in some (few) holes it was observed the existence of uncut fibers of the inner CFRP layer, while drilling the type II configuration. In Figure 50 it is presented the images obtained in the DinoLite digital USB microscope and in the X-ray analysis of the holes with the presence of uncut fibers.

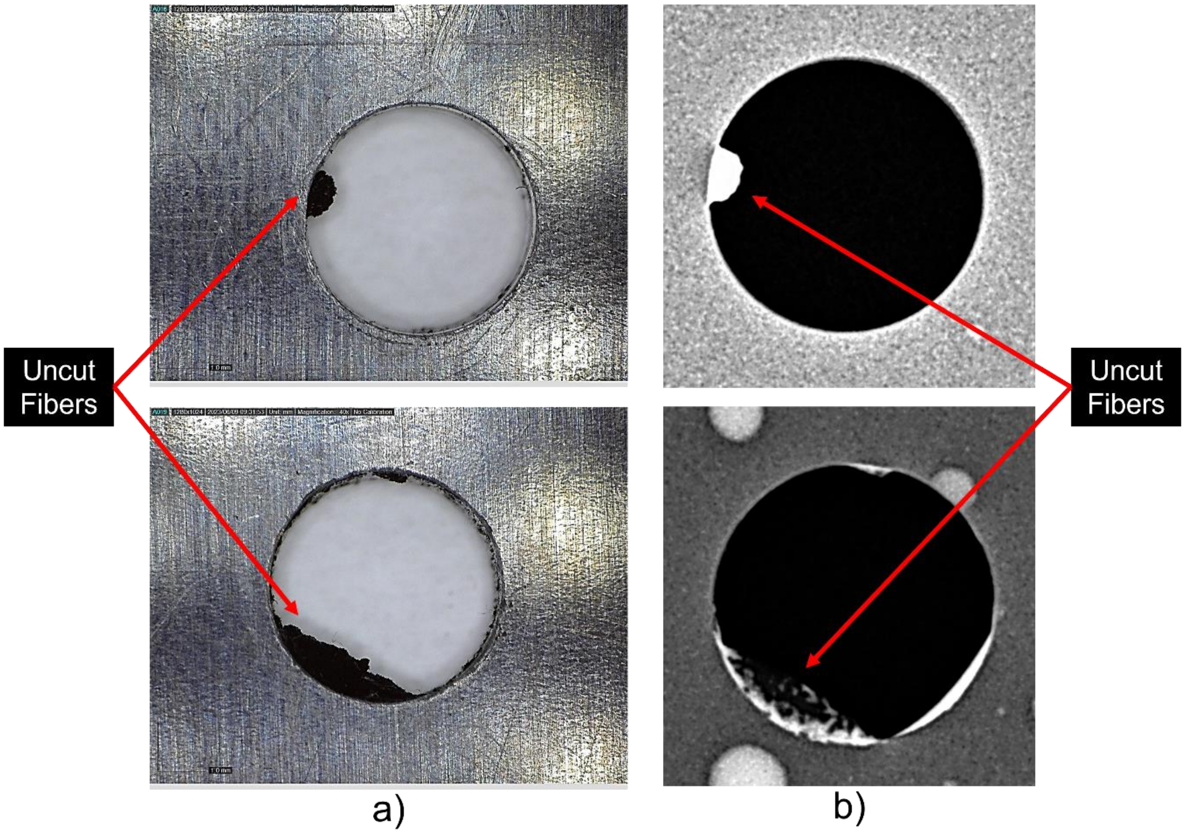

Figure 50. Presence of uncut fibers in the holes produced by the drilling tool 2 (feed – 0.2 mm/rev; cutting speed – 150 m/min) in the configuration type I. Images taken by: (a) DinoLite digital USB microscope; (b) X-ray analysis.

4.4. Hole' Surface Roughness

By analyzing the roughness values – arithmetic average roughness (Ra) and average maximum height of the profile (Rz) – from the graphs in Figures 51, 52, 53 and 54, it can be seen that the surface quality of the holes obtained with the drilling tool 2 were better than those obtained with the drilling tool 1, in both plate configurations.

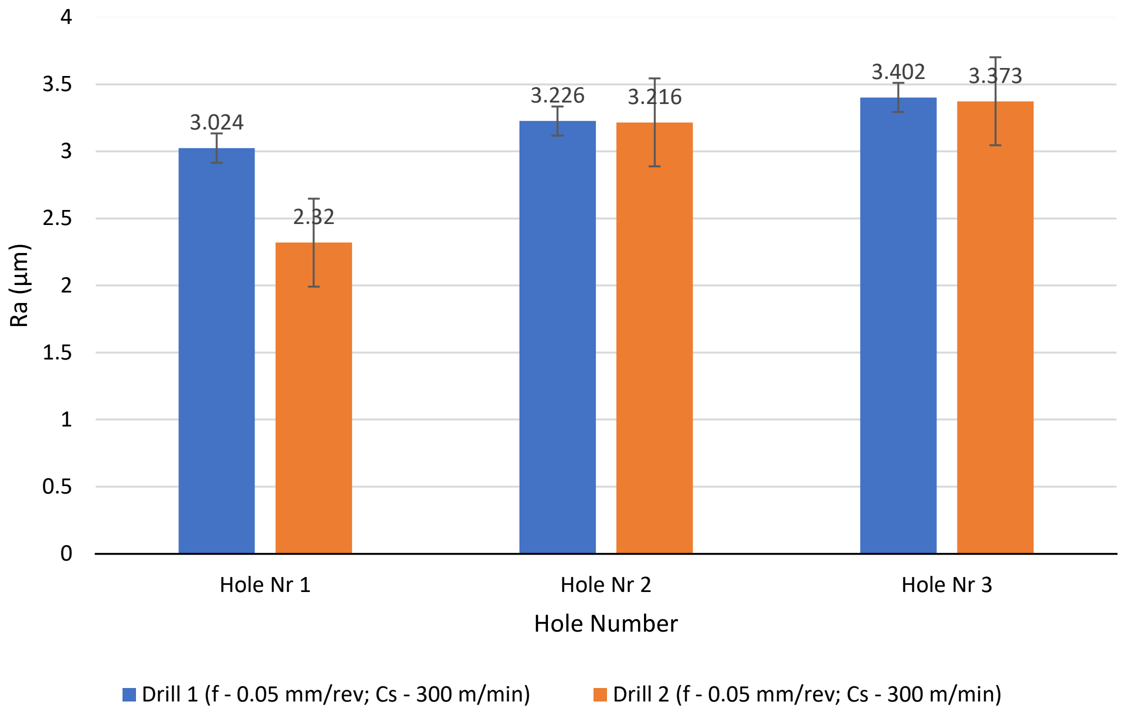

Figure 51. Arithmetic average roughness (Ra) in the holes of the configuration type I.

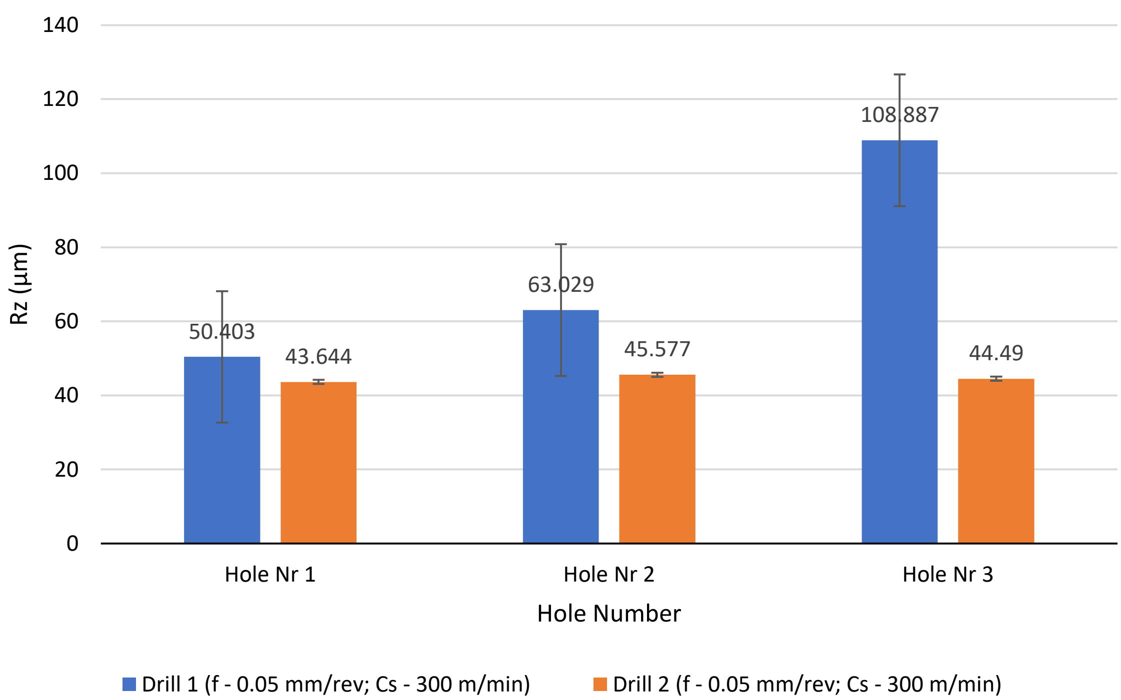

Figure 52. Average Maximum Height of the Profile (Rz) in the holes of the configuration type I.

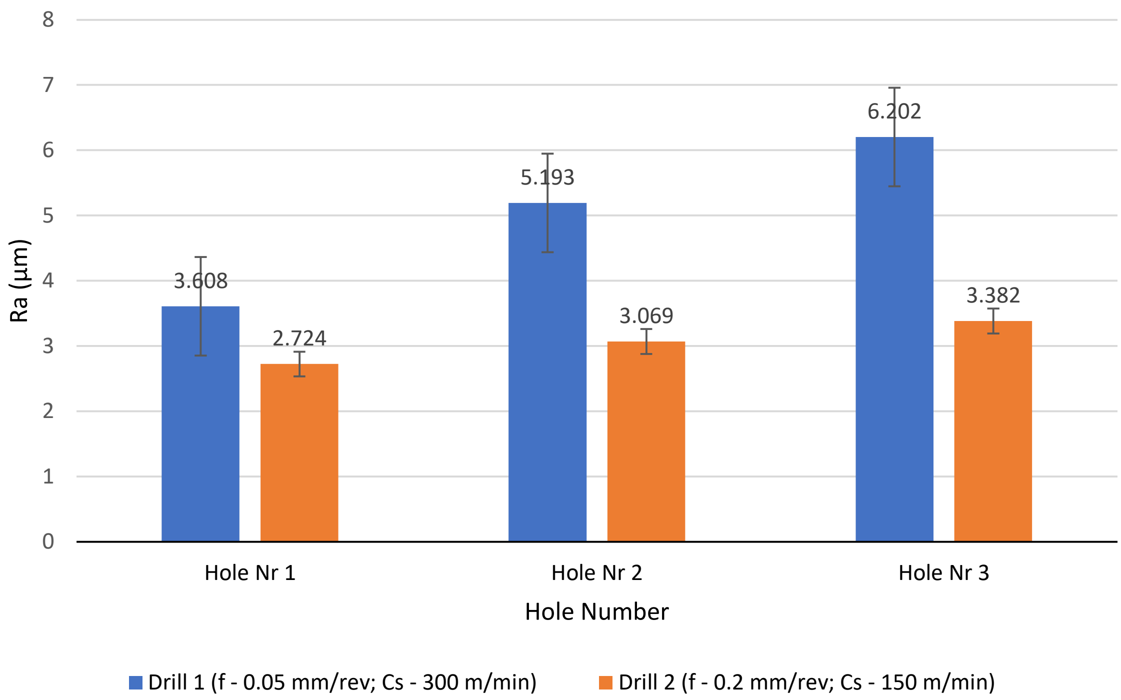

Figure 53. Arithmetic average roughness (Ra) in the holes of the configuration type II.

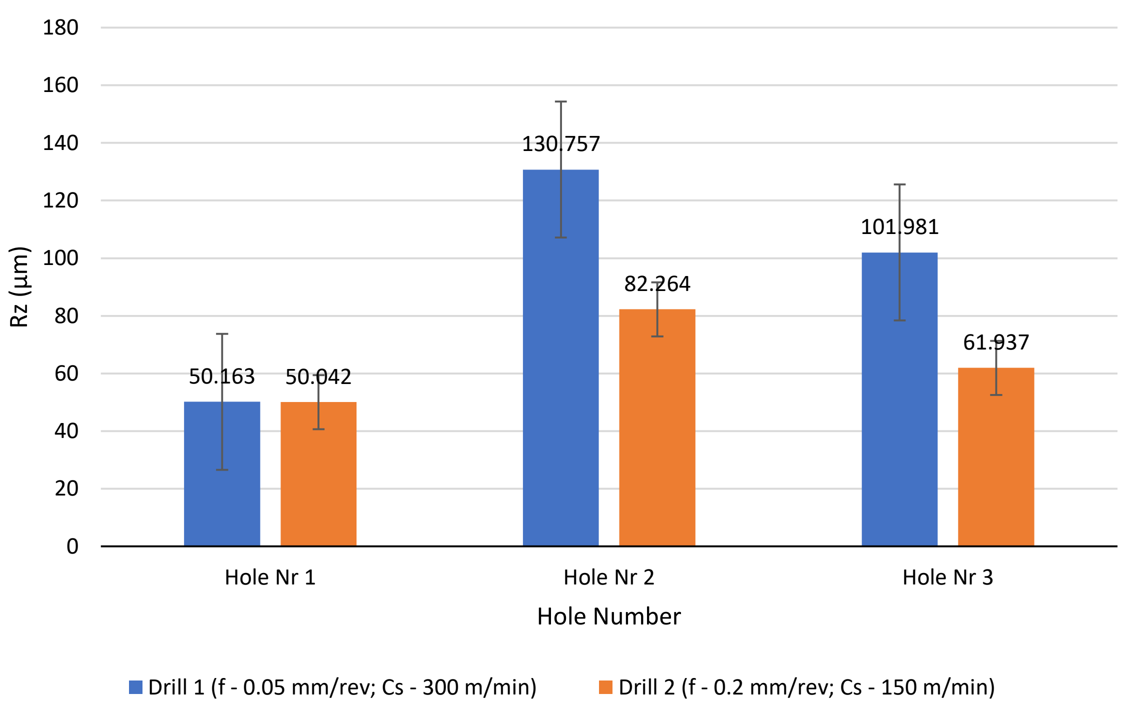

Figure 54. Average Maximum Height of the Profile (Rz) in the holes of the configuration type II.

4.5. Chip Analysis

The problem of chip removal, which has a direct impact on the quality of the drilled hole's wall surface, is one of the major difficulties in drilling CFRP/AA laminates. Non-fragmented drilling chips that are stuck in the aluminum layer have tendency to entangle around the drilling tool. When the CFRP layer is positioned above the aluminum layer, the rolling up of the chips can adversely affect the geometric and dimensional properties of the hole [1].

For type II plate configuration two distinct chip morphologies could be observed. Whereas for the upper layer uniform and long spiral chips were collected, for the bottom layer tangled chips occurred. Such fact evidences the more effective chip evacuation in the upper layer. Among possible explanations: (i) as the drilling tool gets deeper in the manufactured hole, there is a bigger difficulty in successful chip evacuation; (ii) the CFRP middle layer seems to interrupt uniform spiral chip formation and to hinder its formation at the third layer (AA). The relative higher softening (and also higher surface roughness) of the CFRP may promote chip entrapment at the composite layer. As can be seen from the schematic in Figure 55, through the uniform chip geometry visualized in the upper aluminum layer it can be seen that the chip was effectively evacuated by the drilling tool. As the lower aluminum layer is drilled after the inner CFRP layer, it was verified that the chip generated at that moment presented an irregular geometry, as the CFRP layer did not allow the correct evacuation of the chip.

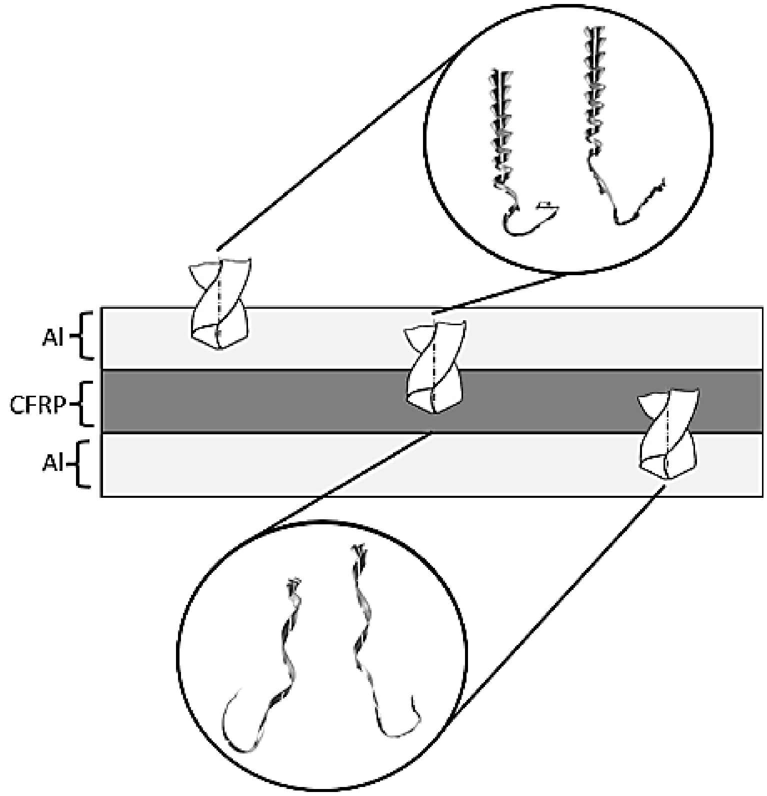

Figure 55. Chip geometry in different stages during the drilling of the configuration type II with the drilling tool 2 with the drilling parameters: feed – 0.2 mm/rev and cutting speed – 150 m/min.

In the case of the type I configuration only the irregular geometry of the aluminum chip was verified, as presented in the scheme of Figure 56. As previously explained, the CFRP layer prior to the aluminum layer did not allow the correct evacuation of the chip. The fragmented CFRP chips observed in both configurations are illustrated in Figure 57.

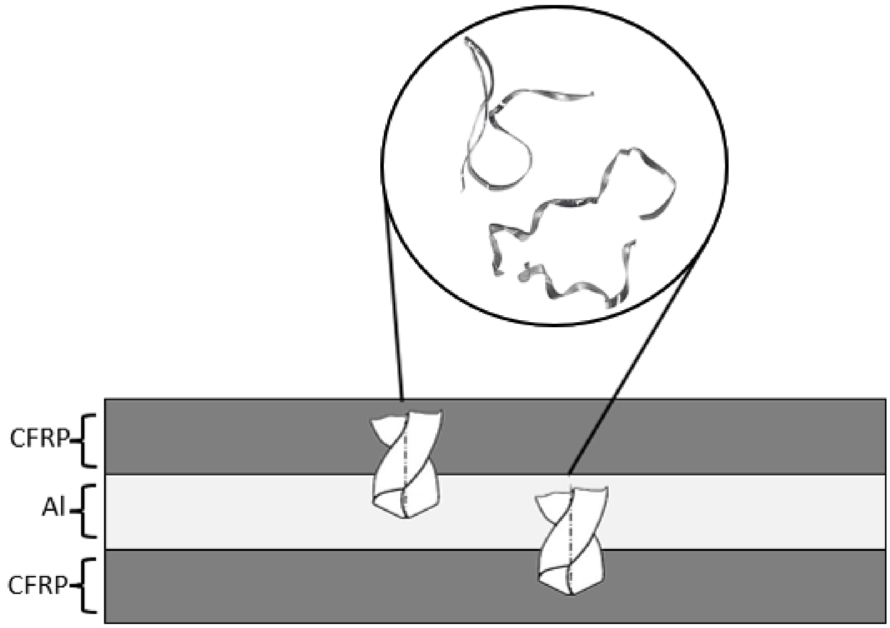

Figure 56. Chip geometry in different stages during the drilling of the configuration type I with the drilling tool 2 with the drilling parameters: feed – 0.05 mm/rev and cutting speed – 300 m/min.

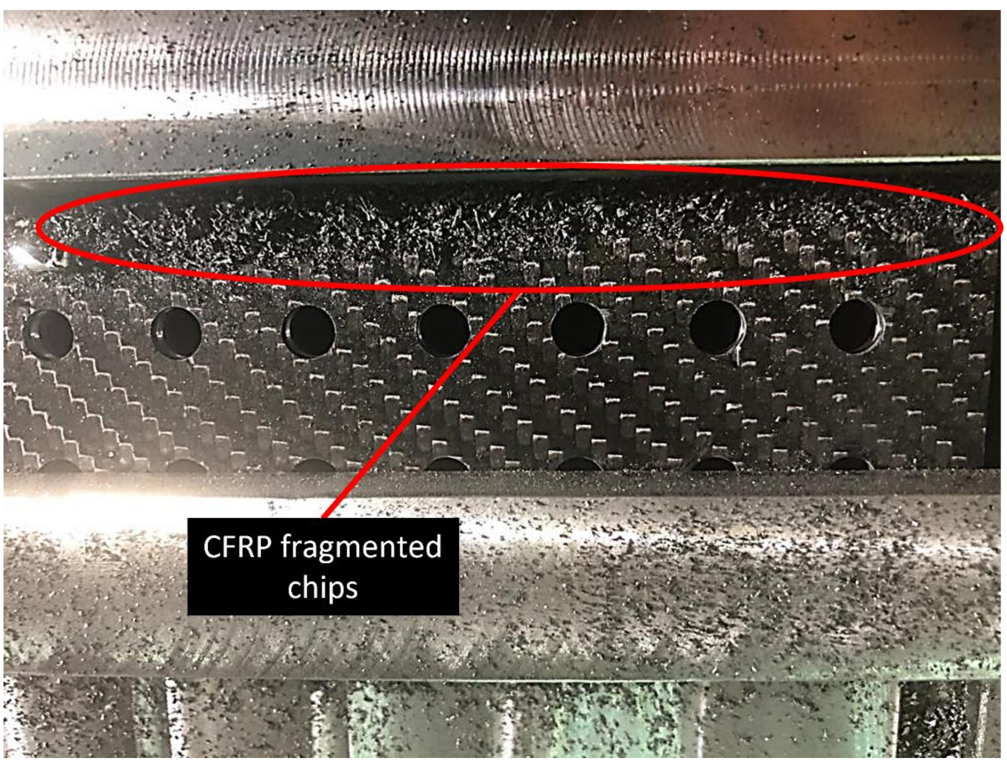

Figure 57. CFRP fragmented chips.

These aspects concerning chip formation and evacuation were observed during the drilling campaign (ii) of the two multi-material plate configurations. When drilling the two configurations, the chip adherence to the drilling tool, as shown in Figure 58, was verified for the cases where there was no correct chip evacuation due to the presence of a CFRP layer prior to another aluminum layer. In the case of the type II configuration, the chips that could be effectively evacuated in the first aluminum layer were those that were not coiled in the tool and presented a uniform geometry. Regarding the drilling of the CFRP layer, powder-like chips were observed. Figure 59 demonstrate the adherence of these CFRP chips to the non-fragmented aluminum chips.

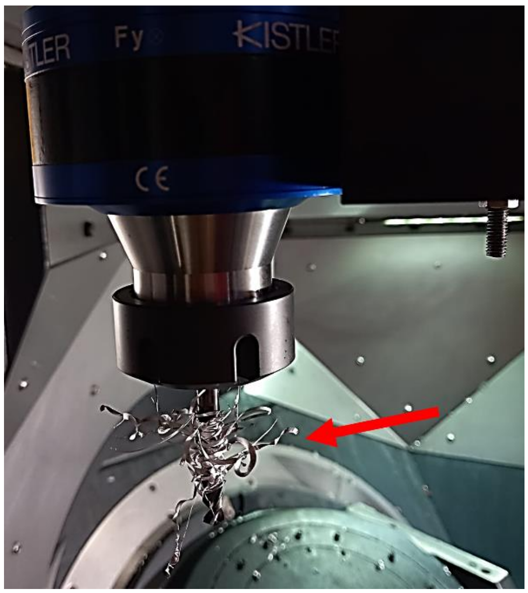

Figure 58. Chip adherence to the drilling tool 2 observed during the drilling campaign (ii).

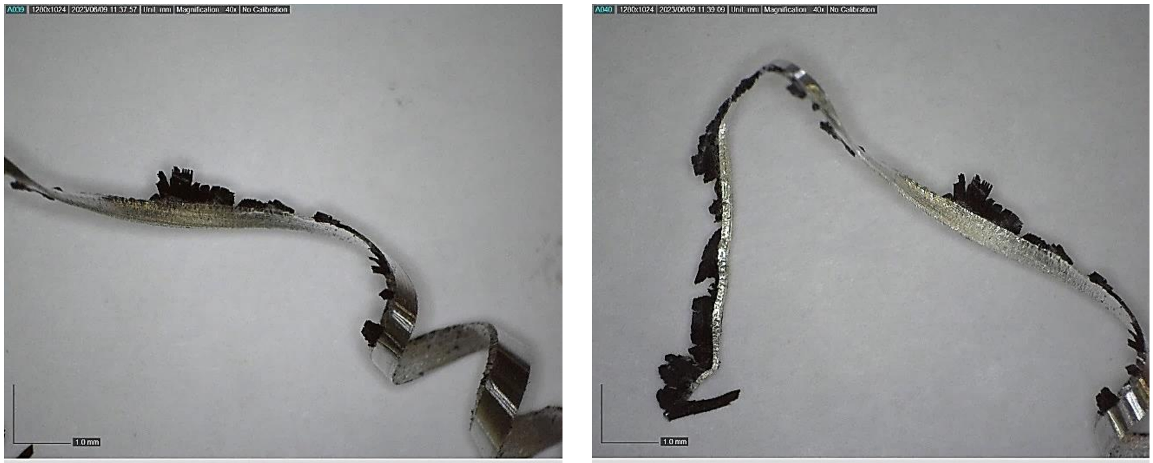

a) b)

Figure 59. CFRP chips with adherence to the non-fragmented aluminum chips – images taken in the DinoLite microscope.

Another problem that was observed in the drilling campaigns was the surface quality of the holes, as long and non-fragmented aluminum chips that were not evacuated properly created circular scratches on the surface of the hole. Figure 60 shows these defects during preliminary tests with the drilling tool 1 (Figure 60a) and in subsequent tests with the drilling tool 2 (Figure 60b).

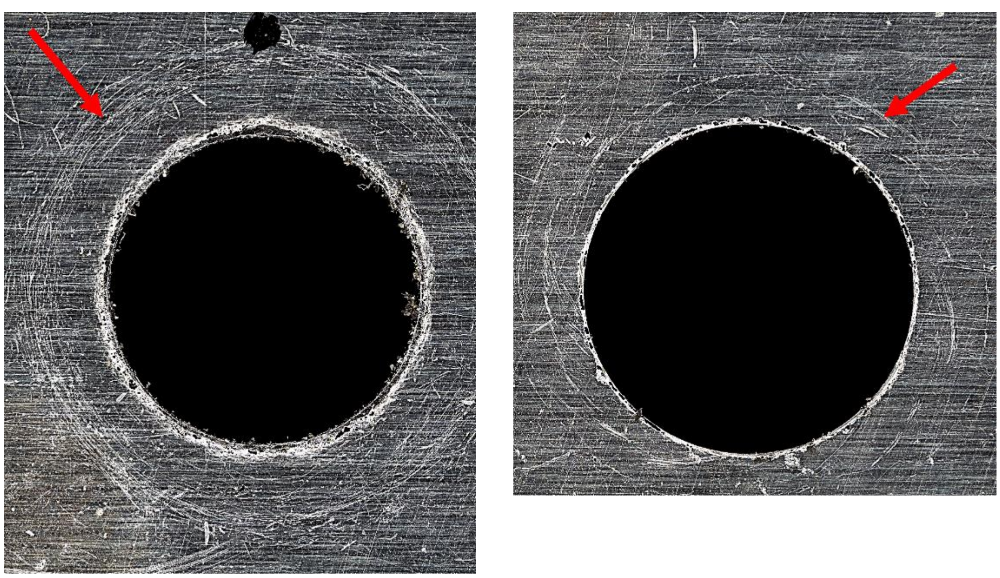

a) b)

Figure 60. Circular surface scratches created by the entangled aluminum chips in the drill in the configuration type II with: (a) the drilling tool 1 (feed – 0.05 mm/rev; cutting speed – 300 m/min) and (b) drilling tool 2 (feed – 0.2 mm/rev; cutting speed – 150 m/min).

By comparing the two situations, it's possible to assume that despite different cutting speeds, the chips in aluminum are longer for low feed rates, being this the cause for the appearance of more circular scratches defects in the first situation (Figure 60a). These results are in accordance with the study of Sridhar et al. [47], where it was concluded that as the feed rate increased from 0.1 mm/rev to 0.4 mm/rev, the size of the aluminum chips decreased. At lower feed rates, the shearing section is smaller, which makes it easier for the chips to wind up and produce long, continuous chips.

4.6. Tool Wear Inspection

The two main wear mechanisms (abrasive wear and tool edge chipping) on cutting tools that are, normally, noticed when drilling CFRPs, where not present during the drilling campaign (ii) in this work. However, while drilling aluminum alloys, the main wear mechanisms impacting cutting tools are adhesion wear, diffusion, and built-up edge (BUE), which is the term to describe the erratic and unstable structure created by the material being deposited on the tool-chip contact. The CFRP/AA laminate drilling wear processes seem to be a combination of adhesion wear and abrasive wear [1].

Regarding the tool wear analysis with the drilling tool 2 used in the type I configuration, it was not verified the existence of abrasive wear. This is proved by the comparison made in Figure 61, where the cutting edges of the tool are represented after drilling the first 15 holes (Figure 61a) and at the end of 345 holes (Figure 61b).

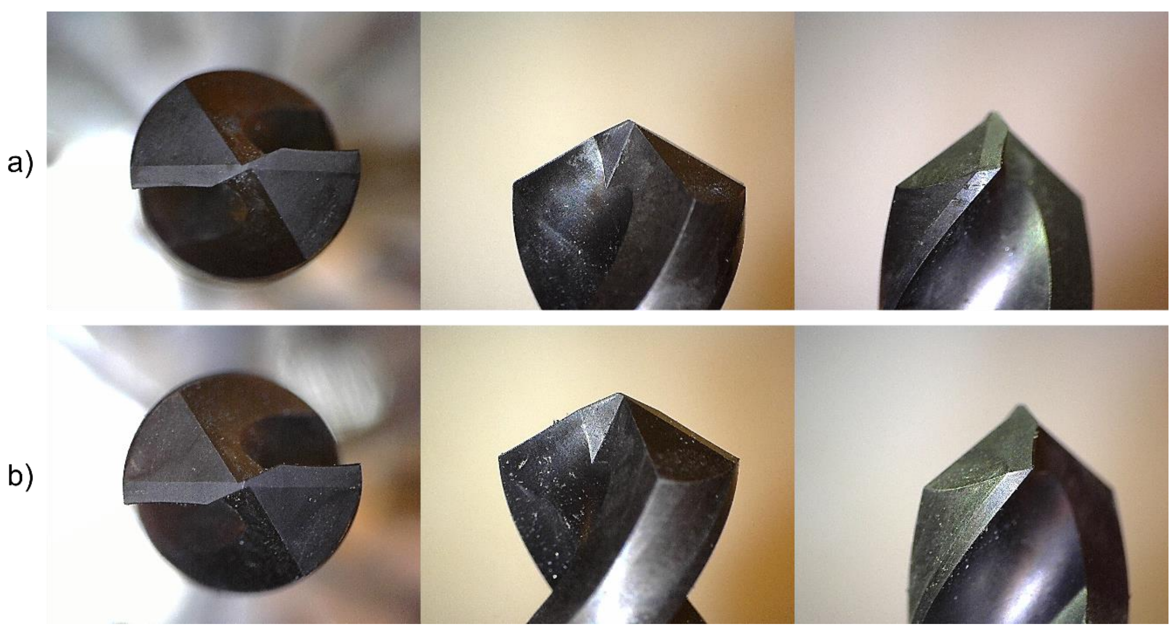

Figure 61. Wear analysis of the cutting edges of the drilling tool 2 after drilling: (a) 15 holes and (b) 345 holes (feed – 0.05 mm/rev; cutting speed – 300 m/min) in the configuration type I.

For the case of the drilling tool 2 used in the type II configuration, it is also verified the inexistence of abrasive wear on the cutting edges when compared in Figure 62 the drilling tool geometry at the end of the drilling of the first 15 holes (Figure 62a) and at the end of the 345 holes (Figure 62b). In this configuration (AA/CFRP/AA) only a greater adherence of aluminum chips to the edges of the drilling tool (BUE) is observed since this configuration has more layers of aluminum than the type I configuration. This adherence of aluminum to the drilling tool could be detrimental to the tool life if the experimental drilling campaign did not end at 345 holes. However, for this number of holes tested in the experimental drilling campaign, this had little impact on wear and tool life.

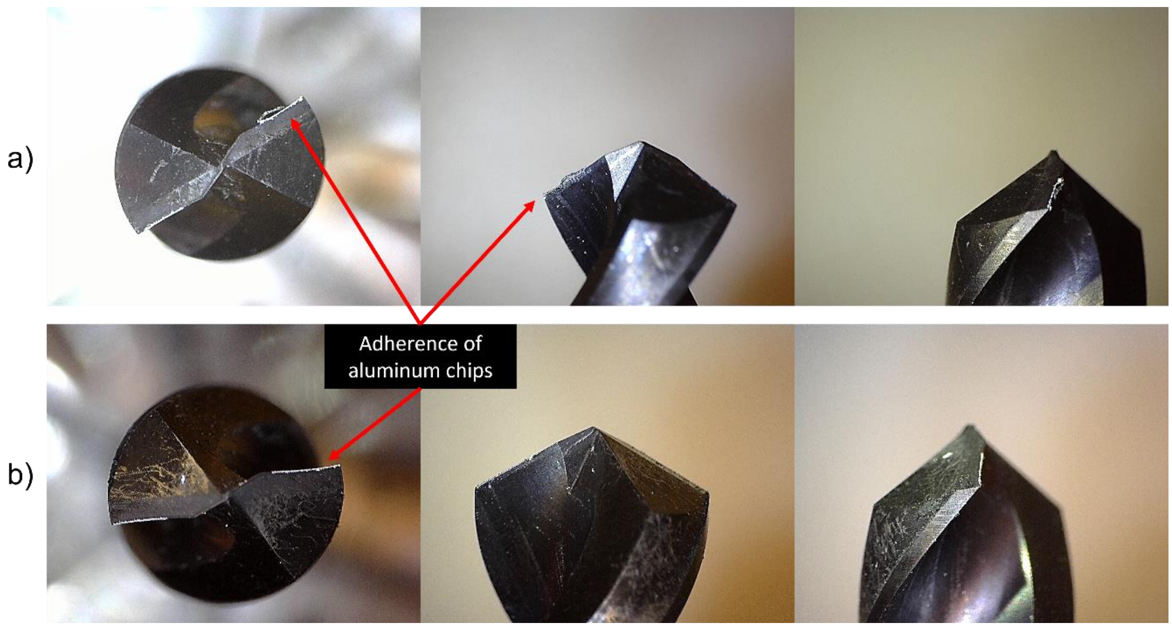

Figure 62. Wear analysis of the cutting edges of the drilling tool 2 after drilling: (a) 15 holes and (b) 345 holes (feed – 0.2 mm/rev; cutting speed – 150 m/min) in the configuration type II.

For each drilling tool 2 used in each configuration, the other results of the wear analysis in the number holes between the first 15 and the last 345, are presented in Appendix C.

Chapter 5

Conclusions and Future Works

5.1. Conclusions

The drilling of CFRP/AA multi-materials utilizing WC-Co CVD diamond coated tools were experimentally studied and the impact of the drilling parameters, including feed rate and cutting speed, as well as the drilling tools geometry was analyzed. Comparisons were made utilizing the cutting loads (thrust force and drilling torque), as well as metrics for the quality of the holes (delamination, burr, uncut fibers, and surface quality). Additionally, a wear study was carried out to access the wear patterns on the tested CVD diamond coated tools and a chip analysis was done to better understand the drilling process in these materials. The following will be a presentation of the key findings from the study that was developed.

Regarding cutting loads, both thrust force and torque were evaluated in the two multi-material configurations. It was found that the cutting forces are substantially higher in the aluminum layers when compared to the CFRP layers, confirming the relative brittleness of CFRP fibers when loaded in shear/compression. On the other hand, higher cutting loads were observed when drilling the AA/CFRP/AA configuration plate, when compared to the CFRP/AA/CFRP configuration plate. Although the cutting speed was lower in the former plate (150 m/min instead of 300 m/min), it was found that the feed increase (0.2 mm/rev instead of 0.05 mm/rev) in this configuration was the main contribution to the appearance of higher values of the cutting loads, thus validating its relation with the geometrical definition of the cutting phenomena.

The delamination factor calculation was only performed on the holes obtained by the drilling tool 1 on the type I configuration plate (CFRP/AA/CFRP), since such defects were not observed using the drilling tool 2 and also the absence of inner delamination was observed through X-ray analysis. The results show an increase of the delamination area with the increase of the drilling parameters. However, it was found that increasing the feed rate contributed more substantially than increasing the cutting speed to the evolution of the delamination defects.

Regarding burr occurrence, more severe defects were noticed when drilling the AA/CFRP/AA configuration plate with the drilling tool 1. However, with the optimization of the drilling parameters (feed – 0.2 mm/rev; cutting speed – 150 m/min) and with the drilling tool 2, such defect was corrected. Despite this optimization with the drilling tool 2, uncut fibers of the inner CFRP layer were still present in some holes.

In the chip analysis, the presence of CFRP powdered chips were observed, while regarding the aluminum chips, it presented a long and non-fragmented geometry. Regarding the evacuation of the aluminum chips, it was concluded that, in the upper aluminum layer of AA/CFRP/AA configuration plate, this was effectively managed by the drill tool, while in the inner and lower aluminum layers challenges in chip evacuation occurred, leaving the chips stuck in the drilling tool, creating circular scratches on the surface of the plate. CFRP layers seemed to act as barrier for the correct evacuation of the chip subsequent aluminum layer.

Finally, no significant wear was noticed on each of the two drilling tools employed on the two distinct plate configurations (for an approximate drilled distance of 1550 mm). Still, aluminum adhesion was noticed on the flank face of drilling tool 2 used for drilling the AA/CFRP/AA configuration plate, which may indicate further possible wear in this tool region. In sum, drilling operational conditions that promote a very stable (minimal) tool wear within acceptable productivity range were identified.

5.2. Future Works

Following the creation of this work, a number of other areas connected to this theme might be explored in order to improve the outcomes and increase information about the subject under study. Several ideas include the following:

- Thermal sensing technology analysis of drilling experiments would give more information into the drilling process;
- Inspect wear tendencies for higher removal rates using the drilling tool 2 to estimate maximum level of wear allowed;
- Correlate thrust force levels with delamination occurrence and possible identification of load thresholds. The usage of a fracture mechanics approach (including an experimental mode I and II fracture characterization campaign) may be useful for the linkage of fracture properties of the present laminates and its delamination-based failure;
- Understanding the intralaminar delamination through orthogonal/oblique cutting testing methodologies in order to scale down the drilling operation and be able to perform predictive finite element analysis.

References

[1] G. Franz, P. Vantomme, and M. H. Hassan, "A Review on Drilling of Multilayer Fiber-Reinforced Polymer Composites and Aluminum Stacks: Optimization of Strategies for Improving the Drilling Performance of Aerospace Assemblies," *Fibers*, vol. 10, no. 9. MDPI, Sep. 01, 2022.

[2] F. C. Campbell, *Structural Composite Materials*, ASM International. 2010.

[3] R. Hsissou, R. Seghiri, Z. Benzekri, M. Hilali, M. Rafik, and A. Elharfi, "Polymer composite materials: A comprehensive review," *Composite Structures*, vol. 262. Elsevier Ltd, Apr. 15, 2021.

[4] S. T. Peters, *Handbook of Composites*. 1998.

[5] B. Parveez, M. I. Kittur, I. A. Badruddin, S. Kamangar, M. Hussien, and M. A. Umarfarooq, "Scientific Advancements in Composite Materials for Aircraft Applications: A Review," *Polymers*, vol. 14, no. 22. MDPI, Nov. 01, 2022.

[6] D. Gay, S. V. (Suong V.) Hoa, and S. W. Tsai, *Composite materials : design and applications*. CRC Press, 2003.

[7] W. S. University, *DEPARTMENT OF DEFENSE HANDBOOK COMPOSITE MATERIALS HANDBOOK VOLUME 3. POLYMER MATRIX COMPOSITES MATERIALS USAGE, DESIGN, AND ANALYSIS AMSC N/A AREA CMPS DISTRIBUTION STATEMENT A. Approved for public release; distribution unlimited*, vol. 3. SAE International, 2002.

[8] M. Maria, "Advanced composite materials of the future in aerospace industry," *INCAS BULLETIN*, vol. 5, no. 3, pp. 139–150, Sep. 2013.

[9] M. Hirz and P. Rossbacher, "Enhanced knowledge-based 3D-CAD methods supporting automotive body-in-white production engineering Alternative propulsion technologies, new mobility conceps View project Robot Charging View project ENHANCED KNOWLEDGE-BASED 3D-CAD METHODS SUPPORTING AUTOMOTIVE BODY-IN-WHITE PRODUCTION ENGINEERING," 2016. [Online]. Available: https://www.researchgate.net/publication/303749155

[10] A. Brent. Strong, *Fundamentals of composites manufacturing : materials, methods and applications*. Society of Manufacturing Engineers, 2008.

[11] J. Fleischer, R. Teti, G. Lanza, P. Mativenga, H. C. Möhring, and A. Caggiano, "Composite materials parts manufacturing," *CIRP Annals*, vol. 67, no. 2, pp. 603–626, Jan. 2018.

[12] K. Bilisik, N. S. Karaduman, and N. E. Bilisik, "3D Fabrics for Technical Textile Applications," in *Non-woven Fabrics*, InTech, 2016.

[13] "Satin vs Twill | Fabric Weaves Explained – LYVANNA." https://lyvanna.com/blogs/blog/silk-satin-vs-silk-twill-what-are-fabric-weaves (accessed Apr. 12, 2023).

[14] S. M. Sapuan, “Composite Materials,” in *Composite Materials*, Elsevier, 2017, pp. 57–93.

[15] B. Suresh Kumar, N. Baskar, and K. Rajaguru, “Drilling operation: A review,” in *Materials Today: Proceedings*, Elsevier Ltd, 2020, pp. 926–933.

[16] F. Klocke, *Manufacturing Processes 1*. in RWTHedition. Berlin, Heidelberg: Springer Berlin Heidelberg, 2011.

[17] L. Zhang, Z. Liu, W. Tian, and W. Liao, “Experimental studies on the performance of different structure tools in drilling CFRP/Al alloy stacks,” *International Journal of Advanced Manufacturing Technology*, vol. 81, no. 1–4, pp. 241–251, Oct. 2015.

[18] Y. Zhang, D. Wu, and K. Chen, “A theoretical model for predicting the CFRP drilling-countersinking thrust force of stacks,” *Compos Struct*, vol. 209, pp. 337–348, Feb. 2019.

[19] L. G. Turnad and A. Bambang, “Cutting force and temperature variation in bone drilling - A review,” *Adv Mat Res*, vol. 845, pp. 934–938, 2014.

[20] C. Y. Wang, Y. H. Chen, Q. L. An, X. J. Cai, W. W. Ming, and M. Chen, “Drilling temperature and hole quality in drilling of CFRP/aluminum stacks using diamond coated drill,” *International Journal of Precision Engineering and Manufacturing*, vol. 16, no. 8, pp. 1689–1697, Jun. 2015.

[21] M. Sato, H. Tanaka, and K. Yamamoto, “Temperature variations in drilling of CFRP/aluminum and CFRP/titanium stacks,” *International Journal of Automation Technology*, vol. 10, no. 3, pp. 348–355, 2016.

[22] D. Geng, Y. Teng, Y. Liu, Z. Shao, X. Jiang, and D. Zhang, “Experimental study on drilling load and hole quality during rotary ultrasonic helical machining of small-diameter CFRP holes,” *J Mater Process Technol*, vol. 270, pp. 195–205, Aug. 2019.

[23] I. Sultana, Z. Shi, H. Attia, and V. Thomson, “A new hybrid oscillatory orbital process for drilling of composites using superabrasive diamond tools,” *CIRP Ann Manuf Technol*, vol. 65, no. 1, pp. 141–144, 2016.

[24] M. Aamir, K. Giasin, M. Tolouei-Rad, and A. Vafadar, “A review: drilling performance and hole quality of aluminium alloys for aerospace applications,” *Journal of Materials Research and Technology*, vol. 9, no. 6. Elsevier Editora Ltda, pp. 12484–12500, Nov. 01, 2020.

[25] M. Aamir, M. Tolouei-Rad, K. Giasin, and A. Nosrati, “Recent advances in drilling of carbon fiber–reinforced polymers for aerospace applications: a review,” *International Journal of Advanced Manufacturing Technology*, vol. 105, no. 5–6, pp. 2289–2308, Dec. 2019.

[26] N. Geier, J. P. Davim, and T. Szalay, “Advanced cutting tools and technologies for drilling carbon fibre reinforced polymer (CFRP) composites: A review,” *Composites Part A: Applied Science and Manufacturing*, vol. 125. Elsevier Ltd, Oct. 01, 2019.

[27] E. Brinksmeierl and R. Janssen’, “Drilling of Multi-Layer Composite Materials consisting of Carbon Fiber Reinforced Plastics (CFRP), Titanium and Aluminum Alloys Property Tensile strength Modulus of elasticity.”

[28] S. L. Soo, A. M. Abdelhafeez, M. Li, R. Hood, and C. M. Lim, "The drilling of carbon fibre composite–aluminium stacks and its effect on hole quality and integrity," *Proc Inst Mech Eng B J Eng Manuf*, vol. 233, no. 4, pp. 1323–1331, Mar. 2019.

[29] P. W. May, "CVD diamond: a new technology for the future?"

[30] E. Uhlmann and J. Koenig, "CVD diamond coatings on geometrically complex cutting tools," *CIRP Ann Manuf Technol*, vol. 58, no. 1, pp. 65–68, 2009.

[31] L. Bigelow and L. K. Bigelow, "Diamond coatings," *Journal de Physique IV Proceedings*, vol. 111, no. C7, p. 3, 1993.

[32] E. Hojman, R. Akhvlediani, A. Layyous, and A. Hoffman, "Diamond CVD film formation onto WC-Co substrates using a thermally nitrided Cr diffusion-barrier," *Diam Relat Mater*, vol. 39, pp. 65–72, 2013.

[33] H. Sein, W. Ahmed, M. Jackson, R. Woodwards, and R. Polini, "Performance and characterisation of CVD diamond coated, sintered diamond and WC-Co cutting tools for dental and micromachining applications," in *Thin Solid Films*, Jan. 2004, pp. 455–461.

[34] E. Ashkinazi *et al.*, "Technology Features of Diamond Coating Deposition on a Carbide Tool," *C (Basel)*, vol. 8, no. 4, p. 77, Dec. 2022.

[35] C. C. Tsao, "Experimental study of drilling composite materials with step-core drill," *Mater Des*, vol. 29, no. 9, pp. 1740–1744, Oct. 2008.

[36] N. Duboust *et al.*, "Machining of Carbon Fibre: Optical Surface Damage Characterisation and Tool Wear Study," in *Procedia CIRP*, Elsevier B.V., 2016, pp. 71–74.

[37] X. Wang, P. Y. Kwon, C. Sturtevant, D. D. W. Kim, and J. Lantrip, "Tool wear of coated drills in drilling CFRP," *J Manuf Process*, vol. 15, no. 1, pp. 127–135, 2013.

[38] G. List *et al.*, "Wear behaviour of cemented carbide tools in dry machining of aluminium alloy," *Wear*, vol. 259, no. 7–12, pp. 1177–1189, Aug. 2005.

[39] M. Nouari, G. List, F. Girot, and D. Géhin, "Effect of machining parameters and coating on wear mechanisms in dry drilling of aluminium alloys," *Int J Mach Tools Manuf*, vol. 45, no. 12–13, pp. 1436–1442, Oct. 2005.

[40] J. Y. Sheikh-Ahmad, *Machining of Polymer Composites*, Springer. 2009.

[41] J. Fernández-Pérez, J. Díaz-Álvarez, M. H. Miguélez, and J. L. Cantero, "Combined analysis of wear mechanisms and delamination in CFRP drilling," *Compos Struct*, vol. 255, Jan. 2021.

[42] A. Hrechuk, V. Bushlya, R. M'Saoubi, and J. E. Ståhl, "Experimental investigations into tool wear of drilling CFRP," in *Procedia Manufacturing*, Elsevier B.V., 2018, pp. 294–301.

[43] M. Montoya, M. Calamaz, D. Gehin, and F. Girot, "Evaluation of the performance of coated and uncoated carbide tools in drilling thick CFRP/aluminium alloy stacks," *International*

Journal of Advanced Manufacturing Technology, vol. 68, no. 9–12, pp. 2111–2120, Oct. 2013.

[44] D. Kim and M. Ramulu, "MACHINABILITY OF TITANIUM/GRAPHITE HYBRID COMPOSITES IN DRILLING."

[45] D. Arola, M. Ramulu, and D. H. Wang, "Chip formation in orthogonal trimming of graphite/epoxy composite," 1996.

[46] M. H. Hassan, J. Abdullah, G. Franz, C. Y. Shen, and R. Mahmoodian, "Effect of twist drill geometry and drilling parameters on hole quality in single-shot drilling of CFRP/AL7075-T6 composite stack," *Journal of Composites Science*, vol. 5, no. 7, Jul. 2021.

[47] A. K. Sridhar, G. Bolar, and N. H. Padmaraj, "Comprehensive experimental investigation on drilling multi-material carbon fiber reinforced aluminum laminates," *Journal of King Saud University - Engineering Sciences*, vol. 34, no. 7, pp. 391–401, Nov. 2022.

[48] G. Bolar, A. K. Sridhar, and A. Ranjan, "Drilling and helical milling for hole making in multi-material carbon reinforced aluminum laminates," *International Journal of Lightweight Materials and Manufacture*, vol. 5, no. 1, pp. 113–125, Mar. 2022.

[49] J. Xu, C. Li, S. Mi, Q. An, and M. Chen, "Study of drilling-induced defects for CFRP composites using new criteria," *Compos Struct*, vol. 201, pp. 1076–1087, Oct. 2018.

[50] G. D. Wang, S. K. Melly, N. Li, T. Peng, and Y. Li, "Research on milling strategies to reduce delamination damage during machining of holes in CFRP/Ti stack," *Compos Struct*, vol. 200, pp. 679–688, Sep. 2018.

[51] I. El-Sonbaty, U. A. Khashaba, and T. Machaly, "Factors affecting the machinability of GFR/epoxy composites," *Compos Struct*, vol. 63, no. 3–4, pp. 329–338, 2004.

[52] H. Ho-Cheng and C. K. H. Dharan, "Delamination During Drilling in Composite Laminates," *Journal of Engineering for Industry*, vol. 112, no. 3, pp. 236–239, Aug. 1990.

[53] F. Lachaud, R. Piquet, F. Collombet, and L. Surcin, "Drilling of composite structures," *Compos Struct*, vol. 52, no. 3–4, pp. 511–516, May 2001.

[54] L. B. Zhang, L. J. Wang, and X. Y. Liu, "A mechanical model for predicting critical thrust forces in drilling composite laminates," *Journal of Engineering Manufacture*, vol. 215, no. 2, pp. 135–144, Feb. 2001.

[55] P. Rahmé, Y. Landon, F. Lachaud, R. Piquet, and P. Lagarrigue, "Analytical models of composite material drilling," *International Journal of Advanced Manufacturing Technology*, vol. 52, no. 5–8, pp. 609–617, Feb. 2011.

[56] R. Piquet, B. Ferret, F. Lachaud, and P. Swider, "Experimental analysis of drilling damage in thin carbon/epoxy plate using special drills," *Compos Part A Appl Sci Manuf*, vol. 31, no. 10, pp. 1107–1115, Oct. 2000.

[57] F. Girot, F. Dau, and M. E. Gutiérrez-Orrantia, "New analytical model for delamination of CFRP during drilling," *J Mater Process Technol*, vol. 240, pp. 332–343, Feb. 2017.

[58] Z. F. Massoom and H. A. Kishawy, “Prediction of critical thrust force generated at the onset of delamination in machining carbon reinforced composites,” *International Journal of Advanced Manufacturing Technology*, vol. 103, no. 5–8, pp. 2751–2759, Aug. 2019.

[59] W.-C. Chen, “SOME EXPERIMENTAL INVESTIGATIONS IN THE DRILLING OF CARBON FIBER-REINFORCED PLASTIC (CFRP) COMPOSITE LAMINATES,” 1997.

[60] A. Faraz, D. Biermann, and K. Weinert, “Cutting edge rounding: An innovative tool wear criterion in drilling CFRP composite laminates,” *Int J Mach Tools Manuf*, vol. 49, no. 15, pp. 1185–1196, Dec. 2009.

[61] K. M. John and S. Thirumalai Kumaran, “Backup support technique towards damage-free drilling of composite materials: A review,” *International Journal of Lightweight Materials and Manufacture*, vol. 3, no. 4. KeAi Publishing Communications Ltd., pp. 357–364, Dec. 01, 2020.

[62] J. Campos Rubio, A. M. Abrao, P. E. Faria, A. E. Correia, and J. P. Davim, “Effects of high speed in the drilling of glass fibre reinforced plastic: Evaluation of the delamination factor,” *Int J Mach Tools Manuf*, vol. 48, no. 6, pp. 715–720, May 2008.

[63] A. Haeger *et al.*, “Non-destructive detection of drilling-induced delamination in CFRP and its effect on mechanical properties,” in *Procedia Engineering*, Elsevier Ltd, 2016, pp. 130–142.

[64] C. C. Tsao and H. Hocheng, “Computerized tomography and C-Scan for measuring delamination in the drilling of composite materials using various drills,” *Int J Mach Tools Manuf*, vol. 45, no. 11, pp. 1282–1287, Sep. 2005.

[65] A. T. Zehnder, “Modes of Fracture,” *Encyclopedia of Tribology*, 2013.

[66] D. Geng *et al.*, “Delamination formation, evaluation and suppression during drilling of composite laminates: A review,” *Composite Structures*, vol. 216. Elsevier Ltd, pp. 168–186, May 15, 2019.

[67] A. Rivero, G. Aramendi, S. Herranz, and L. N. L. De Lacalle, “An experimental investigation of the effect of coatings and cutting parameters on the dry drilling performance of aluminium alloys,” *International Journal of Advanced Manufacturing Technology*, vol. 28, no. 1–2, pp. 1–11, Feb. 2006.

[68] C. Devitte, G. S. C. Souza, A. J. Souza, and V. Tita, “Optimization for drilling process of metal-composite aeronautical structures,” *Science and Engineering of Composite Materials*, vol. 28, no. 1, pp. 264–275, Jan. 2021.

[69] J. H. Lee, J. C. Ge, and J. H. Song, “Study on burr formation and toolwear in drilling cfrp and its hybrid composites,” *Applied Sciences (Switzerland)*, vol. 11, no. 1, pp. 1–14, Jan. 2021.

[70] N. Geier, G. Póka, Á. Jacsó, and C. Pereszlai, “A method to predict drilling-induced burr occurrence in chopped carbon fibre reinforced polymer (CFRP) composites based on digital image processing,” *Compos B Eng*, vol. 242, Aug. 2022.

[71] J. Xu, Q. An, and M. Chen, “A comparative evaluation of polycrystalline diamond drills in drilling high-strength T800S/250F CFRP,” *Compos Struct*, vol. 117, no. 1, pp. 71–82, 2014.

[72] D. I. Poór, N. Geier, C. Pereszlai, and J. Xu, “A critical review of the drilling of CFRP composites: Burr formation, characterisation and challenges,” *Composites Part B: Engineering*, vol. 223. Elsevier Ltd, Oct. 15, 2021.

[73] A. D’Orazio, M. El Mehtedi, A. Forcellese, A. Nardinocchi, and M. Simoncini, “Tool wear and hole quality in drilling of CFRP/AA7075 stacks with DLC and nanocomposite TiAlN coated tools,” *J Manuf Process*, vol. 30, pp. 582–592, Dec. 2017.

[74] H. Zhang, J. Dang, Q. An, X. Cai, and M. Chen, “Study on the drilling performances of a newly developed CFRP/invar co-cured material,” *J Manuf Process*, vol. 66, pp. 669–678, Jun. 2021.

[75] C. Kuo, Z. Li, and C. Wang, “Multi-objective optimisation in vibration-assisted drilling of CFRP/Al stacks,” *Compos Struct*, vol. 173, pp. 196–209, Aug. 2017.

[76] N. Geier and C. Pereszlai, “Analysis of characteristics of surface roughness of machined CFRP composites,” *Periodica Polytechnica Mechanical Engineering*, vol. 64, no. 1, pp. 67–80, 2020.

[77] K. Lakshmi Kala and K. Prahlada Rao, “Synthesis and characterization of fabricated fiber metal laminates for aerospace applications,” *Mater Today Proc*, vol. 64, pp. 37–43, Jan. 2022.

[78] B. Zhong, F. Zou, Q. An, M. Chen, H. Zhang, and C. Xie, “Experimental study on drilling process of a newly developed CFRP/Al/CFRP co-cured material,” *J Manuf Process*, vol. 75, pp. 476–484, Mar. 2022.

[79] E. Ekici, A. R. Motorcu, and E. Yıldırım, “An Experimental Study on Hole Quality and Different Delamination Approaches in the Drilling of CARALL, a New FML Composite,” *FME Transactions*, vol. 49, no. 4, pp. 950–961, 2021.

[80] A. Pardo, M. Majeed, and R. Heinemann, “Process signals characterisation to enable adaptive drilling of aerospace stacks,” in *Procedia CIRP*, Elsevier B.V., 2020, pp. 479–484.

[81] M. Nurhaniza, M. K. A. M. Ariffin, F. Mustapha, and B. T. H. T. Baharudin, “Analyzing the Effect of Machining Parameters Setting to the Surface Roughness during End Milling of CFRP-Aluminium Composite Laminates,” *International Journal of Manufacturing Engineering*, vol. 2016, pp. 1–9, Mar. 2016.

[82] F. Marques, F. G. A. Silva, T. E. F. Silva, P. A. R. Rosa, A. T. Marques, and A. M. P. de Jesus, “Delamination of Fibre Metal Laminates Due to Drilling: Experimental Study and Fracture Mechanics-Based Modelling,” *Metals (Basel)*, vol. 12, no. 8, Aug. 2022.

[83] “DIN 1836: Fields of Application of Tool Categories N, H, W - European Standards”, 08-1962.

Attachment A: Technical Drawings of the Drilling Tools

In Figures 63 and 64 are illustrated the definition drawings with the main dimensions of the two drilling tools used in this report, the drilling tool 1 and the drilling tool 2, respectively.

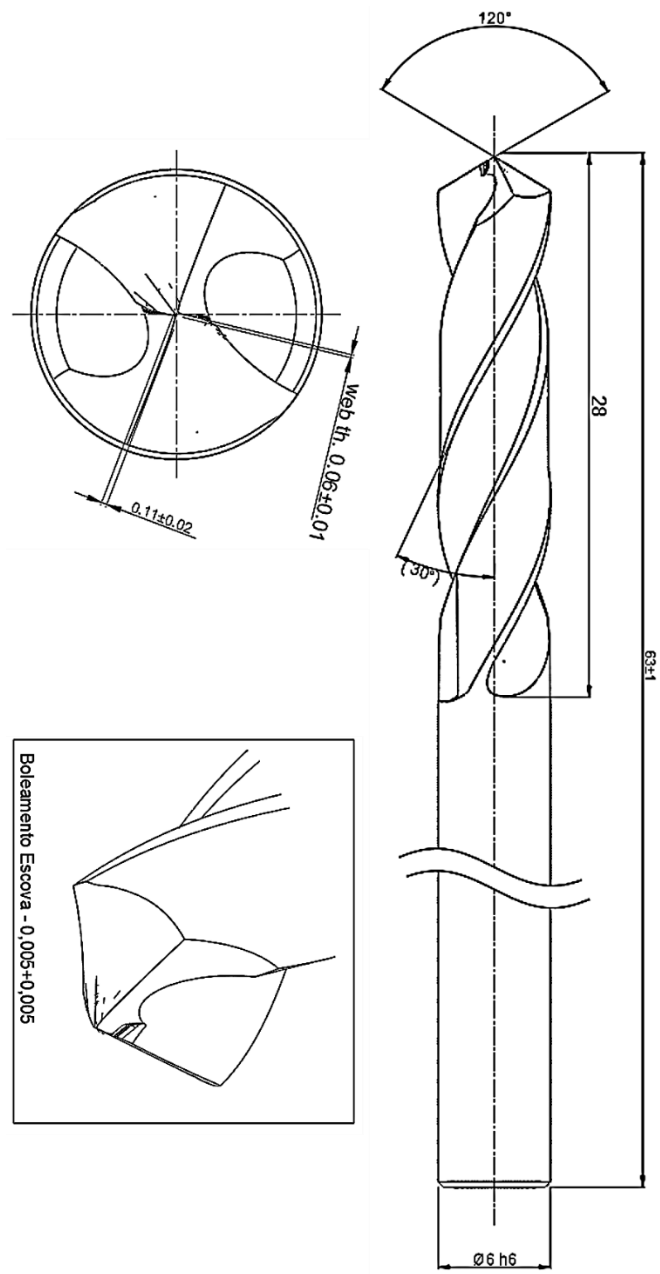

Figure 63. Technical drawing (in mm) of the drilling tool 1 (by PALBIT S.A.).

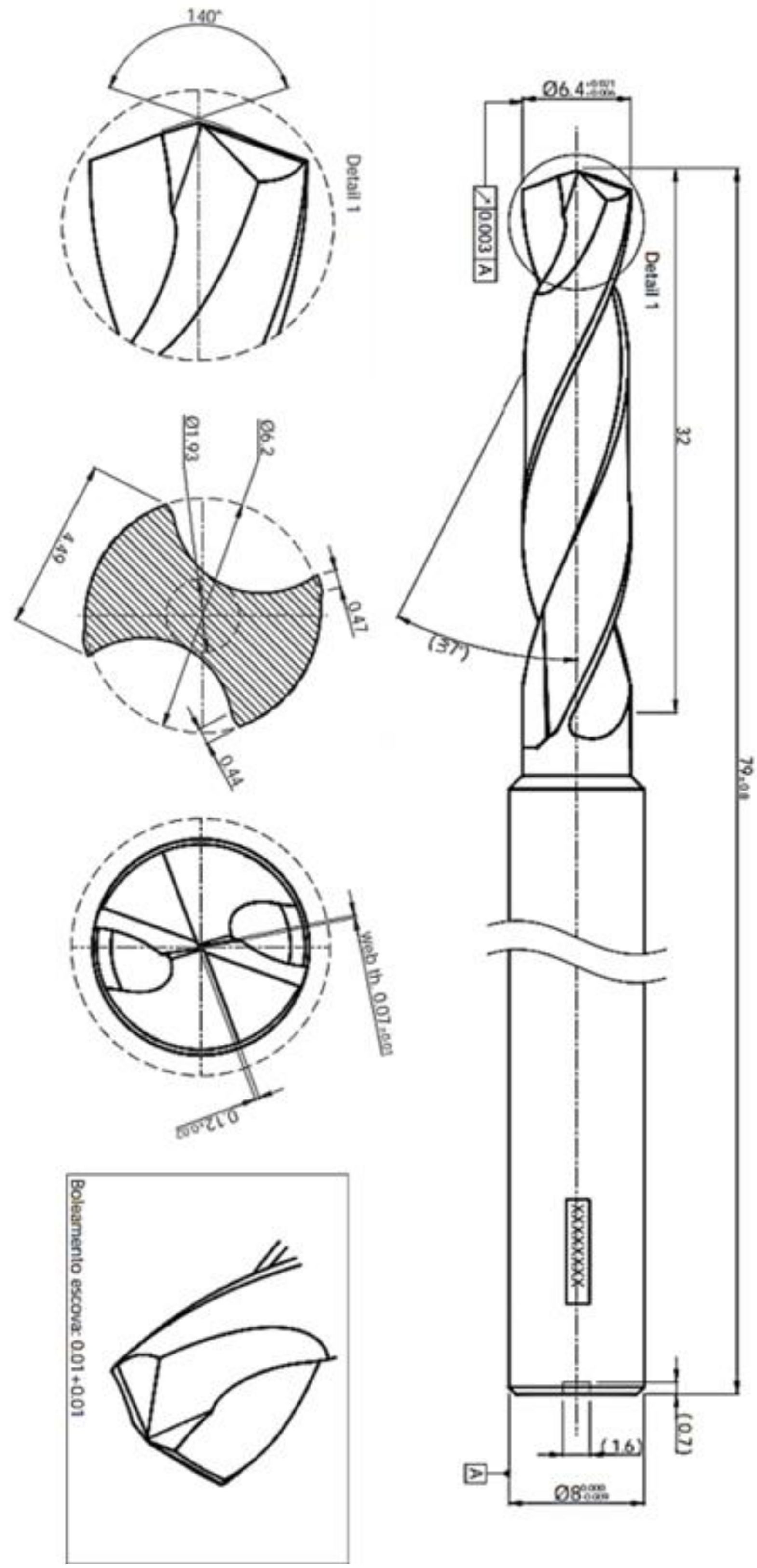

Figure 64. Technical drawing (in mm) of the drilling tool 2 (by PALBIT S.A.).

Appendix A: Preliminary Drilling Campaign and Drilling Campaign

Both the preliminary drilling campaign (i) and the drilling campaign (i) are illustrated in Table 9. In the figures in the table, for the drilling tool 1 the number 1 was used and for the drilling tool 2 the number 2. The numbers following that are used to indicate different tools with the same geometry. The indications in the black boxes correspond to the preliminary drilling campaign (i) while the blue boxes correspond to the drilling campaign (ii).

Table 9. Preliminary drilling campaign (i) and drilling campaign (ii).

Preliminary Drilling Campaign and Drilling Campaign

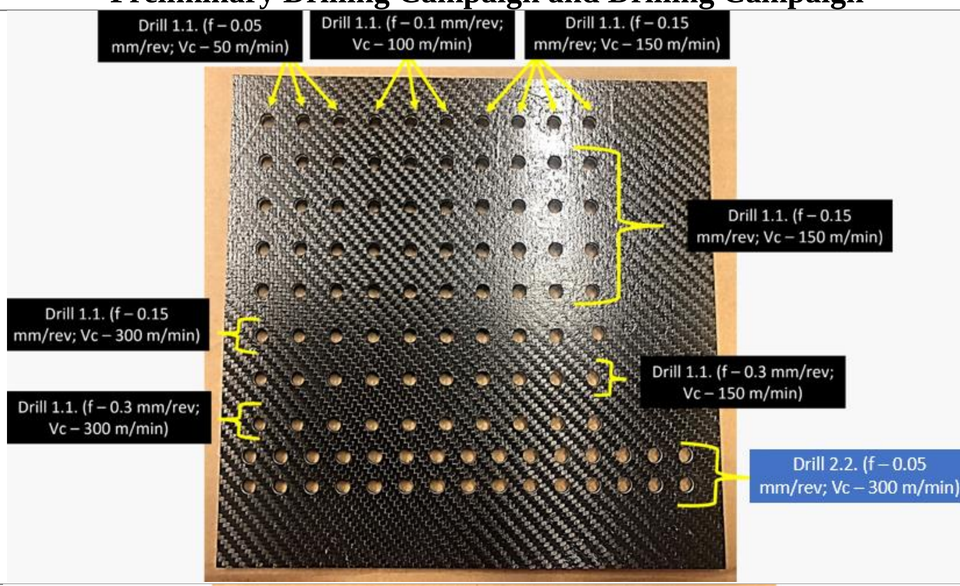

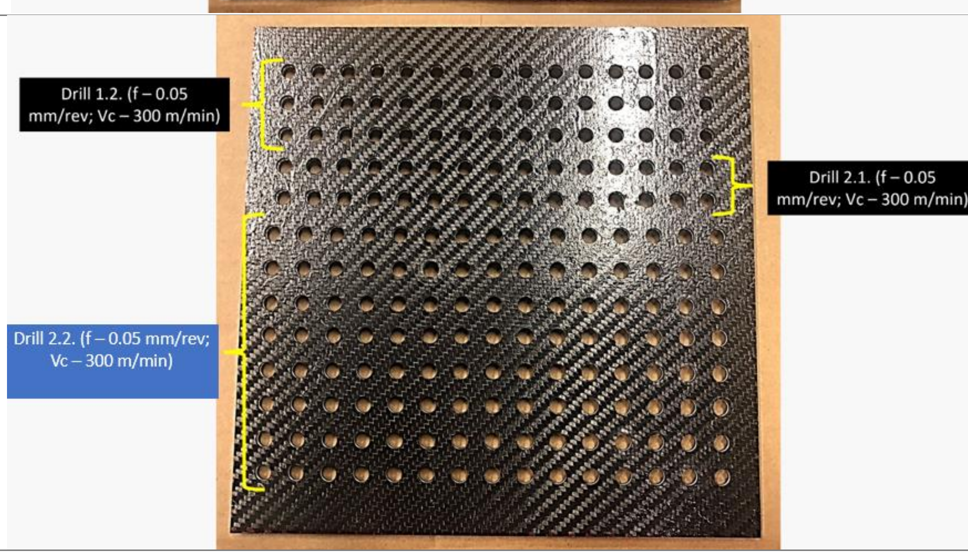

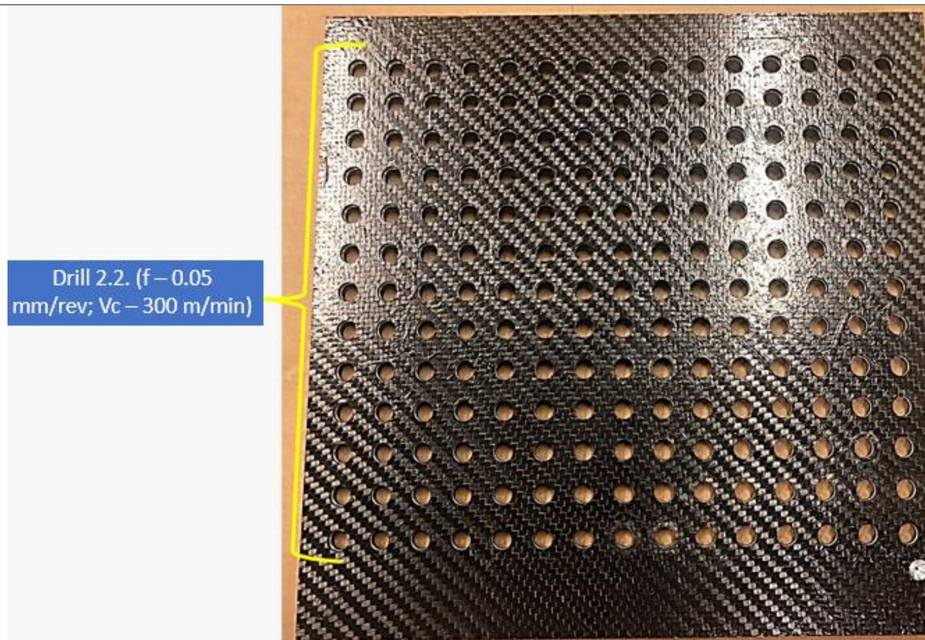
Drill 2.2. (f – 0.05
mm/rev; Vc – 300 m/min)

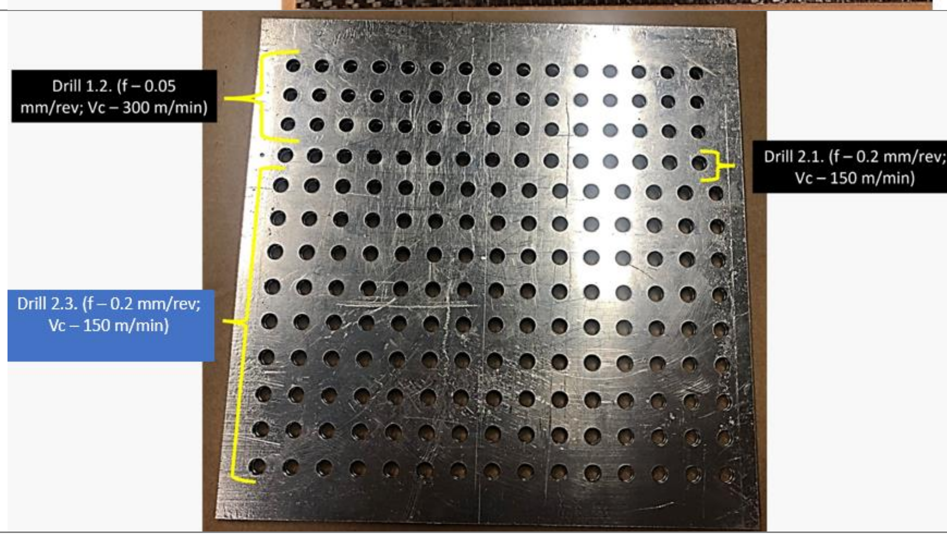
Drill 1.2. (f – 0.05
mm/rev; Vc – 300 m/min)
Drill 2.1. (f – 0.2 mm/rev;
Vc – 150 m/min)
Drill 2.3. (f – 0.2 mm/rev;
Vc – 150 m/min)

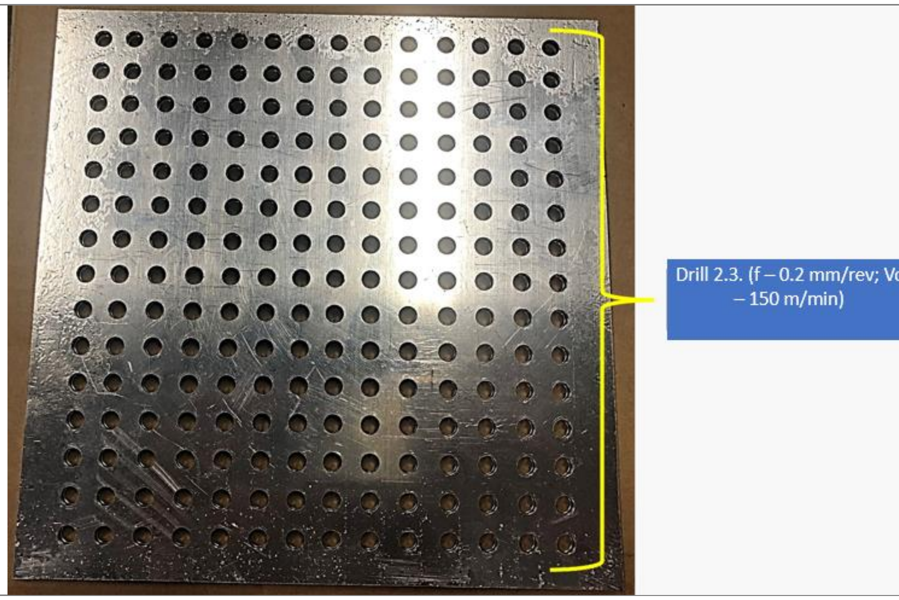
Drill 2.3. (f – 0.2 mm/rev; Vc – 150 m/min)

Appendix B: Delamination Preliminary Results

The delamination preliminary results for the configuration type I are presented in Table 10. The two methods used to compare this type of damage were a microscope analysis (on the left side of the table) and an X-ray analysis (on the right side of the table).

Table 10. Delamination results using DinoLite USB microscope analysis (left) and X-ray analysis (right) for the preliminary drilling campaign (i) with the drilling tool 1.

<table>
<tr><th colspan="2">Feed – 0.05 mm/rev; Cutting Speed – 50 m/min</th></tr>
<tr><td>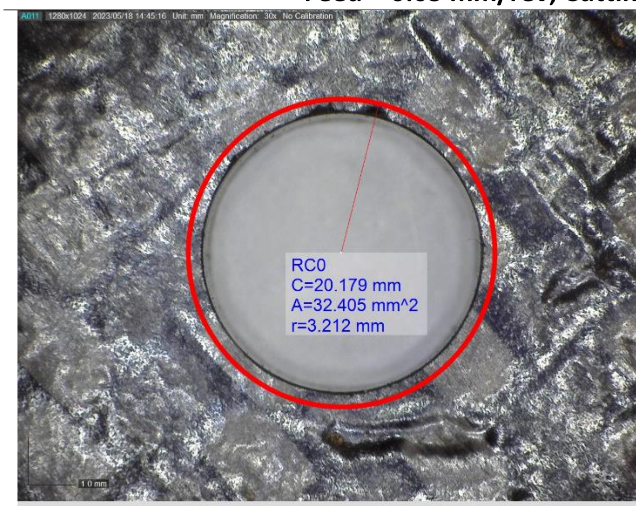
</td><td>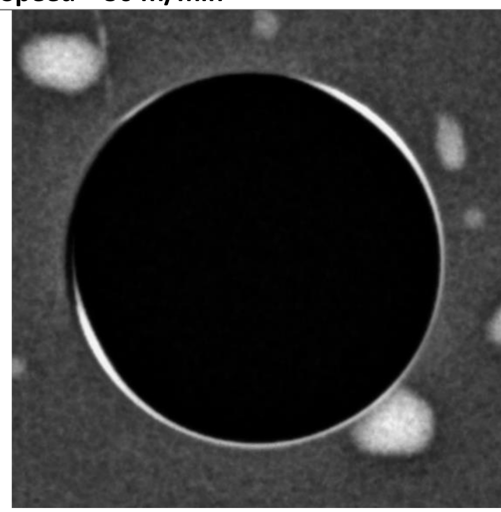</td></tr>
<tr><th colspan="2">Feed – 0.05 mm/rev; Cutting Speed – 300 m/min</th></tr>
<tr><td>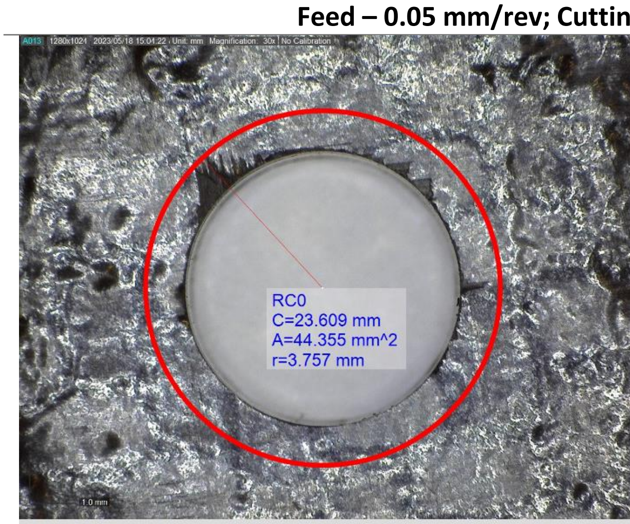
</td><td>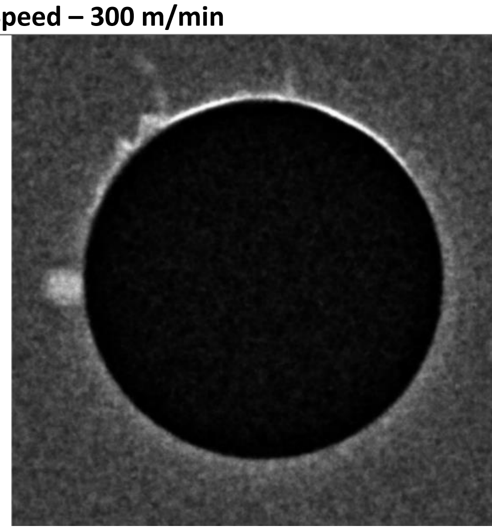</td></tr>
<tr><th colspan="2">Feed – 0.15 mm/rev; Cutting Speed – 150 m/min</th></tr>
</table>

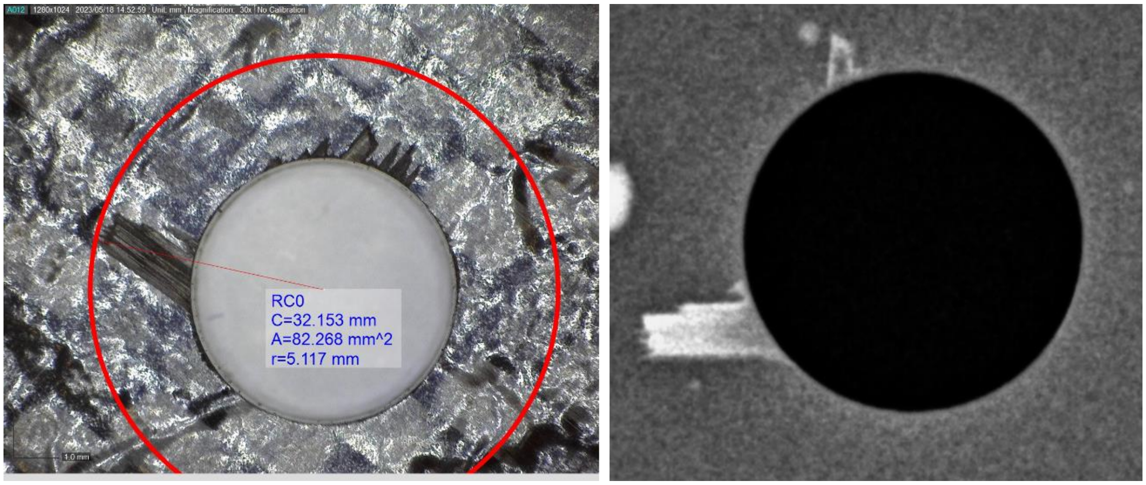

Feed – 0.15 mm/rev; Cutting Speed – 300 m/min

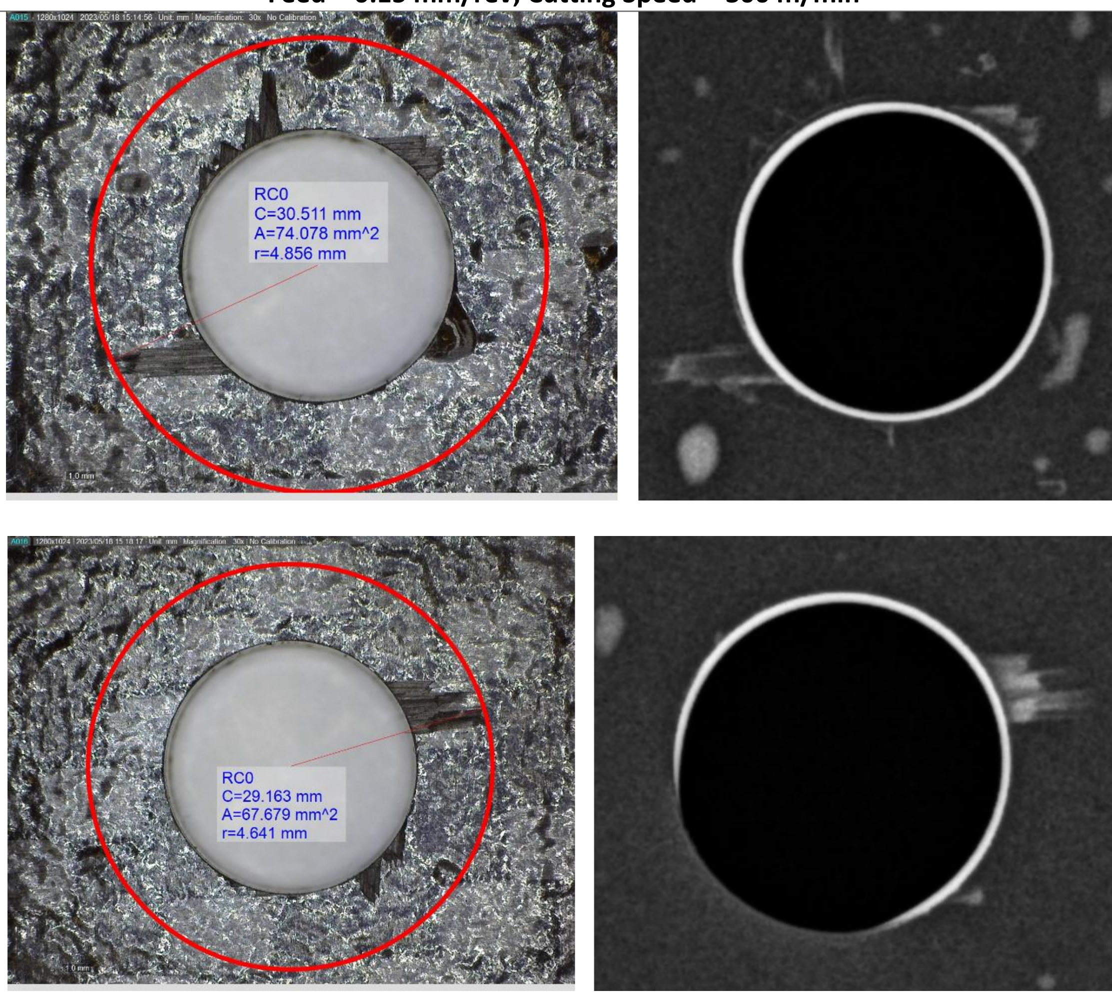

Feed – 0.3 mm/rev; Cutting Speed – 150 m/min

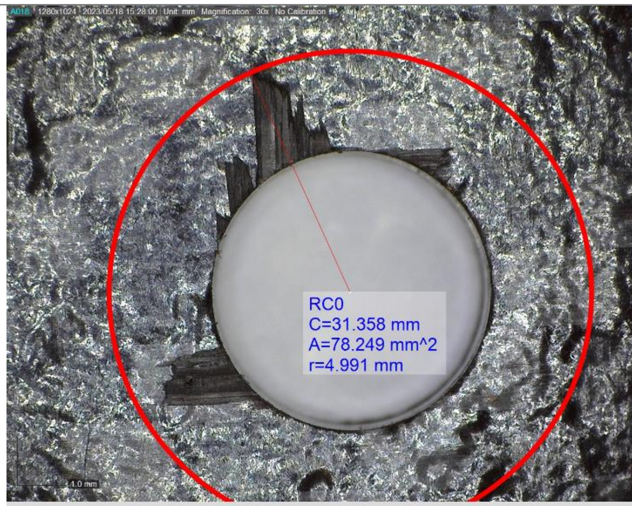

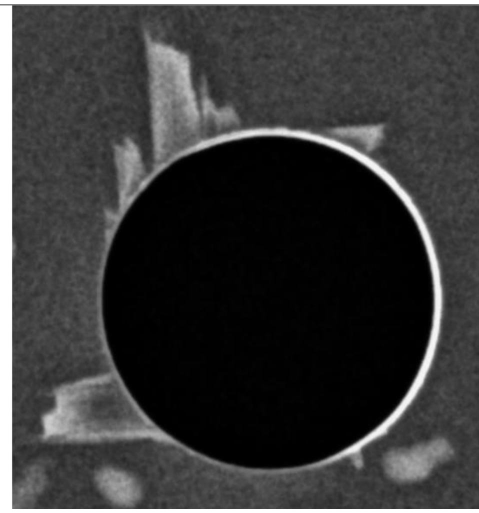

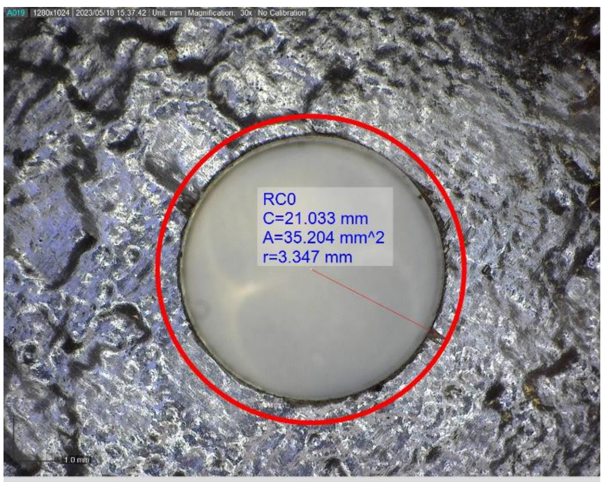

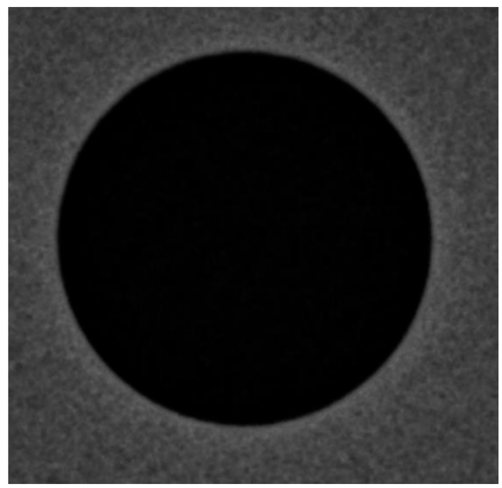

Feed – 0.3 mm/rev; Cutting Speed – 300 m/min

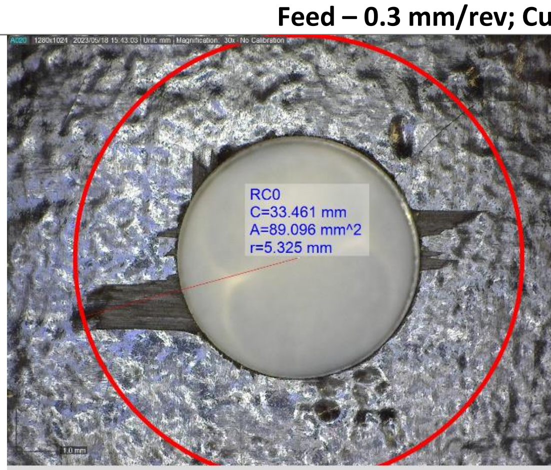

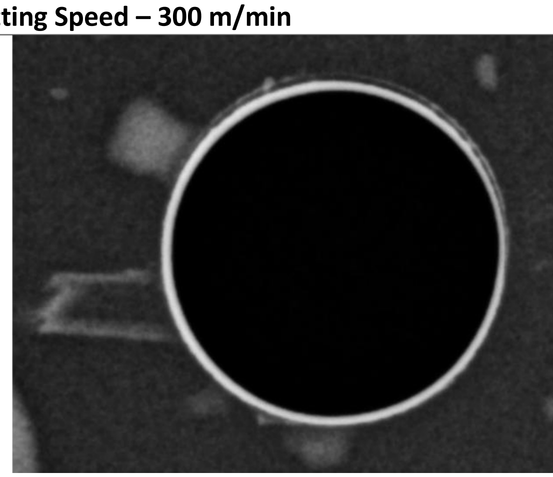

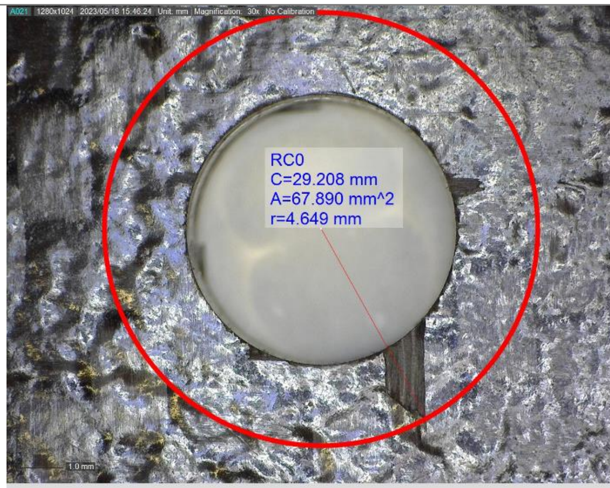
A021
1280x1024
2023/05/18 15:46:24
Unit: mm
Magnification: 30x
No Calibration
RC0
C=29.208 mm
A=67.890 mm^2
r=4.649 mm
1.0 mm
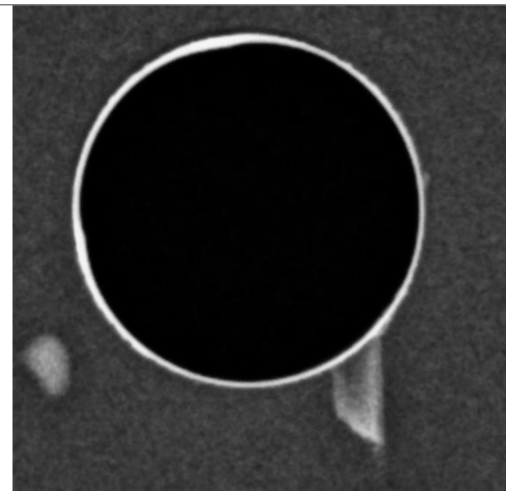

Appendix C: Tool Wear Analysis During the Drilling Campaign

Tables 11 and 12 illustrate three images in different positions of the two drilling tools 2 from drilling the initial 15 holes to a final 345 holes for the configurations type I and type II, respectively, in order to inspect the wear evolution of the drilling tools.

Table 11. Wear inspection of the drilling tool 2 in the drilling campaign (feed – 0.05 mm/rev; cutting speed – 300 m/min) of the plate configuration of type I.

Tool Wear Analysis in the type I configuration (CFRP/AA/CFRP) with the second geometry drill			
Hole Nr.			
15	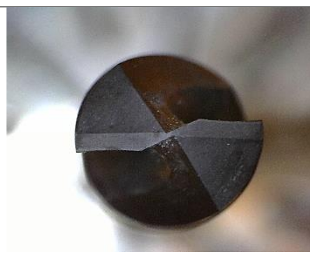		
90	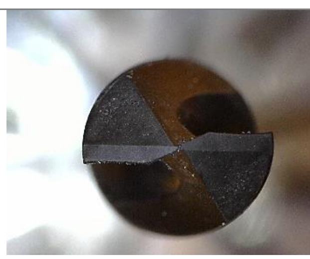		
180	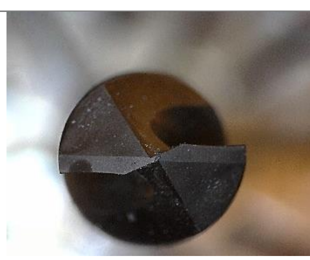		
270	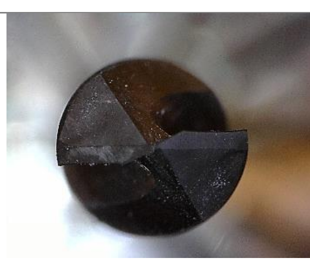		

345	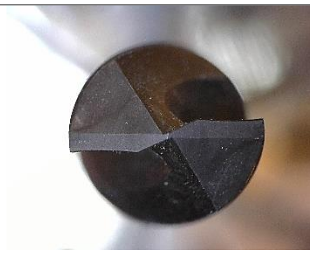		

Table 12. Wear inspection of the drilling tool 2 in the drilling campaign (feed – 0.2 mm/rev; cutting speed – 150 m/min) of plate configuration of type II.

Tool Wear Analysis in the type II configuration (AA/CFRP/AA) with the second geometry drill

Hole Nr.			
15	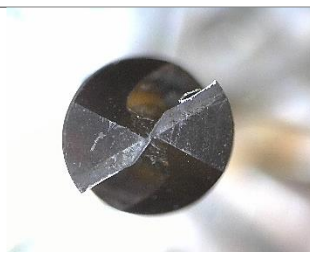		
90	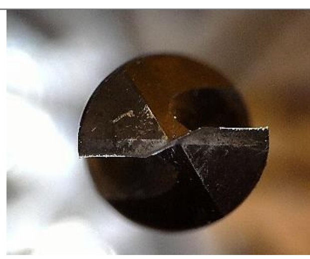	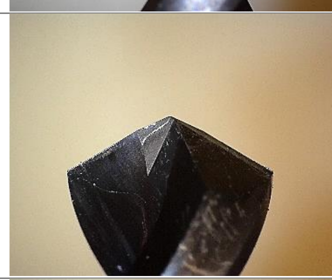	
180	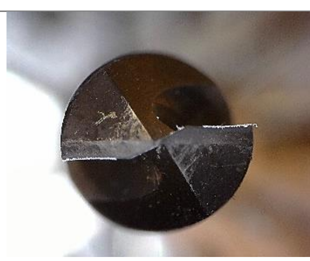		
270	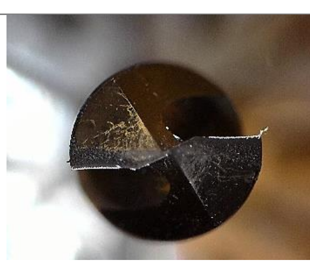	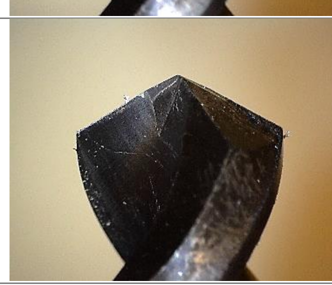	

345